Stony Brook University

Real-time dynamics of the confining string

A Dissertation Presented

by

Frashër Loshaj

to

The Graduate School

in Partial Fulfillment of the Requirements

for the Degree of

Doctor of Philosophy

in

Physics

Stony Brook University

August 2014

Stony Brook University

The Graduate School

Frashër Loshaj

We, the dissertation committee for the above candidate for the
Doctor of Philosophy degree, hereby recommend
acceptance of this dissertation.

Dmitri Kharzeev – Dissertation Advisor
Professor, Department of Physics and Astronomy

George Sterman – Chairperson of Defense
Distinguished Professor, Department of Physics and Astronomy

Xu Du
Assistant Professor, Department of Physics and Astronomy

Larry McLerran
Senior Scientist
Brookhaven National Laboratory, Nuclear Theory Group

This dissertation is accepted by the Graduate School.

Charles Taber
Dean of the Graduate School

Abstract of the Dissertation

Real-time dynamics of the confining string

by

Frashër Loshaj

Doctor of Philosophy

in

Physics

Stony Brook University

2014

Quantum chromodynamics (QCD) describes the interaction of quarks and gluons, which are charged under the color group. Due to confinement of color charge, only colorless hadrons are observed in experiment. At very short distances (hard processes), perturbation theory is a valid tool for calculations and predictions can be made which agree well with experiment. Confinement, which is not yet understood from first principles, is important even for hard processes, because after the perturbative evolution is finished, the final colored particles combine to create the final state hadrons. There are many effective theories of confinement developed over the years. We will consider the Abelian projection; the gauge theory becomes Abelian-like and the theory contains magnetic monopoles. Confinement happens due to the dual Meissner effect, where dual in

this case means the roles of the electric and magnetic fields are reversed. The field between charges resembles that of an Abrikosov-Nielsen-Olesen vortex or string. Based on the Abelian nature of the confining string, because fermion zero modes are localized along the vortex and by considering very energetic jets, we assume that the dynamics along this string is described by massless quantum electrodynamics in 1+1 dimensions. This theory shares with QCD many important properties: confinement, chiral symmetry breaking, theta-vacuum, and is exactly soluble. We use the model to compute the fragmentation functions of jets in electron-positron annihilation and after fixing two adjustable parameters, we study the modification of fragmentation functions of jets in the QCD medium. We address an important puzzle in hadron scattering: the soft photon yield in processes with hadrons in the final state is much larger than what is expected from the Low theorem. We find that soft photons produced from currents induced during the real-time dynamics of jet fragmentation can contribute in the enhancement of photons. We compare the result with the recent DELPHI measurements and a reasonable agreement is found. Finally, assuming the QCD string to be thin, we address the observed phenomenon in recent lattice studies of partial chiral symmetry restoration along the string. Our result agrees well with the data.

Contents

List of Figures

Acknowledgements

I would like to thank my advisor Dmitri Kharzeev for his guidance and support during my last years as a PhD student and for his help in finishing the projects on which this thesis is largely based on.

I thank the members of the committee Xu Du, Larry McLerran and George Sterman for agreeing to participate in the defense.

Over the past few years I have benefited from numerous discussions with professors of the Nuclear Theory group Edward Shuryak, Derek Teaney and Ismail Zahed. I would like to thank also Tigran Kalaydzhyan, Wolfger Peelaers and Ho-Ung Yee for many useful discussions.

I am indebted to Dmitri Kharzeev and George Sterman for reading earlier versions of the thesis and for many useful comments.

I am grateful to Laszlo Mihaly for helping me transfer from the electrical engineering department and for giving me the opportunity to pursue a PhD degree in physics.

Chapter 1

Introduction

At very short distances (high energies), due to *asymptotic freedom* [1, 2], QCD can be viewed as a theory of weakly coupled quarks and gluons. On the other hand, at distances of the order of the proton size, namely ~ 1 fm, the theory becomes strongly coupled and degrees of freedom are hadrons instead of quarks and gluons. The latter do not exist as asymptotic states due to the formation of chromoelectric flux tube or string between color sources - *confinement*.

QCD is not solved yet at these low energies and confinement is not fully understood from first principles. There are, however, indirect indications for its existence. For example, an order parameter that is useful in describing the phases of QCD is the Wilson loop operator [3], defined as

$$W(C) = \mathrm{Tr}\left\{ P \exp\left[i \oint_C A_\mu(x) dx^\mu \right] \right\}. \tag{1.1}$$

P stands for path ordering, C is a closed contour of integration and A_μ is the gauge field. We can imagine the contour as the trajectory of a quark in space-time. For example, in the case of a very heavy quark-antiquark pair, separated by distance R, existing for time T, the contour will be a rectangle as shown in Fig. 1.1. For a very large value of time T, the vacuum expectation value of the Wilson loop operator becomes

$$\langle W(C) \rangle \simeq \exp[-V(R)T], \tag{1.2}$$

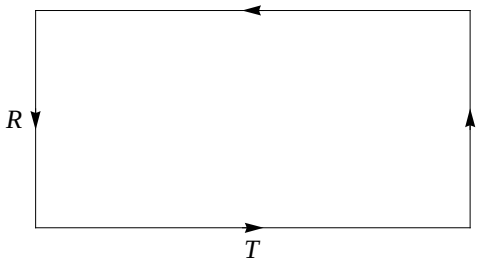

Figure 1.1: Rectangular Wilson loop.

where $V(R)$ is the static potential between the quarks. If the potential is linearly confining, namely $V(R) = \sigma R$, where σ is the string tension, the Wilson loop operator takes the value

$$\langle W(C) \rangle \simeq e^{-\sigma RT}. \tag{1.3}$$

This is known as the *area law* and is an indicator of confinement. The existence of light quarks in the theory, causes the potential between quarks to be screened, in other words, the string stretched between them breaks and the Wilson loop operator obeys the *perimeter law* instead. These properties can be checked for example in lattice QCD.

Another feature of QCD is its complicated and rich vacuum structure. The masses of the light quarks in QCD are very small compared to the characteristic mass scale $M \sim 1$ GeV (the scale below which the perturbative QCD is invalid). Since the interaction between quarks is mediated via a vector exchange, in the limit of zero mass for the quarks, the theory is chirally symmetric - quarks with different chirality do not transform between each other. This symmetry is absent in the spectrum of hadrons, therefore it must be spontaneously broken. From the Goldstone theorem [4], the spontaneous symmetry breaking is accompanied with the appearance of massless bosons (Goldstone bosons) in the spectrum. If $m_u, m_d \to 0$ (SU(2) symmetry), then we have the breaking $SU(2)_L \times SU(2)_R \to SU(2)$. In this case, there should be three Goldsone bosons, which can be identified with the triplet of the π mesons. The spontaneous breaking of the chiral symmetry is accompanied with nonzero value of certain condensates. For example, from the Gell-Mann-Oakes-Renner

relation [5]

$$\langle 0|\bar{q}q|0\rangle = -\frac{1}{2}\frac{m_\pi^2 f_\pi^2}{m_u + m_d}, \tag{1.4}$$

where m_π and f_π are the mass and the decay constant of the pion respectively. Using the numerical values of these parameters (see for example [6]), we get

$$\langle 0|\bar{q}q|0\rangle \simeq -(257 \text{ MeV})^3. \tag{1.5}$$

The interpretation of this result is that a nearly massless quark propagating in the QCD vacuum dynamically obtains a finite mass. Another property is, for example, the large scale fluctuations of the gauge field. This can be illustrated by the so-called gluon condenstate, given by [6]

$$\frac{1}{32\pi^2}\langle 0|F_{\mu\nu}F^{\mu\nu}|0\rangle \simeq (200 \text{ MeV})^4. \tag{1.6}$$

In quenched QCD, the limit of infinitely heavy quarks, one can use the string tension as an order parameter of confinement-deconfinement transition. On the other hand, in the chiral limit (zero fermion mass), the chiral condensate can be an appropriate order parameter of the chiral phase transition. It is well known however that both string tension and chiral condensate are present in both phases, which suggests that we are dealing with a *crossover* instead of a phase transition.

Some nonperturbative aspects can be addressed analytically, as is the case in the so called Shifman-Vainshtein-Zakharov (SVZ) sum rules [7], which is a method for extracting the long distance current correlation functions using the values of certain condensates.

For the most part of this thesis we will be interested in nonperturbative aspects of high energy processes. We should mention that perturbative QCD (pQCD) calculations, over the years, have shown remarkable agreement with experimental results. This success can be attributed to properties like *factorization* (see [8]) - where one can treat independently the hard part of high energy hadron scattering from the soft part, and local parton hadron duality (LPHD) [9] - where distributions of final quarks and gluons (partons) in QCD cascades, seem very similar to the final hadron distribution in experiment.

Let us consider a simplified picture of a high energy event. The hard part of the process can be treated perturbatively, where the dynamical degrees of freedom are quarks and gluons. As we go to large distances, or small momenta, the transition between quark and gluon to hadron degrees of freedom takes place. This process is known as *hadronization*. There are many models that are used to describe the transition of quarks and gluons to hadrons. We will review very briefly below the so-called Lund model, which is based on the semiclassical treatment of the QCD string.

A pedagogical review of the subject is given in [10]. We will mostly follow [10–12]. The starting point of the string model is the fact that the potential between $q\bar{q}$ grows linearly with distance, $V(r) = \kappa r$, where from experiment (for example hadron mass spectroscopy) it is known that $\kappa \simeq 1$ GeV/fm $\simeq 0.2$ GeV^2 (at small distance between quarks, a Coulomb potential is also present, but it is neglected, because it does not affect the fragmentation, only the properties of the final hadrons).

In order for the description to be Lorentz covariant and causal, the most straightforward way is to require that the endpoints of the strings be massless and to neglect transverse degrees of freedom. The string formed this way is referred to as the massless relativistic string. Consider for example a quark q and antiquark $\bar{q}$ moving back to back, with a linear potential stretching between them. As the quarks move, the energy of the string increases and when it equals the initial kinetic energy of the system, the quark-antiquark abruptly change direction and start moving back (see Fig. 1.2). The mass of the system is proportional to the area spanned by the endpoints of the string.

After including dynamical fermions, the string should break, splitting into two color singlet states. This is illustrated in Fig. 1.3. The thick horizontal lines indicate the electric field stretched between the pairs. The two systems move apart and the electric field between the two vanishes as indicated in Fig. 1.3. If the invariant masses of the new strings are large, they continue to break, until the masses reach values comparable to masses of hadrons. Thus, in the process of pair creation, the original string breaks into n strings, which form the primary hadrons (in Fig. 1.3 we illustrate a formation of a hadron in the

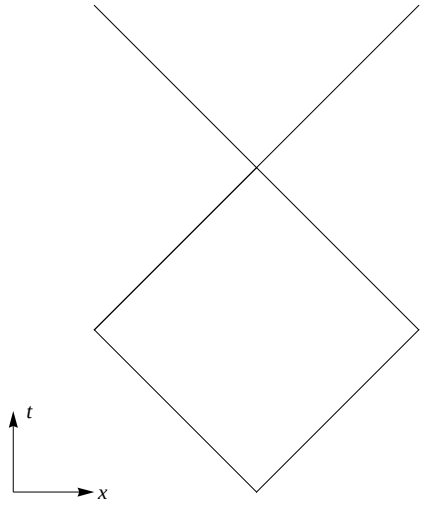

Figure 1.2: Space-time diagram of the motion of the massless relativistic string.

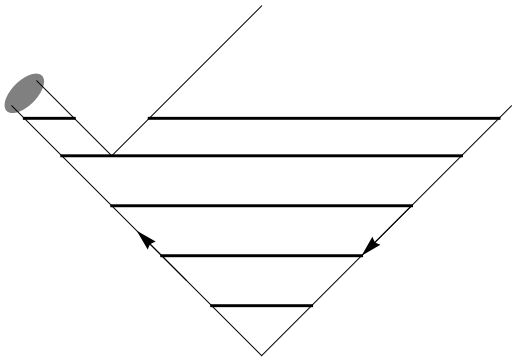

Figure 1.3: Breaking of the QCD string.

far left). The time ordering of the breaking is irrelevant because the points where the string breaks are space-like separated. This can be seen as follows. Since the string has a constant tension κ,

$$\left|\frac{dE}{dz}\right| = \left|\frac{dp_z}{dt}\right| = \kappa. \tag{1.7}$$

Now assume that the string breaks at points 1 and 2, as shown in Fig. 1.4, with coordinates (t_1, z_1) and (t_2, z_2) respectively. The energy and momentum

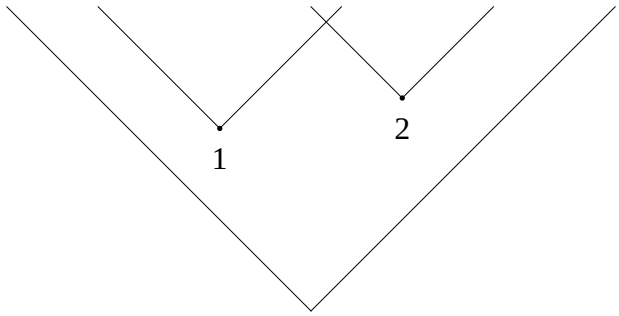

Figure 1.4: String breaking in two points.

of the system between points 1 and 2 are given by

$$E = \kappa\Delta z = \kappa(z_1 - z_2), \quad p_z = \kappa\Delta t = \kappa(t_1 - t_2). \tag{1.8}$$

The total mass is

$$E^2 - p_z^2 = m^2 = (z_1 - z_2)^2 - (t_1 - t_2)^2, \tag{1.9}$$

and is positive only for space-like separation of the points. The breaking then occurs independently. This enables one to define an iterative procedure, which guaranties that the produced hadrons are on mass shell.

It should be pointed out that heavy quarks like charm and bottom are not produced as the string breaks, but they can only be at the endpoints of the initial string. This can be argued by using the Heisenberg and Euler theory of pair creation in a strong field [13] (for a review see [14]). The probability for creating a pair of particles with mass m and transverse momentum $p_\perp$ is

given by

$$\exp\left(-\frac{\pi m_\perp^2}{\kappa}\right) = \exp\left(-\frac{\pi m^2}{\kappa}\right)\exp\left(-\frac{\pi p_\perp^2}{\kappa}\right), \tag{1.10}$$

where $m_\perp = \sqrt{p_\perp^2 + m^2}$. We see that this expression implies suppression of production of heavy pairs, namely $u : d : s : c \simeq 1 : 1 : 0.3 : 10^{-11}$.

The Lund model has proven to be very successful in describing many experimental results. Its usage however, is quite limited when the quantum dynamics of the string breaking is required. The quark gluon plasma formed in heavy ion collisions is strongly coupled and its effect on jets involves nonperturbative physics. One needs a dynamical theory of confinement in this case (see chapter 4). Another example would be in the case of photon production from the real-time dynamics of jet fragmentation (see chpater 5).

Despite all the successes of perturbative QCD, there is a need to understand better the nonperturbative aspects of it. A lot of data from the soft-physics part from LHC, for example, may challenge the standard fragmentation picture. It should also be questioned if this picture applies in heavy ion physics as well. Another reason to understand the fragmentation of quarks and gluons comes when studying ultra high energy cosmic rays. The extrapolation of the known models from collider energies to these processes seems to be challenged (see for example [15]).

In this thesis, using a very well known exactly soluble theory, which shares with QCD many key properties, we will develop a simple model of dynamical string breaking. More details will be given in chapter 2. We will give the basic idea here, but first we have to say something about another model of confinement, the dual superconductor theory.

The mechanism of confinement in terms of the dual Meissner effect is due to Nambu, Mandelstam, 't Hooft and many others (see for example [16–18]). The basic idea is as follows. Since quarks contain chromoelectric charge, if a quark q and an antiquark $\bar{q}$ are put at a distance R from each other, there will be a chromoelectric field stretching between them. If these particles are embedded in a non-superconducting medium, then a Coulomb like field is stretched in between. On the other hand, if the medium is a superconductor, then the field between quark and antiquark will resemble a flux tube, which is the result of

Meissner effect (for type II superconductors). The field cannot be expelled completely, because the flux should be conserved. As the distance between particles increases, the flux tube becomes longer, but it maintains the same minimal thickness and the transverse profile is unchanged. These flux tubes are similar to the Abrikosov-Nielsen-Olesen vortices, which we will review in the next chapter. The effect we described so far is referred to as the dual superconductivity, because as we can see the roles of the electric and magnetic fields are interchanged, compared to the usual superconductor. For the usual type II superconductor, the electric charges condense, into the so called Cooper pairs, and magnetic flux tubes are formed between magnetic monopoles. In our case, the flux tubes are electric and in turn magnetic monopoles should condense. Furthermore, it is assumed that the field between the quark and antiquark is Abelian. In this case the dual superconductor is described via the Landau-Ginzburg model. This "Abelianization" can be achieved, for example, through the method of Abelian projection, which we will also briefly review in the next chapter.

Based on the dual superconductor theory of confinement, we assume that the dynamics along the QCD string is Abelian. The electric field between charged particles is similar to that of the vortex in the Landau-Ginzburg theory. Moreover, as we will see in the next chapter, if one introduces fermions to this theory, the zero modes can be seen to be localized along the core of the vortex. For the most part of this work, we consider very energetic jets, therefore the longitudinal scale, along the jet axis, is much larger than transverse. We then assume a $1+1$ dimensional dynamics. Our assumption therefore will be that the dynamics of fermions on the string is described by massless QED in $1+1$ dimensions, also known as the Schwinger model. The theory is exactly soluble. String breaking due to massless fermions is similar to the Lund model as shown above.

We will give many details in subsequent chapters, but let us mention an important difference between the semiclassical treatment of the Lund model and our case. Let us consider again a quark-antiquark pair moving back to back as in Fig. 1.5. In the Lund model model, as we saw above, the string breaks due to the creation of massless pairs and the electric field between them

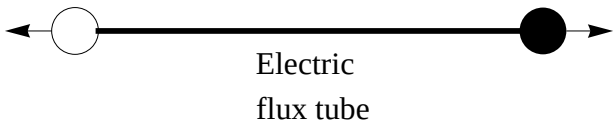

Figure 1.5: Electric flux tube formed between a quark-antiquark pair moving back to back.

vanishes. In the Schwinger model the situation is different. As the new pair is created, the field between them is not completely canceled (see Fig. 1.6). Instead, as new pairs are created, they create a dynamical fluctuation of the field. In $1+1$ dimensions, the chirality of fermions is determined by their

Figure 1.6: String breaking by formation of a massless pair of quark-antiquark. The electric field between the created pair does not vanish.

direction of motion and charge. The right moving fermion and a left moving antifermion have the same chirality. This means that the system in Fig. 1.5 has two units of chirality, which is "encoded" in the electric field due to the index theorem in $1+1$ dimensions

$$N_R - N_L = \frac{g}{2\pi} \int d^2x \; \epsilon^{\mu\nu} F_{\mu\nu}. \tag{1.11}$$

N_R and N_L are the number of right and left handed particles respectively (in our conventions, the system has two units of right chirality). The axial anomaly is precisely given by the integrand of (1.11), therefore it determines the particle creation. We will discuss more about the role of the anomaly in particle creation in Chapter 5.

The following is the outline of this thesis.

In chapter 2 we review the so-called Abelian projection of gauge theories. The diagonal part of the gauge field remains massless and the theory can be thought of as having a $U(1)^{N-1}$ gauge invariance. In the simplest case of $SU(2)$ it is shown that singular points of the transformed field can be interpreted as containing magnetic monopoles. From these considerations, we assume that

the QCD string resembles a dual Abrokosov-Nelsen-Olesen vortex. If one introduces fermions into the theory, it is well known that zero modes will be confined along the core of the string. We therefore conjecture that the dynamics of massless fermions along the QCD string is described by QED in $1+1$ dimensions, also known as the Schwinger model. The theory is exactly soluble. We illustrate this in a simple way using bosonization. We review this theory and notice that it shares with QCD many important features, including confinement, screening of charge, chiral symmetry breaking, anomalies and θ-vacuum.

In chapter 3 we use the Schwinger model to study the real-time dynamics of jet fragmentation. Our aim is to calculate analytically the fragmentation function of the quark. The coupling of the theory has dimension of mass. In the bosonized version of the theory the coupling is interpreted as the mass of the produced hadron in the fragmentation of QCD string. We introduce another parameter Q_0, whose physical interpretation is that of the scale at which the perturbative cascade stops. We fit these parameters by comparing with data from e^+e^- annihilation to hadrons. Our result, by choosing the hadron mass to correspond the σ meson mass and $Q_0 \simeq 2$ GeV, agrees reasonably well with the data. The most significant discrepancy is seen for soft hadrons and this is due to the fact that we neglect the produced gluons in the perturbative cascade.

In chapter 4, we adopt the model to include the effect of QCD medium, produced in heavy-ion collisions, in jets. We consider a very simple case of a static medium. As the jet propagates, it scatters off the static sources, which are placed at equal distance from each other. After each scattering, the quark rotates in color space, creating many independent antennae giving off radiation, by which the jet loses energy. This scenario seems to explain well the experimental observation of soft hadron enhancement for in-medium jet fragmentation. We then consider the case where the jet exchanges momentum with the medium and gives off a final gluon outside the medium. As a result of partial screening of the color charge of the jet from the final gluon, we obtain the observed suppression for intermediate momentum hadrons.

A long lasting puzzle in high energy hadron scattering is the phenomenon

of anomalous soft photon production. It corresponds to the observed fact that in many experiments the soft photon yield cannot be explained from the Low theorem - the observed yield is up to five times higher than expected. The phenomenon is only observed in processes with hadronic final states. It is reasonable to assume that part of the enhancement of photons can come from the real-time dynamics of QCD string breaking in the process of jet fragmentation. We use the model introduced in the previous chapters. By assuming a non-zero width of the hadron propagator and taking into account the fluctuations of the string, we can describe the recent DELPHI measurements in photon enhancement. This will be the focus of chapter 5.

Recently, a lattice measurement of the chiral condensate was performed in the presence of static quarks (QCD string stretched between them). It was shown that the chiral condensate decreases at the core of the string, which signals partial chiral symmetry restoration. In chapter 6 we assume a thin string between the quarks, with a probabilistic fluctuation in the transverse plane. Assuming the same energy density per unit length in the full $3+1$ dimensional string and the $1+1$ dimensional case, we derive the probability distribution. In order to compare with the data, we have to fix the effective width of the string, which is shown to be of the order of the lattice spacing.

We give a summary of all the results of the thesis and mention some of the future prospects in chapter 7.

Chapter 2

Abelian model of the QCD string

In this chapter we will argue that the dynamics along the string formed between color charges, if we consider light fermions in the theory, is described by a $1+1$ dimensional, Abelian model. In order to do that, we first review some facts about the Abelian projection of $SU(N)$ gauge theory (we only consider $SU(2)$ for simplicity). The Abelian projected theory contains magnetic monopoles. These monopoles can condense, giving rise to a dual superconductor, described by the Landau-Ginzburg theory. Duality here means that the roles of the magnetic and electric fields are interchanged. Between colored sources, a (chromo-) electric field flux tube is formed and confinement ensues. This scenario is similar to the case of the usual superconductor where the magnetic monopoles are confined. In later chapters we use this model to study the real-time dynamics of jet fragmentation. The jets under consideration are very energetic; the longitudinal (along jet axis) scale is much larger than transverse, therefore we neglect the transverse degrees of freedom in our treatment. We propose that the dynamics of jet fragmentation at late stages, where the perturbative QCD emission ends, is described effectively by massless QED_2, also known as the Schwinger model. We review below some basic facts about this model and show that it shares with QCD many important aspects, needed to describe jet fragmentation. These include confinement, chiral

symmetry breaking, anomalies and θ-vacuum.

2.1 Abelian Projection

In this section we review the so-called Abelian projection (also known as Abelian gauge fixing). The basic ideas shown here have been introduced in the seminal papers by Polyakov [19] and 't Hooft [20, 21]. For a review see [22, 23]. The aim of the Abelian projection is to find a gauge where the $SU(N)$ gauge field $A^a_\mu T^a$ is diagonal (T^a are the generators of $SU(N)$). This would reduce the non-Abelian theory to an Abelian one. This however cannot be achieved - not all components of the gauge field can be diagonalized simultaneously. We can instead proceed in the following way. Let's consider a scalar in the adjoint representation of the gauge group

$$\phi(x) = \phi^a(x) T^a. \tag{2.1}$$

The scalar can be constructed out of the fields of the gauge theory, for example $\phi = G_{12}$, where $G_{\mu\nu}$ is the field strength. The goal of this procedure is to choose a gauge where the field $\phi(x)$ is diagonal, in other words

$$\Omega(x)\phi(x)\Omega^\dagger(x) = \mathrm{diag}(\lambda_1(x), \lambda_2(x), \ldots, \lambda_N(x)). \tag{2.2}$$

This gauge is called the Abelian gauge and in general it depends on the choice of $\phi(x)$. We will discuss below how the monopoles appear in this gauge for the case of $SU(2)$. The gauge fixing (2.2) now becomes

$$\phi(x) \to \Omega(x)\phi(x)\Omega^\dagger(x) = \begin{pmatrix} \lambda & 0 \\ 0 & \lambda \end{pmatrix}, \quad \lambda = \sqrt{(\phi^1)^2 + (\phi^2)^2 + (\phi^3)^2}. \tag{2.3}$$

We notice that the eigenvalues are degenerate when $\lambda = 0$, which means that all components of $\phi(x)$ vanish. Let's consider the points where this happens, namely

$$\phi^1(\boldsymbol{r}_0) = \phi^2(\boldsymbol{r}_0) = \phi^3(\boldsymbol{r}_0) = 0 \tag{2.4}$$

We have three equations and three unknowns, which are the components of the vector $\boldsymbol{r}_0$. At the point $\boldsymbol{r}_0$, it is not possible to define the gauge, and we will see that the gluon field develops a singularity at that point. Let us Taylor expand the field $\phi(\boldsymbol{r})$, where $\boldsymbol{r} = (x^1, x^2, x^3)$, at the vicinity of the point $\boldsymbol{r}_0$

$$\phi(\boldsymbol{r}) = \phi^a(\boldsymbol{r})T^a = T^a C^{ab}(x_a - x_{0b}) \tag{2.5}$$

where

$$C^{ab} = \frac{\partial \phi^a(\boldsymbol{r})}{\partial x_b}\Big|_{x_a = x_{0a}}, \tag{2.6}$$

and x_{0a} are the components of $\boldsymbol{r}_0$. We see that in this new coordinate system, defined by the transformation C^{ab}, the field takes the form

$$\phi(\boldsymbol{r}) = x'^a T^a, \quad x'^a = C^{ab}(x_b - x_{0b}). \tag{2.7}$$

The scalar has now the form of the *hedgehog* field. From now on, we assume to be in the new frame and we drop the primes. Let (r, θ, ϕ) be the spherical coordinates of the vector $\boldsymbol{r}$. The hedgehog field $\phi(x) = x^a T^a$ takes the form

$$\phi(\boldsymbol{r}) = x^a T^a = T^1 r \sin\theta\cos\phi + T^2 r \sin\theta \sin\phi + T^3 r\cos\theta \tag{2.8}$$

In the case of $SU(2)$, the generators are given by $T^a = \frac{1}{2}\sigma^a$, where σ^a are the Pauli matrices (see (A.4)). We then have

$$\phi(\boldsymbol{r}) = \frac{r}{2}\begin{pmatrix} \cos\theta & e^{-i\phi}\sin\theta \\ e^{i\phi}\sin\theta & -\cos\theta \end{pmatrix}. \tag{2.9}$$

It is easy to see that the gauge transformation

$$\Omega(\theta, \phi) = \begin{pmatrix} e^{i\phi}\cos\frac{\theta}{2} & \sin\frac{\theta}{2} \\ -\sin\frac{\theta}{2} & e^{-i\phi}\cos\frac{\theta}{2} \end{pmatrix}, \tag{2.10}$$

diagonalizes the field $\phi(x)$. In other words,

$$\Omega(x)\phi(x)\Omega^\dagger(x) = \frac{r}{2}\begin{pmatrix} 1 & 0 \\ 0 & -1 \end{pmatrix} = rT^3. \tag{2.11}$$

We next check how the gluon field looks like in this gauge

$$A_\mu \equiv A_\mu^a T^a \to \Omega \left(A_\mu + \frac{1}{ie} \partial_\mu \right) \Omega^\dagger, \tag{2.12}$$

where e is the coupling constant. To check how the spatial components of the gauge field transform, we first have to compute

$$\Omega \boldsymbol{\nabla} \Omega^\dagger = \hat{\boldsymbol{r}} \left(\Omega \frac{\partial}{\partial r} \Omega^\dagger \right) + \hat{\boldsymbol{\theta}} \left(\Omega \frac{1}{r} \frac{\partial}{\partial \theta} \Omega^\dagger \right) + \hat{\boldsymbol{\phi}} \left(\Omega \frac{1}{r \sin\theta} \frac{\partial}{\partial \phi} \Omega^\dagger \right). \tag{2.13}$$

From the explicit expression of the transformation matrix (2.10), we get

$$\Omega \frac{\partial}{\partial r} \Omega^\dagger = 0, \tag{2.14}$$

$$\Omega \frac{\partial}{\partial \theta} \Omega^\dagger = -ie^{i\phi} T^2, \tag{2.15}$$

$$\Omega \frac{\partial}{\partial \phi} \Omega^\dagger = -i(1+\cos\theta) T^3 + i \sin\theta \cos\phi T^1 - i \sin\theta \sin\phi T^2. \tag{2.16}$$

Finally,

$$\frac{1}{ie} \Omega \boldsymbol{\nabla} \Omega^\dagger = \frac{1}{e} \left(-\hat{\boldsymbol{\theta}} \frac{1}{r} e^{i\phi} T^2 - \hat{\boldsymbol{\phi}} \frac{1+\cos\theta}{r \sin\theta} T^3 + \hat{\boldsymbol{\phi}} \frac{1}{r} (\cos\phi T^1 - \sin\phi T^2) \right). \tag{2.17}$$

We can write the result in the following form

$$\boldsymbol{A} = \boldsymbol{A}^a T^a = \boldsymbol{A}_R^a T^a - \frac{1}{e} \hat{\boldsymbol{\phi}} \frac{1+\cos\theta}{r \sin\theta} T^3, \tag{2.18}$$

where $\boldsymbol{A}_R$ is the *regular* part of the gauge field, whereas the second term is singular as $\theta \to 0$ and has the form of the potential of a magnetic monopole (see Appendix B). Comparing this result to the expression for the potential of a magnetic monopole, we get the magnetic charge

$$g = -\frac{1}{e}. \tag{2.19}$$

The Dirac quantization condition $2eg = n$, where n is an integer, is fulfilled. We have thus shown that at the points where the Abelian gauge is ill defined (or singular), the diagonal (Abelian) part of the gauge field behaves as if at those points there are magnetic monopoles with magnetic charge $g = -\frac{1}{e}$. It can be shown that the theory contains an Abelian gauge field and massive scalars. In the case of $SU(N)$, this procedure leads to a theory with $U(1)^{N-1}$ symmetry and charged massive scalars that contain two types of charges (from two different $U(1)$ sectors) [22, 23]. Magnetic monopoles also appear at points where the gauge field is singular. It is shown that indeed in this gauge, magnetic monopoles exist and if they condense, confinement can be viewed as appearing due to the dual Meissner effect.

2.2 Abrikosov-Nielsen-Olesen (ANO) Vortex

Let us now see how the vortex is formed by considering an Abelian-Higgs model. The vacuum expectation value of the Higgs boson plays the role of the order parameter, which in the case of the ordinary superconductor is the condensate of Cooper pairs and in the dual superconductor picture is the condensate of magentic monopoles. It is well known that this theory contains vortex solutions, which were first found by Abrikosov [24] for the case of superconductivity and later were generalized to the relativistic case by Nielsen and Olesen [25]. We consider the Lagrangian in $2+1$ dimensions

$$\mathcal{L} = -\frac{1}{4}F_{\mu\nu}F^{\mu\nu} + \frac{1}{2}\left(D_\mu\phi\right)^\dagger\left(D^\mu\phi\right) - \frac{\lambda}{4}\left(|\phi|^2 - \frac{\mu^2}{\lambda}\right)^2, \tag{2.20}$$

where ϕ is a complex scalar field, $D_\mu = \partial_\mu\phi + ieA_\mu\phi$ and e is the $U(1)$ coupling constant. It is clear that the scalar field acquires a vacuum expectation value

$$\langle\phi\rangle = \sqrt{\frac{\mu^2}{\lambda}} = v, \tag{2.21}$$

and the $U(1)$ symmetry is spontaneously broken. The Higgs field $\phi(x)$ and the gauge field acquire masses $m_\phi = \sqrt{2\lambda}v$ and $m_A = ev$ respectively. The

Lagrangian is invariant under the gauge transformations

$$\begin{aligned} \phi(x) &\rightarrow e^{ie\Lambda(x)}\phi(x) \\ A_\mu(x) &\rightarrow A_\mu(x) - \partial_\mu\Lambda(x). \end{aligned} \tag{2.22}$$

We can define, for any smooth configuration of ϕ, the winding number

$$N[C] = \frac{1}{2\pi}\oint_C d\boldsymbol{x}\cdot\boldsymbol{\nabla}(\arg\phi), \tag{2.23}$$

where C is the circle at $|\boldsymbol{x}| = \infty$. If ϕ is nonzero everywhere on the circle C, then this quantity is well defined and measures the total rotation of the phase of ϕ. It follows from the definition (2.23) that this quantity is an integer. It is easy to see that for $\Lambda(x)$ single-valued everywhere, the winding number is gauge invariant. If we take the gauge field at large distances to be pure gauge (this means that the field strength vanishes)

$$\boldsymbol{A}(x) = \frac{1}{e}\boldsymbol{\nabla}\alpha(x), \tag{2.24}$$

the winding number is given by

$$N[C] = n = \frac{1}{2\pi}\oint_C d\boldsymbol{x}\cdot\boldsymbol{\nabla}\alpha = \frac{e}{2\pi}\oint_C d\boldsymbol{x}\cdot\boldsymbol{A} = \frac{e}{2\pi}\int d^2xB = \frac{e}{2\pi}\Phi, \tag{2.25}$$

where $B = -F_{12}$ is the magnetic field in the z direction and we have used Stokes' theorem to get the fourth equality. The last surface integral, is over the area bounded by the curve C. This tells us that the flux is quantized

$$\Phi = \frac{2\pi n}{e}. \tag{2.26}$$

We will look for static solutions and set $A_0 = 0$. Assuming the most general rotationally symmetric solution and requiring that the solution is invariant under reflection about the x-axis (the scalar field gets complex conjugated),

we adopt the following ansatz

$$\begin{aligned} \phi(\boldsymbol{x}) &= v e^{i\theta} f(evr) \\ A_j(\boldsymbol{x}) &= \epsilon_{jk}\hat{x}^k \frac{a(evr)}{er}, \end{aligned} \tag{2.27}$$

with functions f and a real. This solution has winding $n = 1$. It can be checked that the solution (2.27) has finite energy and it scales like

$$E = v^2 F\left(\frac{\lambda}{e^2}\right) = \frac{m_\phi^2}{2\lambda} F\left(\frac{\lambda}{e^2}\right), \tag{2.28}$$

where the function F is of the order of unity. The equations of motion, in terms of f and a are

$$\begin{aligned} a'' - \frac{1}{u}a' + (1-a)f^2 &= 0, \\ f'' + \frac{1}{u}f' - \frac{(1-a)^2}{u^2}f + \frac{\lambda}{e^2}(1-f^2)f &= 0, \end{aligned} \tag{2.29}$$

where $u = evr$ and the primes denote derivatives with respect to u. The requirement that the solution is regular at the origin gives the condition

$$f(0) = a(0) = 0, \tag{2.30}$$

whereas requiring finite energy solution gives us

$$f(\infty) = a(\infty) = 1. \tag{2.31}$$

Having set the boundary conditions, the equations can be solved numerically. We show the solutions for $\lambda/e^2 = 1/2$ in Fig. 2.1, which was taken from [26]. We see that the magnetic field is localized around the core and falls exponentially away from it. In the dual picture, the magnetic field is replaced by the electric field and between electric charges an electric flux tube is formed.

Let us mention some facts about the multi vortex solution, or $n > 1$. In this case, we cannot argue that the minimal energy configuration necessarily gives a

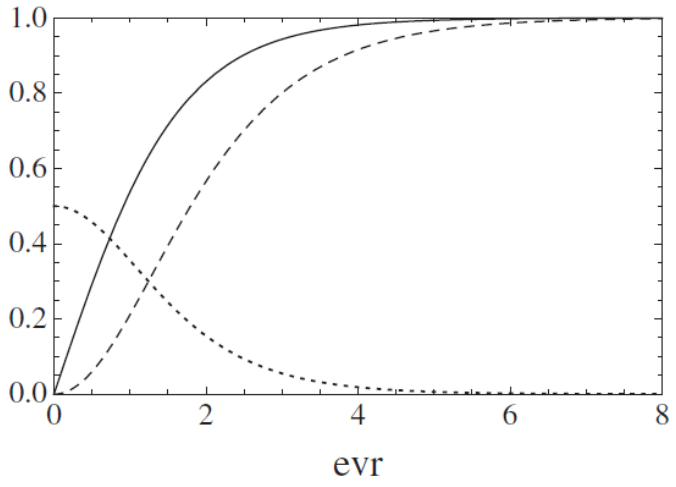

Figure 2.1: Numerical solutions of equations (2.29). Solid line is f, dashed line is a and e times the magnetic field B is the dotted line.

static solution. In other words, this means that not all zeros of ϕ are located at the origin. Qualitatively, in order to see if the n vortex solution dissociates into n unit vortices, we should consider the interaction between two well separated vortices. There are two types of interactions, the electromagnetic and the scalar. The sign of the force depends on which of these interactions dominates. The electromagnetic force is repulsive, whereas the scalar force is attractive. Both forces fall off exponentially at large distance, therefore the dominating force is the one falling off more slowly. We have an attractive force for $m_\phi < m_A$, and repulsive if $m_\phi > m_A$ [26]. In the superconductor phenomenology, the first case corresponds to Type I superconductor, whereas the second to Type II.

We now add fermions to a $3+1$ dimensional Abelian-Higgs model and see what are the consequences. We assume that the vortex is situated along the z-axis. The fermions are given by four component spinors ψ, satisfying

$$\gamma^5 \psi_R = \psi_R, \tag{2.32}$$

$$\gamma^5 \psi_L = -\psi_L, \tag{2.33}$$

where $\gamma^5 = i\gamma^0\gamma^1\gamma^2\gamma^3$ and $\psi_{L,R} = \frac{1}{2}(1 \mp \gamma^5)\psi$. We introduce the fermions to

the theory by adding

$$\mathcal{L}_f = i\bar{\psi}_R\gamma^\mu D_\mu\psi_R + i\bar{\psi}_R\gamma^\mu D_\mu\psi_R - g\phi\bar{\psi}_L\psi_R - g\phi^*\bar{\psi}_R\psi_L, \tag{2.34}$$

to Lagrangian (2.20). g is real and is the fermion-scalar coupling constant and $D_\mu\psi = (\partial_\mu + iqA_\mu)\,\psi$. The gauge symmetry requires that $e = 2q$, where e is the charge of ϕ. The Lagrangian has the symmetry

$$\psi \to e^{i\beta\gamma^5}\psi,\ \ \phi \to e^{-2i\beta}\phi, \tag{2.35}$$

and doesn't have a bare (independent of ϕ) mass term. The Dirac equation can be written as

$$\begin{aligned} i\gamma^\mu D_\mu\psi_L - g\phi\psi_R &= 0, \\ i\gamma^\mu D_\mu\psi_R - g\phi^*\psi_L &= 0. \end{aligned} \tag{2.36}$$

We look for solutions $\psi^{(0)}_{L,R}$, which depend only on the transverse radial direction $r = \sqrt{(x^1)^2 + (x^2)^2}$. We also assume that

$$\begin{aligned} i\gamma^1\gamma^2\psi^{(0)}_L &= \psi^{(0)}_L, \\ i\gamma^1\gamma^2\psi^{(0)}_R &= -\psi^{(0)}_R \end{aligned} \tag{2.37}$$

Let us consider the first of equations (2.36). We can write it as

$$i\left(\gamma^1 D_1 + \gamma^2 D_2\right)\psi^{(0)}_L - g\phi\psi^{(0)}_R = 0. \tag{2.38}$$

We multiply both sides by γ^1 and recall that $(\gamma^1)^2 = -1$. We get

$$\left(D_1 - \gamma^1\gamma^2 D_2\right)\psi^{(0)}_L - ig\phi\gamma^1\psi^{(0)}_R = 0. \tag{2.39}$$

We use the property (2.37), relations (2.27) and

$$D_1 \pm iD_2 = e^{\pm i\theta}\left[\partial_r \pm \frac{i}{r}\partial_\theta \pm \frac{a(r)}{2r}\right], \tag{2.40}$$

to get

$$\left[\partial_r + \frac{a(r)}{2r}\right] \psi_L^{(0)} - igvf(r)\gamma^1 \psi_R^{(0)} = 0. \tag{2.41}$$

Similarly, for the second of equations (2.36), we have

$$\left[\partial_r + \frac{a(r)}{2r}\right] \psi_R^{(0)} - igvf(r)\gamma^1 \psi_L^{(0)} = 0. \tag{2.42}$$

Note that the sign before $a(r)$ is the same in both equations, despite the fact that there is a sign difference in relations (2.27). This is due to the fact that ψ_L and ψ_R have opposite charges. The solution of equations (2.41) and (2.42) is given by

$$\psi_L^{(0)} = C \exp\left\{-\int_0^r dr' \left[gvf(r') + \frac{a(r')}{2r'}\right]\right\} \chi \tag{2.43}$$

and

$$\psi_R^{(0)} = -i\gamma^1 \psi_L^{(0)}. \tag{2.44}$$

χ is a constant, left-handed spinor, which satisfies

$$i\gamma^1\gamma^2\chi = \chi. \tag{2.45}$$

We assume that the general solution has the form

$$\begin{aligned} \psi_L &= b(t,z)\psi_L^{(0)}(r), \\ \psi_R &= b(t,z)\psi_R^{(0)}(r), \end{aligned} \tag{2.46}$$

where $b(t,z)$ is an arbitrary function of coordinates t and z. The Dirac equation above gives

$$(\gamma^0\partial_0 + \gamma^3\partial_3) b(t,z)\chi = 0. \tag{2.47}$$

From the definition of γ^5 in $3+1$ dimensions, and multiplying the equation above by $\gamma^0\gamma^3$, we notice that the spinor χ satisfies

$$\gamma^0\chi = -\gamma^3\chi. \tag{2.48}$$

The solution of equation (2.47) is given by an arbitrary function of $t-z$. The

modes with definite energy have $b = e^{-i\omega(t-z)}$. The case $\omega > 0$ corresponds to a "right-moving" particle with energy $E = \omega$ that moves with the speed of light along the vortex core (in the z-direction), whereas $\omega < 0$ corresponds to an antiparticle with energy $E = |\omega|$. Since the particles move with the speed of light, they must be massless. As we move away from the core, into the transverse plane, the fermionic field falls off exponentially. We see that along the vortex core we have an effective theory in $1 + 1$ dimensions, where massless fermions are coupled to a gauge field. In the case of an Abelian gauge theory, as the one considered here, the effective theory will be QED in $1 + 1$ dimensions (QED_2). Below, we review some facts about this theory.

2.3 The Schwinger model

We saw above that confinement can be understood in terms of the "dual Meissner" effect. This means that due to condensation of magnetic monopoles, the vacuum can be considered as a superconductor, where compared to the usual superconductor, the roles of the electric and magnetic fields are reversed. Confinement happens as a result of monopole currents which expel the electric field from the superconductor, and due to the conservation of flux, the field between electric charges is stretched along a thin tube. In the following, we assume that the dynamics of fermions along these tubes is described in terms of massless QED_2.

QED_2 (the Schwinger model) has been used a long time ago [27–29] as an effective theory capable to model the transformation of partons into hadrons at high energies [30] (see also [31, 32]). The high energy justifies the dimensional reduction to $(1 + 1)$ dimensions even further, and the Schwinger model with massless fermions shares many key properties with QCD, including: i) the Higgs phenomenon (local electric charge conservation is spontaneously broken); ii) the spontaneous breaking of global chiral symmetry; iii) the screening of color charge (similar to the scenario of confinement for QCD with light quarks proposed by Gribov [33], see [34] for a review); iv) axial anomaly and the θ-vacuum. The main advantage of the Schwinger model with massless fermions (quarks) is that it is exactly soluble and can be used to investigate

e.g. the role of LPM effect at strong coupling. Of course, for our purposes we have to generalize it to allow for the rotation of quarks in color space (see Chapter 4) as they traverse the quark-gluon plasma (recently the effects of the color flow were addressed in [35]).

The dynamics of QED_2 is described by the action

$$S = \int d^2x \mathcal{L} \tag{2.49}$$

where the Lagrangian is given by

$$\mathcal{L} = -\frac{1}{4} F_{\mu\nu} F^{\mu\nu} + \bar{\psi} i \not{D} \psi \tag{2.50}$$

where, $\not{D} \equiv \gamma^\mu D_\mu$, $F_{\mu\nu} = \partial_\mu A_\nu - \partial_\nu A_\mu$ and $D_\mu = \partial_\mu + igA_\mu$[1]. This Lagrangian is invariant under gauge transformations

$$\psi \to e^{i\alpha(x)}\psi, \quad A_\mu \to A_\mu - \frac{1}{g}\partial_\mu \alpha(x). \tag{2.51}$$

The fields have the following mass dimensions

$$[A] = 0, \quad [\psi] = \frac{1}{2}, \tag{2.52}$$

which means that the coupling constant

$$[g] = 1. \tag{2.53}$$

There are two classically conserved currents, the vector current

$$j^\mu(x) = \bar{\psi}(x)\gamma^\mu\psi(x), \tag{2.54}$$

and the axial current

$$j_5^\mu = \bar{\psi}(x)\gamma^\mu\gamma^5\psi(x). \tag{2.55}$$

[1]The index $\mu = 0, 1$; A_μ is the gauge field and g is the coupling constant. Other conventions are given in Appendix A

Their conserved charges are

$$Q = \int dx j^0(x), \quad Q_5 = \int dx j_5^0(x). \tag{2.56}$$

After including the quantum corrections, if we want to preserve gauge invariance, then the axial current becomes anomalous. We will derive the axial anomaly in an intuitive way in the next section.

2.3.1 The anomaly and Dirac sea - spectral flow

In $1+1$ dimensions it is very easy to see that the anomaly can be understood in terms of the Dirac sea (see for example [36–39]). Let's assume a compact spatial extension, namely $x \in [-L/2, L/2]$. We impose the following boundary conditions

$$\begin{aligned} A_\mu\left(t, x = -\frac{L}{2}\right) &= A_\mu\left(t, x = \frac{L}{2}\right) \\ \psi\left(t, x = -\frac{L}{2}\right) &= -\psi\left(t, x = \frac{L}{2}\right). \end{aligned} \tag{2.57}$$

By choosing an appropriate gauge, it is always possible to to remove x dependence for A_1, so $A_1 = A_1(t)$. We will assume that $A_1(t)$ is an external field, which changes adiabatically with time. We also assume that the Coulomb potential $A_0 = 0$, which is a reasonable approximation in the limit $gL << 1$ [38]. We still have some gauge freedom left. It is easy to see, by looking at the gauge transformation of fermions, that we are still left with

$$A_1 \to A_1 + \frac{2\pi n}{gL}, \tag{2.58}$$

where $n = 0, \pm 1, \ldots$. This means that the configuration space for the gauge field is a circle with length $\frac{2\pi}{gL}$. From the Lagrangian (2.50), we get the equation of motion

$$(i\partial\!\!\!/ - gA\!\!\!/)\psi = 0. \tag{2.59}$$

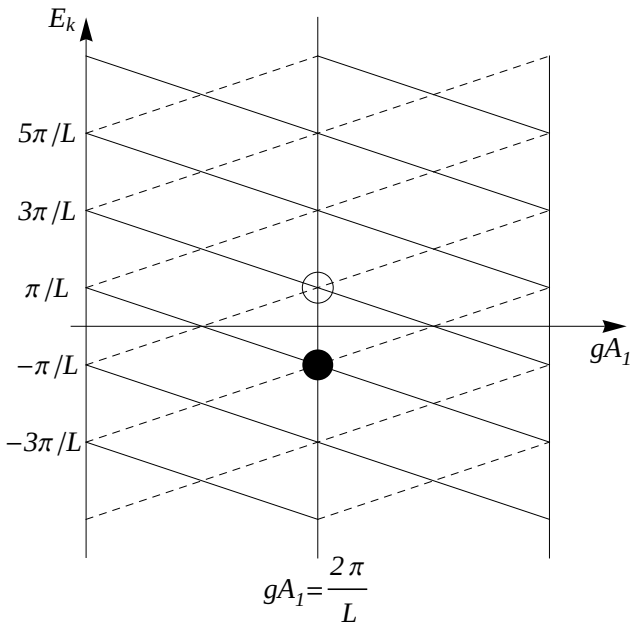

Figure 2.2: Level crossing in background electric field.

Using the conventions in Appendix A, we can write

$$\left[i\frac{\partial}{\partial t}+\sigma_3\left(i\frac{\partial}{\partial x}-gA_1\right)\right]\psi=0. \tag{2.60}$$

The general solution to the equation (2.60), taking into account boundary conditions (2.57), can be written as (we omit an overall constant)

$$\psi(t,x)\sim\frac{1}{\sqrt{L}}\sum_k u(k)\exp(-iE_kt)\exp\left(i\frac{2\pi}{L}\left(k+\frac{1}{2}\right)\right)x. \tag{2.61}$$

where E_k is the energy of the kth mode. By plugging in the solution (2.61) to (2.60), we get the following energy spectra for left and right handed fermions

$$\begin{aligned}E_k^L&=\frac{2\pi}{L}\left(k+\frac{1}{2}\right)+gA_1\\ E_k^R&=-\frac{2\pi}{L}\left(k+\frac{1}{2}\right)-gA_1\end{aligned} \tag{2.62}$$

We illustrate this in Fig 2.2. In this figure, the dashed and solid lines show the

levels for left and right components respectively. In the usual way, we fill up all negative energy levels and leave empty all positive ones, so at $A_1 = 0$ we have the vacuum state. As we change $gA_1 = 0$ to $gA_1 = \frac{2\pi}{L}$ (see for example the case when $k = 0$), the levels L-levels move up, whereas the R-levels move down, in such a way that we arrive at the same ground state. This illustrates the above mentioned fact that the gauge field is compact. In process though, since the levels have shifted, we have created an L-particle (white circle) and an R-hole (black circle). The total electric charge is conserved, because the particle and the hole have opposite charge. On the other hand, the axial charge is just the difference between left and right handed fermions, namely

$$Q_5 = N_L - N_R. \tag{2.63}$$

In our conventions, a left-handed fermion has axial charge +1, whereas a right-handed antifermion has also axial charge +1. The total change in the axial charge is then

$$\Delta Q_5 = 2. \tag{2.64}$$

If we write

$$\Delta Q_5 = \frac{L}{\pi} g \Delta A_1 \tag{2.65}$$

and divide both sides by Δt, we get

$$\dot{Q}_5 = \frac{L}{\pi} g \dot{A}_1. \tag{2.66}$$

Using (2.56)

$$\partial_0 \int_0^L dx j_5^0 = \frac{g}{\pi} \partial_0 \int_0^L dx A_1. \tag{2.67}$$

This gives

$$\partial_0 j_5^0 = \frac{g}{\pi} \partial_0 A_1. \tag{2.68}$$

If we write the last equation in a Lorentz covariant way, we get

$$\partial_\mu j_5^\mu = \frac{g}{2\pi} \epsilon^{\mu\nu} F_{\mu\nu}, \tag{2.69}$$

which is the well known anomaly in $1+1$ dimensions. The anomaly can also be derived by considering the behavior at some ultra violet (UV) cutoff, as is the case in the perturbative treatment. When working with the Dirac sea, since the total energy and charge of the vacuum (we have infinitely many filled states) are ill-defined, one has to regularize the currents. The most often used procedure is the point splitting method of Schwinger, which preserves the gauge invariance. This method leads to the same result for the anomaly (see references given in the beginning of the section).

To summarize, we have considered the Dirac sea and we have switched on, adiabatically, an external gauge field. As a result, the energy levels in the infinite sea shift; L-levels move up in energy and R-levels move down - spectral flow. This difference in energy levels gives the index of the Dirac operator. The total electric charge is conserved, but the axial charge changes by ± 2 (depending on the sign of the gauge potential). By considering the UV behavior of the theory, we arrive at the same result. We haven't used any perturbative calculation and we see that that the anomaly is a purely topological effect.

2.3.2 Bosonization

In one spatial dimension, the fermionic degrees of freedom can be expressed in terms of bosonic ones in an exact way. This correspondence is usually expressed as a duality between fermionic bilinears and a real scalar field. This procedure is known as *bosonization*. In the $U(1)$ case the correspondence is given by the following relations [40, 41]

$$\begin{aligned} \bar{\psi}(x) i\gamma^\mu \partial_\mu \psi(x) &\rightarrow \frac{1}{2}\partial_\mu \phi(x) \partial^\mu \phi(x) \\ \bar{\psi}(x)\gamma^\mu \psi(x) &\rightarrow -\frac{1}{\sqrt{\pi}} \epsilon^{\mu\nu}\partial_\nu \phi(x) \\ \bar{\psi}(x)\psi(x) &\rightarrow -c\frac{g}{\sqrt{\pi}} \cos(2\sqrt{\pi}\phi(x)) \end{aligned} \tag{2.70}$$

where $c = \frac{e^\gamma}{2\pi}$ and γ is the Euler constant. This is known as the Abelian bosonization. Note that the scalar field has mass dimension $[\phi] = 0$. We

now show, using bosonization, that the Schwinger model is dual to a free scalar theory. Let us start from the Lagrangian (2.50) and substitute the bosonization relations

$$\mathcal{L} = -\frac{1}{4}F_{\mu\nu}F^{\mu\nu} + \frac{1}{2}\partial_\mu\phi\partial^\mu\phi + \frac{g}{\sqrt{\pi}}\epsilon^{\mu\nu}\partial_\nu\phi A_\mu - j^\mu_{ext}A_\mu, \tag{2.71}$$

where we have introduced an external current j^μ_{ext}. Let's assume that we can parametrize this current as

$$j^\mu_{ext}(x) = -\frac{1}{\sqrt{\pi}}\epsilon^{\mu\nu}\partial_\nu\phi_{ext}(x). \tag{2.72}$$

We substitute this into the previous Lagrangian. We also note that the gauge field has only one component F_{01} and $\epsilon^{\mu\nu}\partial_\mu A_\nu = F_{01}$. Using these facts and after integration by parts, we get

$$\mathcal{L} = \frac{1}{2}F_{01}^2 + \frac{1}{2}\partial_\mu\phi\partial^\mu\phi + \frac{g}{\sqrt{\pi}}(\phi + \phi_{ext})F_{01}. \tag{2.73}$$

The field F_{01} is non-propagating, therefore we can eliminate it by substituting its equation of motion into the Lagrangian above. This gives

$$\mathcal{L} = \frac{1}{2}\partial_\mu\phi\partial^\mu\phi - \frac{1}{2}\left(\frac{g}{\sqrt{\pi}}\right)^2(\phi + \phi_{ext})^2. \tag{2.74}$$

The result (2.74) is quite surprising. We have started with an interacting theory and we ended up with a free theory instead (for $\phi_{ext} = 0$). The effective theory we got is just Klein-Gordon coupled to a classical source. We should emphasize that this Lagrangian, even though classical, captures all quantum effects of the fermionic theory from which we started with. As an illustration, let's assume that $\phi_{ext} = 0$. The equation of motion for the scalar then is just the Klein-Gordon equation

$$(\Box + m^2)\phi = 0. \tag{2.75}$$

where $m = \frac{g}{\sqrt{\pi}}$. On the other hand, from Maxwell's equations and using bosonization relations, we get

$$\partial_1 F^{10} = g j^0 = -\frac{g}{\sqrt{\pi}} \partial_1 \phi. \tag{2.76}$$

Assuming that fields vanish at spatial infinity, we have

$$F_{01} = -\frac{g}{\sqrt{\pi}} \phi. \tag{2.77}$$

In $1+1$ dimensions, the following relation between the gamma matrices holds

$$\gamma^\mu \gamma^5 = -\epsilon^{\mu\nu} \gamma_\nu. \tag{2.78}$$

Using this and bosonization relations, we can write for the axial current

$$j_5^\mu = \frac{1}{\sqrt{\pi}} \partial^\mu \phi. \tag{2.79}$$

Combining (2.79) with (2.77) and using the equation of motion for ϕ, we derive again the anomaly

$$\partial_\mu j_5^\mu = \frac{g}{2\pi} \epsilon^{\mu\nu} F_{\mu\nu}. \tag{2.80}$$

The duality between the Schwinger model and the free Klein-Gordon theory, illustrates that the former is exactly soluble. We show below that the Schwinger model shares with QCD many important properties, which are crucial for the treatment of the dynamics of fermions along the QCD string which will be the topic of the later chapters.

2.3.3 The θ-vacuum

We consider the case of a constant background electric field F [42]. The solution to Maxwell's equations, in the gauge $A_1 = 0$, is

$$F_{01} = g \partial^{-1} j^0 + F. \tag{2.81}$$

In three spatial dimensions we usually do not assume such a field, because it is always energetically favorable to produce pairs of charged particles which will screen it. In one spatial dimension the situation is different. Let's now put a pair of oppositely charged particles a distance L from each other, as shown in Fig. 2.3, and look at the energy difference

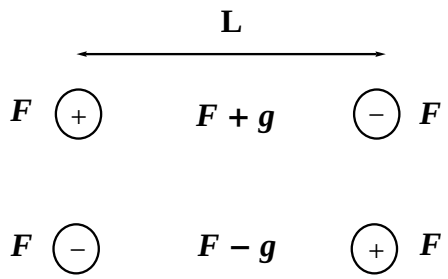

Figure 2.3: Field configuration after a pair production.

$$\Delta E = \frac{1}{2}\int dx\ [F_{01}^2 - F^2] = \frac{1}{2}L\ [(F \pm g)^2 - F^2]. \tag{2.82}$$

It is clear that it is energetically favorable to produce pairs if $|F| > \frac{1}{2}g$, until the field is reduced to $|F| < \frac{1}{2}g$. The physics is periodic, with period g. This can be illustrated if we plot the energy as a function of F, as shown in Fig. 2.4.

As F increases, at the point where $|F| = \frac{1}{2}g$, a pair is created and therefore instead of the energy increasing further, it continues into another branch and so on. This is similar to tunneling into another vacuum, with a different topological number. We introduce the parameter

$$\theta = \frac{2\pi F}{g}, \tag{2.83}$$

to parametrize the vacuum structure, and it plays a similar role to the θ-vacuum in QCD. Let us use the bosonized version of the theory to make this more clear. In A.4, it is shown that the axial charge is a generator of

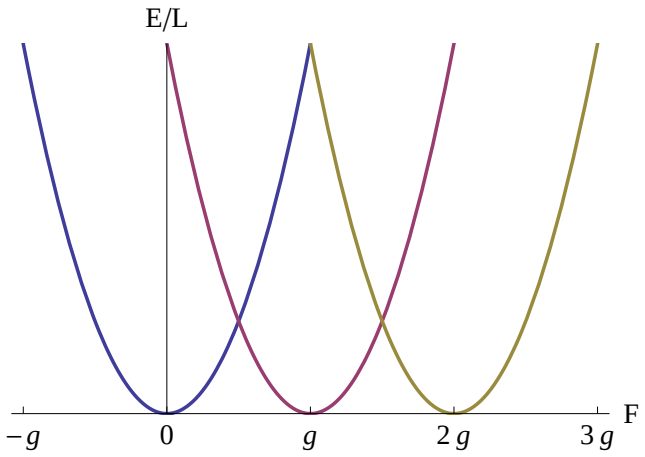

Figure 2.4: Ground state energy in units of length L.

translations in the bosonic field ϕ, introduced above

$$e^{i\alpha\sqrt{\pi}Q_5}\phi e^{-i\alpha\sqrt{\pi}Q_5} = \phi + \alpha \tag{2.84}$$

and due to the compactness of the the gauge group, the field ϕ was shown to be compact. We should make the identification

$$\phi \to \phi + n\sqrt{\pi}, \tag{2.85}$$

where n is an integer. Let us write the field ϕ as a sum of a massive scalar $\hat{\phi}$, where $\hat{\phi} \in [0, \sqrt{\pi}]$, and a constant electric field θ. The axial charge operator acts on these fields in the following way

$$\begin{aligned} e^{i\alpha\sqrt{\pi}Q_5}\hat{\phi}e^{-i\alpha\sqrt{\pi}Q_5} &= \hat{\phi} \\ e^{i\alpha\sqrt{\pi}Q_5}\theta e^{-i\alpha\sqrt{\pi}Q_5} &= \theta + \alpha. \end{aligned} \tag{2.86}$$

The states of the system can now be considered to be a direct product of the states of the field $\hat{\phi}$, which we denote by $|\Phi)$, and states $|n\}$, which are the eigenstates of operator $\frac{1}{2}Q_5$. We can define raising and lowering operators of states $|n\}$ as $a^{\pm} = \exp(\pm 2i\sqrt{\pi}\theta)$. They change the chirality of the system by

two units

$$a^{\pm}\left|n\right\} = \left|n \pm 1\right\}. \tag{2.87}$$

The eigenstates of the raising and lowering operators can be written in a similar way as for the harmonic oscillator, namely

$$\left|\theta_0\right\} = \frac{1}{\pi^{1/4}} \sum_n e^{-2i\sqrt{\pi}n\theta_0} \left|n\right\}. \tag{2.88}$$

The state (2.88) can be thought of as corresponding to the case of a constant electric field $\frac{g\theta_0}{\sqrt{\pi}}$. We should now look at the vacuum state of the theory. We could choose $\left|0\right\rangle = \left|0\right)\left|0\right\}$, but there could be processes which change the chirality of the system (as we will see later), therefore this is not a good candidate. This means that we cannot choose any particular $\left|n\right\}$ state. As we saw above, the θ-vacuua are eigenstates of chirality changing processes, therefore the correct choice of the vacuum state would be $\left|0\right\rangle = \left|0\right)\left|\theta_0\right\}$, with θ_0 defined in (2.88).

2.3.4 String tension and chiral symmetry breaking

Another feature of QCD is the chiral symmetry breaking introduced in the previous chapter. As the massless quarks move in the QCD vacuum, they dynamically obtain mass. This leads to the vacuum having a nonzero condensate $\langle\bar{q}q\rangle$. In order to compute this condensate, we first consider the massive Schwinger model and then we put the mass to zero at the end [43]. Similarly as in the previous section we consider a constant background electric field F. We can imagine that the field is created between a charge and an anticharge separated by a distance $2L$. We define $\theta = \frac{2\pi F}{g}$. The Hamiltonian of the massive Schwinger model, using bosonization relations, can now be written as [42]

$$H = \int dx \left[\frac{1}{2}(\dot{\phi})^2 + \frac{1}{2}(\partial_1\phi)^2 + \frac{1}{2}m^2\phi^2 - cmM\cos\left(2\sqrt{\pi}\phi - \theta\right)\right]. \tag{2.89}$$

The string tension is defined as the increase in vacuum energy per unit length due to external sources (or external field). If we denote the vacuum energy in

the presence of sources and without the sources as $E_0(\theta)$ and $E_0(0)$ respectively, the string tension, to lowest order in M, is given by

$$\sigma = \frac{E_0(\theta) - E_0(0)}{2L} = cMm(1 - \cos\theta). \tag{2.90}$$

The tension is nonzero for external fields being non-integer multiples of g. This leads to permanent confinement of charges. We will discuss confinement and screening in the next section. The chiral condensate can be computed by using the Feynman-Hellman theorem and Hamiltonian (2.89)

$$\langle\bar{\psi}\psi\rangle_0 = \frac{\partial}{\partial M} E_0(\theta)\Big|_{m=0} = -c\cos\theta. \tag{2.91}$$

where the constant c depends on the Euler number γ and was defined in (2.70). We see that the vacuum of the Schwinger model breaks chiral symmetry in analogy with QCD. We will use (2.91) in Chapter 6 to investigate the modification of the chiral condensate in the presence of the QCD string.

2.3.5 Confinement and screening

We already saw in the previous section that if we give mass to fermions the theory becomes confining. On the other hand, if the theory possesses light fermions, they lead to the screening of the charge. In the following we will derive the potential between two static quarks to illustrate these phenomena. Let us start from the bosonized Lagrangian (2.73) with a mass term and an external current j_{ext}, which in this case will be the current of static charges separated by a distance L. In the gauge $A_1 = 0$, the Lagrangian is given by

$$\begin{aligned} \mathcal{L} &= \frac{1}{2}(\partial_1 A_0)^2 + \frac{1}{2}\partial_\mu\phi\partial^\mu\phi + \frac{g}{\sqrt{\pi}}(\phi + \phi_{ext})(-\partial_1 A_0) \\ &+ cmM\cos\left(2\sqrt{\pi}\phi\right). \end{aligned} \tag{2.92}$$

Let us consider a general case where the charges constituting the external current have a different charge from the dynamical fermions (external charges have charge $q_{ext}g$, where q_{ext} is a constant). The equations of motion from

(2.92) are

$$
\begin{aligned}
-\frac{1}{2}\partial_1^2 A_0 + \frac{g}{\sqrt{\pi}}(\partial_1\phi + \partial_1\phi_{ext}) = 0 \\
-\partial_1^2\phi + cmM2\sqrt{\pi}\sin(2\sqrt{\pi}\phi) + \frac{g}{\sqrt{\pi}}\partial_1 A_0 = 0.
\end{aligned}
\tag{2.93}
$$

It was argued in [44] that in the case when $q_{ext} << 1$,

$$
\sin(2\sqrt{\pi}\phi) \simeq 2\sqrt{\pi}\phi. \tag{2.94}
$$

Using the fact that ϕ is compact (see A.4), the approximation above is valid also for $q_{ext} \simeq n$, where n is an integer. From now on we take $n = 1$. Using the definition of ϕ_{ext}, after eliminating the bosonic field ϕ, we can compute the potential in momentum space

$$
\tilde{A}_0(k) = \frac{g\left(k^2 + 4\pi cmM\right)}{k^2\left(k^2 + \frac{g^2}{\pi} + 4\pi cmM\right)}\tilde{j}^0_{ext}(k). \tag{2.95}
$$

where

$$
\begin{aligned}
\tilde{A}_0(k) &= \int dx\ e^{-ikx}A_0(x), \\
\tilde{j}^0_{ext}(k) &= \int dx\ e^{-ikx}j^0_{ext}(x).
\end{aligned}
\tag{2.96}
$$

Note that the problem is time independent, therefore the integrals are over the spatial direction only. To compute the inverse Fourier transform we first define

$$
\begin{aligned}
m_1^2 &= 4\pi cmM, \\
m_2^2 &= 4\pi cmM + \frac{g^2}{\pi}.
\end{aligned}
\tag{2.97}
$$

The potential (2.95) can now be cast in the following form

$$
\tilde{A}_0(k) = g\left[\frac{m_1^2}{m_2^2}\frac{1}{k^2} + \left(1 - \frac{m_1^2}{m_2^2}\right)\frac{1}{k^2 + m_2^2}\right]\tilde{j}^0_{ext}(k). \tag{2.98}
$$

Recall that the charge density is that of a charge-anticharge separated by a distance L,

$$j^0_{ext}(x) = \delta\left(x - \frac{L}{2}\right) - \delta\left(x + \frac{L}{2}\right). \tag{2.99}$$

To compute the inverse Fourier transform of (2.98) we use another approximation, namely $cmM << g^2$. We now get

$$\begin{aligned} A_0(x) &= \frac{2\pi^2 cmM}{g}\left(\left|x - \frac{L}{2}\right| - \left|x + \frac{L}{2}\right|\right) \\ &- \frac{\sqrt{\pi}}{2}\left(e^{-\frac{g}{\sqrt{\pi}}\left|x-\frac{L}{2}\right|} - e^{-\frac{g}{\sqrt{\pi}}\left|x+\frac{L}{2}\right|}\right). \end{aligned} \tag{2.100}$$

Finally, the potential can be computed from

$$V = -g\frac{1}{2}\int dx\ A_0(x) j^0_{ext}(x). \tag{2.101}$$

Using (2.100), we get [28]

$$V(L) = 2\pi^2 cmML + \frac{g\sqrt{\pi}}{2}\left(1 - e^{-\frac{g}{\sqrt{\pi}}L}\right). \tag{2.102}$$

The first term is the linear confining term, which vanishes in the chiral limit $M \to 0$. The second term is the charge screening, which appears as a result of having light fermions in the theory. We have shown that indeed the Schwinger model, as QCD in $3+1$ dimensions, manifests the phenomenon of confinement and screening of charge. The result (2.102) will be useful later when we speak about soft photon production in real-time dynamics of jet fragmentation (see Chapter 5).

2.4 Discussion

In this section we have reviewed some facts about the Abelian projection of non-Abelian gauge theories and the mechanism by which magnetic monopoles appear in the theory. If these monopoles condense, then confinement can be understood to arise from the dual Meissner effect - (chromo-) electric charges

are connected by (chromo-) electric flux tubes. The effective theory describing these flux tubes (or vortices) is the Abelian-Higgs model. By introducing fermions to this theory, we see that zero modes are localized along the core of the string and move with the speed of light. From this argument and later by considering high energy jets, we assume that the dynamics of fermions along the string core (the flux tube stretched between charges) is governed by massless QED_2 or the Schwinger model. We have emphasized by concrete examples that this model shares with QCD many important features, such as confinement, charge screening, chiral symmetry breaking and θ-vacuum.

Chapter 3

Fragmentation functions of jets in vacuum

Jets are a collimated stream of hadrons produced after collisions of hadrons or leptons at high energies. We illustrate this in Fig. 3.1. The incoming particles move along the horizontal axis and after the collision two narrow cones of particles are produced back-to-back. The processes creating the jet

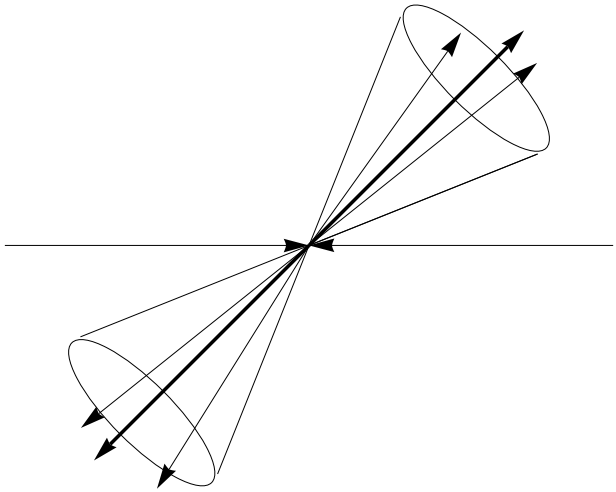

Figure 3.1: Di-jet event in high energy scattering.

involve high momentum transfers. Initially, a quark or a gluon with large virtuality is formed, which in turn radiates more quarks and gluons. These

in turn hadronize and become hadrons. The process of *hadronization* of jets is a nonperturbative phenomenon and cannot be studied within perturbation theory. In the previous chapter we introduced the Schwinger model and we saw that it shares with QCD many important properties. The theory is exactly soluble and we will use it to model the real-time dynamics of jet hadronization. Dimensional reduction is justified further by assuming very high energy jets. The model is assumed to describe the evolution of the jet at late stages, where perturbative emission has stopped. Before introducing the detais of the model we will review some basic facts about perturbative treatment of jets, which has proven to be very successful over the years. We will mostly follow [45].

3.1 Space-time picture of jet evolution

Let's consider the case of electron-positron annihilation to hadrons. In the perturbative QCD language, this corresponds to the process $e^+e^- \to \bar{q}q$. The question arises how is it possible to arrive to final color neutral state from the initial colored one. It is well established and we mentioned several times before that between color charges there stretches a chromoelectric flux tube, with a potential rising linearly with distance (this means that charges are confined). Now we have to answer the question of how this mechanism works in the case of fast moving quarks (nonadiabatic process). The main argument about the validity of perturbation theory is based on the fact that nonperturbative effects for very fast moving quarks happen in macroscopic time scales, therefore there is enough time for perturbative treatment. We will review the main arguments leading to this reasoning. Let's consider a classical charge moving along the z axis with velocity $v \approx 1$ after being accelerated for example from $v = 0$ at $t = 0$. At times $t >> 0$, the charge will be surrounded with a disc of contracted electromagnetic field. In the reference frame where the charge is at rest, the field at distance r' can only be observed at time $t' \geq r'$. In the laboratory frame, the field at distance r away from the z axis is observed much later due to time dilation

$$t = \gamma t' = \frac{E}{m} r. \tag{3.1}$$

where E is the energy of the particle in the lab frame and m is its mass. The distance r can be thought of as the distance between constituent quarks, which is a typical hardonic size we denote by R. If we consider the charge in question to be a quark, then we arrive at the conclusion that the quark will hadronize only after the time (3.1). For light quarks the mass and the distance are related

$$m \sim R^{-1}. \tag{3.2}$$

For heavy (Q) and light (q) quarks we then can estimate the *hadronization times*

$$\begin{aligned} t_q^{hadr} &\approx \frac{E}{m} R = ER^2 \\ t_Q^{hadr} &\approx \frac{E}{m_Q} R. \end{aligned} \tag{3.3}$$

Another important scale is the so-called *formation time* which we will define shortly. Let us consider gluon Bremsstrahlung radiation. The differential spectrum of gluons radiated off a quark is given by

$$dw = \frac{\alpha_s(k_\perp^2)}{4\pi} 2C_F \left[1 + \left(1 - \frac{k}{E}\right)^2\right] \frac{dk}{k} \frac{dk_\perp^2}{k_\perp^2}, \tag{3.4}$$

where E is the energy of the quark and k^μ is the 4-momentum of the gluon (see Fig. 3.2). The strong coupling constant α_s in this case runs with the transverse momentum $k_\perp$. From expression (3.4), we see that the probability

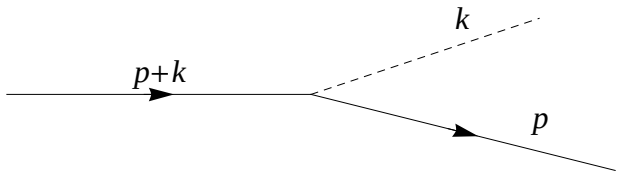

Figure 3.2: Gluon emission from a quark.

of having a multi-jet event, namely

$$k_\perp \sim k \sim E, \tag{3.5}$$

is very small, $w \sim \frac{\alpha_s}{\pi} << 1$. This means that the bulk of radiation doesn't lead to any additional visible jets, but instead will accompany the original quark (quasicollinear, soft)

$$k_\perp << k << E, \quad w \sim \frac{\alpha_s}{\pi} \log^2 E \sim 1. \tag{3.6}$$

The formation time is important in determining how offspring partons influence the final hadronic yield. From Fig. 3.2, using the uncertainty relation between energy and time, we can write the formation time of the gluon

$$t_g^{form} \sim \frac{E}{(p+k)^2} \approx \frac{E}{kE\theta^2} \approx \frac{k}{k_\perp^2}, \tag{3.7}$$

where θ is the angle between the incoming quark and the gluon. In order for the gluon to be emitted perturbatively, we need $t_g^{form} < t_g^{hadr} \approx kR^2$. This puts the following restriction

$$k_\perp > R^{-1}. \tag{3.8}$$

This restriction puts limits on what range of $k_\perp$ perturbation theory can be used. This bound can also be seen from the running of the coupling $\alpha_s(k_\perp)$, where for small transverse momenta, the coupling becomes too large for the perturbative approach to be valid. For very energetic processes, with a momentum transfer scale $\sqrt{Q^2}$, there is a large range where perturbation theory is valid, namely

$$R^{-1} << k_\perp \lesssim k \lesssim \sqrt{Q^2}. \tag{3.9}$$

The parameter that regulates the "lifetime" of the secondary parton is $(k_\perp R)$. Gluons satisfying $k_\perp R >> 1$ are within the perturbative regime and live for a long time, giving off more offspring partons.

As an offspring parton is radiated, one might expect that it is suppressed by a factor of α_s. As we saw above, the probability to emit a new soft parton is $w \sim \frac{\alpha_s}{\pi} \log^2 E \sim 1$. This means that all these emissions should be resumed. A way to do this is to use the Dokshitzer-Gribov-Lipatov-Altarelli-Parisi (DGLAP) equations. We will shortly review the basic idea: let's consider as a target a "dressed" parton of species A ($A = q, \bar{q}, g$), with transverse

size $1/k_0$, or virtuality $k^2 = k_0^2$ (in the case of jets the virtuality is time-like). We denote with $D_A^B(x, Q^2, k_0^2)$ the probability to find the parton of species B inside the cloud of the parton A, with momentum fraction x and transverse virtuality up to Q^2. In this expression it is assumed that we sum over color and polarizations of the field B and average those for the field A. Introducing the variable

$$\xi(Q^2) = \int_{\mu^2}^{Q^2} \frac{dk^2}{k^2} \frac{\alpha_s(k^2)}{4\pi}, \tag{3.10}$$

where μ^2 is an infrared cutoff, the evolution of D_A^B with respect to Q^2 can be written as

$$D_A^B(x, \xi) = \sum_C \int_0^\xi d\xi' \int_0^1 \frac{dz}{z} \Phi_A^C \left[D_C^B(x/z, \xi') - z^2 D_A^B(x, \xi') \right]. \tag{3.11}$$

where Φ_A^B are the splitting functions of parton A to parton B, defined by

$$dw^{A \to B+C} = \frac{dk_\perp^2}{k_\perp^2} \frac{\alpha_s(k_\perp^2)}{4\pi} dz \; \Phi_A^{BC}(z) \tag{3.12}$$

After the perturbative emission of partons stops, the color sources are connected to each other via the chromoelecric string. The string should break due to the presence of light fermions in the theory and the fragments turn into the observed hadrons. The energetic quarks pull from vacuum pairs of fermion-antifermion, which hadronize to give the final state hadrons. This will be the topic of the next section.

3.2 QCD string breaking and particle creation

We now consider particle creation when two color sources are connected by a flux tube or string and move in opposite direction. The dynamics along the string is described by the Schwinger model. The color sources will be introduced as external charges and the situation is illustrated in Fig. 3.3.

Pairs of charge-anticharge are produced dynamically as the sources recede. These pairs in turn form charge neutral bound states, which we interpret

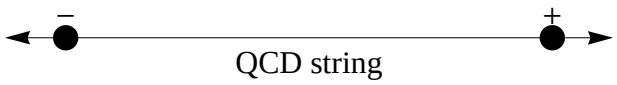

Figure 3.3: Quark and antiquark moving in opposite direction.

to be the final state hadrons. The bosonized form of the Schwinger model, introduced in the previous chapter, is assumed to describe the dynamics of these hadrons. From Lagrangian (2.74) we get the following equation of motion

$$(\Box + m^2)\phi(x) = -m^2\phi_{ext}(x), \tag{3.13}$$

which is just the equation of motion of a scalar field ϕ coupled to a classical source $-m^2\phi_{ext}$. As is well known, this situation leads to coherent particle creation and describes the real-time dynamics of the process. To illustrate the breaking of the string we first consider the external sources to move with the speed of light. The external charge density is given by

$$j^0_{\text{ext}}(x) = -\delta(z+t)\theta(-z) + \delta(z-t)\theta(z). \tag{3.14}$$

Assuming Lorentz invariance, the field ϕ can only depend on $\sqrt{t^2 - x^2}$. We can solve it either by using the Green's function (A.17) or by noting that the equation becomes an inhomogenous Bessel equation and we can solve it directly (see section A.3). We only quote the final answer

$$\phi(x) = \sqrt{\pi}\theta(t^2 - z^2)[1 - J_0(m\sqrt{t^2 - z^2})]. \tag{3.15}$$

The normalized result is plotted in Fig. 3.4 for fixed values of m and t. The interpretation of Fig. 3.4 is as follows. Since in $1+1$ dimensions the potential between charge and anti-charge at short distances is linear, initially we form a string. We can see that the string formed between receding particles breaks into the quark-antiquark pairs – indeed, as it follows from (2.70), the kinks and anti-kinks of the scalar field represent the charged fermions and anti-fermions respectively (see Fig. 3.5).

Recalling bosonization relations, we notice that the axial and vector cur-

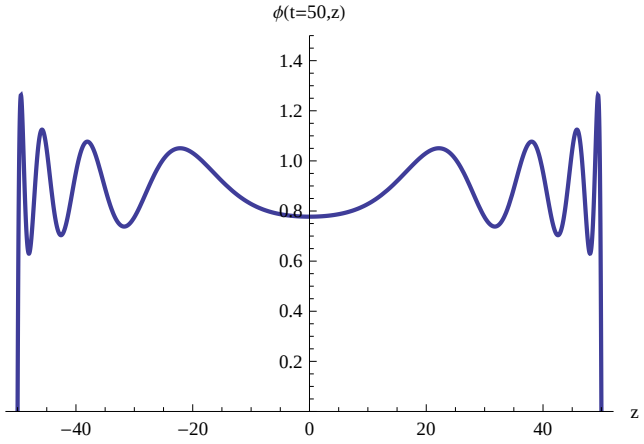

Figure 3.4: Scalar field ϕ as a function of the spatial coordinate z for $m = 0.6$ GeV and $t = 10$ fm.

Figure 3.5: String breaking by creation of pairs of charge-anticharge.

rents both depend on the scalar ϕ and are related. As the the string breaks, there's a dynamical generation of vector and axial currents, a fact we will use later when studying the production of soft photons from the dynamics of jet fragmentation. An interesting fact to notice is that particle production in this model is driven by the anomaly and it would be interesting to investigate if this phenomenon shows up in $3+1$ dimensions as well.

We would like to point out a crucial difference between string breaking in the Schwinger model, after including quantum effects, and the semi-classical picture of the Lund model. In the case of the Lund model, after the string breaks, the field between the produced particles vanishes. In the Schwinger model on the other hand, the induced electric field, in the process of string breaking, is given by (see (2.77))

$$E^{ind}(x) = -\frac{g}{\sqrt{\pi}}\phi(x). \tag{3.16}$$

We interpreted the produced particles to correspond to kinks and antikinks. It is clear that in this model the field doesn't vanish completely between the

produced pair. This changes the dynamics of the process and can lead to observable consequences.

In our treatment of the string breaking we have neglected the back-reaction to the source. This leads to energy non-conservation and the question should be asked of how large this effect is. A recent study of the massive Schwinger model on a lattice [46] addresses this question. In Fig. 3.6, taken from [46], the electric field between two receding charges is shown. In the case of the solid line, two receding, nearly massless fermions with $g/M = 100$, peak momentum $p/M \simeq 700$ and width $\Delta x \simeq 2/(5g)$ are created by a pulse of the electric field. These fermions are referred to as self-consistent. The resulting electric field is then calculated taking into account the full back-reaction to the source. The dashed line is the result with external sources. The snapshot of the field is taken at $t \simeq 38/g$.

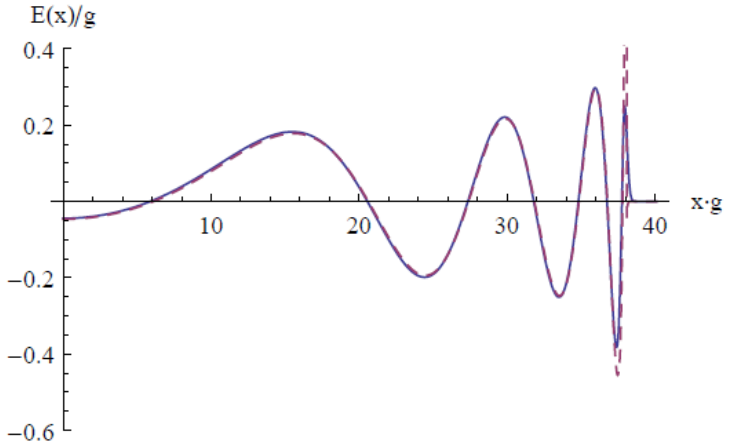

Figure 3.6: Electric field $E(t \simeq 38/g, x)$ for self-consistent fermions (solid line) and external charges (dashed line) for $g/M = 100$, with $E(t, -x) = E(t, x)$.

From the figure we notice two important facts. First, we see that the massless Schwinger model calculation gives reasonable result when the mass is much smaller than coupling and second, not conserving energy by putting external sources does not affect the final result much in the case of very energetic initial sources.

We now move on to describe jets with a given finite energy. The partons

residing in the string ends in general do not move with the speed of light. We consider a general source $-m^2\phi_{ext}(x) = j(x)$

$$(\Box + m^2)\phi = j(x) \tag{3.17}$$

The solution to the equation of motion can be written as

$$\phi(x) = \phi_0(x) + i\int d^2y D_R(x-y)j(y) \tag{3.18}$$

where ϕ_0 is the solution to the Klein-Gordon equation. $D_R(x)$ is the retarded Green's function which was defined in A.2. The free field can be decomposed in the usual way

$$\phi_0(x) = \int \frac{dp}{2\pi}\frac{1}{(2E_p)^{1/2}}\left(a_p e^{-ip\cdot x} + a_p^\dagger e^{ip\cdot x}\right) \tag{3.19}$$

The retarded propagator is

$$D_R(x-y) = \int \frac{dp}{2\pi 2E_p}(e^{ip\cdot(x-y)} - e^{-ip\cdot(x-y)})\theta(x^0-y^0)$$

Combining the expressions above, we get

$$\begin{aligned}\phi(x) &= \int \frac{dp}{2\pi(2E_p)^{1/2}}\left[\left(a_p - \frac{i}{(2E_p)^{1/2}}\tilde{j}^*(p)\right)e^{-ipx}\right. \\ &+ \left.\left(a_p^\dagger + \frac{i}{(2E_p)^{1/2}}\tilde{j}(p)\right)e^{ipx}\right]\end{aligned} \tag{3.20}$$

where we have taken the Fourier transform of the source

$$\tilde{j}(p) = \int d^2x\ e^{ip\cdot x}j(x). \tag{3.21}$$

The Hamiltonian for the free particle is

$$H = \int \frac{dp}{2\pi}E_p\left[a_p^\dagger a_p + \frac{1}{2}[a_p, a_p^\dagger]\right]. \tag{3.22}$$

If we compute the vacuum expectation value with respect to the free particle vacuum (of the normal ordered part), we get

$$\langle 0|H|0\rangle = \int \frac{dp}{2\pi} E_p \frac{|\tilde{j}(p)|^2}{2E_p}. \tag{3.23}$$

This leads to the distribution in momentum of the produced particles.

$$\frac{dN}{dp} \equiv \langle 0|a_p^\dagger a_p|0\rangle = \frac{|\tilde{j}(p)|^2}{2E_p}. \tag{3.24}$$

3.3 Fragmentation functions in $e^+e^- \to$ hadrons

We will use (3.24) to compute the quark fragmentation function [47]. To do this, we have to construct the proper current $j(x) = -m^2\phi_{ext}$. In order to do that, let us return again to the perturbative evolution of the jet.

Similarly as in [30], to describe e^+e^- annihilation into hadrons, we add an external current j^μ_{ext} to the theory, but the quarks now move with velocity $v < 1$, which is determined from the center of mass energy $\sqrt{s}$ and a parameter Q_0, which is comparable to the nonperturbative scale R^{-1} introduced above, in the following way[1]

$$v = \frac{\sqrt{s}/2}{\sqrt{(\sqrt{s}/2)^2 + Q_0^2}}. \tag{3.25}$$

The current is then given by

$$j^0(x) = \delta(z - vt)\theta(z) - \delta(z + vt)\theta(-z) \tag{3.26}$$

We will compute the momentum distribution of produced mesons from this current, therefore we use (3.24). In momentum space $p^\mu = (E_p, p)$, where $E_p = \sqrt{p^2 + m^2}$ (the produced mesons are on-shell), using (2.72), we get

$$\tilde{\phi}_{ext}(p) = i\frac{\sqrt{\pi}}{p}\tilde{j}^0_{ext}(p). \tag{3.27}$$

[1] One jet takes up half of the center of mass energy.

We have to compute the Fourier transform of the charge density

$$\tilde{j}^0_{ext}(p) = \int d^2x \; e^{ip\cdot x} j^0_{ext}(x). \tag{3.28}$$

The resulting integral is not well defined, so to regularize it we give a small negative imaginary part $-\epsilon$ to E_p and set it to zero at the end. In other words,

$$\begin{aligned}
\tilde{j}^0_{ext}(p) &= \int d^2x e^{ip\cdot x} \left[\delta(z-vt)\theta(z) - \delta(z+vt)\theta(-z)\right] \\
&= \lim_{\epsilon\to 0} \int_0^\infty dt \left[e^{i(E_p - pv)t - \epsilon t} - e^{i(E_p+pv)t-\epsilon t}\right] \\
&= i\left(\frac{1}{E_p - pv} - \frac{1}{E_p + pv}\right) = i\frac{2pv}{E_p^2 - p^2v^2}.
\end{aligned} \tag{3.29}$$

Substituting in (3.27)

$$\tilde{j}(p) = -m^2\tilde{\phi}_{ext}(p) = \sqrt{\pi}\frac{2vm^2}{E_p^2 - v^2p^2} \tag{3.30}$$

from where we compute

$$\frac{dN}{dp} = 2\pi\frac{v^2m^4}{E_p(E_p^2 - v^2p^2)^2}. \tag{3.31}$$

One might expect a factor of N_c, but it is missing because we consider hadron yield per produced jet (with a fixed color orientation). For $v = 1$, we get $dN/dp \propto 1/E_p$ familiar from the usual bremsstrahlung spectrum in $(3+1)$ dimensions. Let us define the usual fragmentation variable $z = p^h/p^{jet} \equiv p/p^{jet}$ as the fraction of jet's momentum p^{jet} carried by the hadron of momentum $p^h = p$. As an application of the model, we use (3.31) to evaluate dN/dz and fit it to the data on $e^+e^- \to$ hadrons at $\sqrt{s} = 201.7$ GeV [48]. The result is shown in Fig. 3.7; the fit parameters are the scalar meson mass m and the matching scale Q_0 at which the DGLAP evolution has to be matched onto our model. From the fit we find $m = 0.6$ GeV that is consistent with the PDG value for the σ meson, and $Q_0 = 2$ GeV (the velocity $v = P_{jet}/\sqrt{P_{jet}^2 + Q_0^2}$). At small $z \leq 0.1$, our result is below the data points signaling the need for perturbative

QCD evolution; however the spectrum at $z \geq 0.15$ is reproduced reasonably well. For lower center of mass energies, the fit seems to be better, because

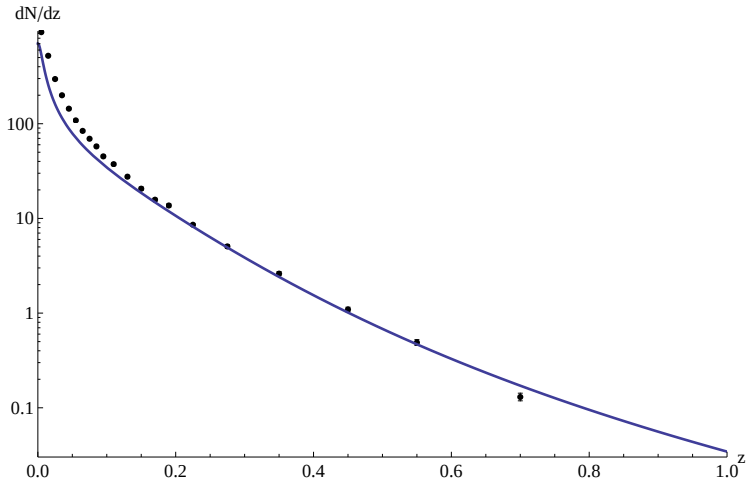

Figure 3.7: The spectrum of charged hadrons in e^+e^- annihilation at $\sqrt{s} = 201$ GeV; solid line is obtained from (3.31).

there is less contribution from the perturbative cascade. We have shown in Fig. 3.8 the rapidity distribution of produced hadrons in e^+e^- annihilation for center of mass energy $\sqrt{s} = 29$ GeV, measured by TPC/Two Gamma collaboration and reported in [49].

In order to compute dN/dy, we have made the change of variables $(p \to y)$, where

$$y = \frac{1}{2} \ln \frac{E_p + p}{E_p - p}. \tag{3.32}$$

In turn

$$E_p = m \cosh y, \quad p = m \sinh y. \tag{3.33}$$

3.4 Discussion

In this chapter we investigated the particle production by external sources, where the latter model the color sources in high energy scattering processes. We observed that particle creation is driven by the anomaly. We then computed the fragmentation function for e^+e^- to hadrons using an exactly soluble

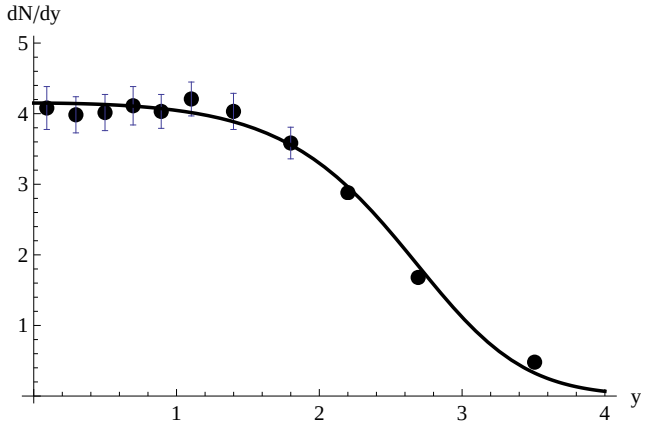

Figure 3.8: Rapidity distribution of charged pions in e^+e^- annihilation experiment, with center of mass energy $\sqrt{s} = 29$ GeV. Solid curve is calculated from (3.31).

model, which was motivated in the previous chapter. The model has two parameters, the mass of the hadrons, m, and the nonperturbative scale Q_0. By setting $m \simeq 0.6$ GeV and $Q_0 \simeq 2$ GeV, we observed that the data are described reasonably well. The values we get for the parameters could be interpreted as follows: m correponds to the mass of σ meson and Q_0 is a QCD nonperturbative scale at which the QCD cascade is assumed to stop. We see a reasonable agreement with experimental data.

Chapter 4

Jets in medium - Energy Loss

The focus of this chapter will be the role of the QCD medium (formed in heavy ion collisions) in the modification of jet fragmentation functions.

Let us recall shortly the space-time evolution of jet evolution. The perturbatively produced high transverse momentum partons are in general far off mass shell and evolve emitting gluons and quark-antiquark pairs; this evolution towards smaller parton virtualities is governed by the QCD renormalization group and described by DGLAP equations as we outlined above. At $Q_0^2 \sim 1-3$ GeV^2 the non-perturbative effects of confinement set in and transform the radiated partons into the observed hadrons. The longitudinal distance a parton moves before hadronizing is then given by $L_h \simeq zP_{jet}/Q_0^2$, where z is the fraction of the jet transverse momentum P_{jet} carried by the parton with virtuality Q_0. Using for the sake of an estimate the values $z = 0.2$, $P_{jet} = 100$ GeV and $Q_0 = 2$ GeV^2 (this is the value we found above), we get $L_h \simeq 2$ fm. In Pb-Pb collisions, this estimate suggests that the jet evolves down to the scales at which the dynamics becomes non-perturbative well within the produced medium.

It is widely believed that the quark-gluon plasma at temperatures $T \leq (2-3)T_c$ produced at RHIC and LHC is non-perturbative and strongly coupled at scales of the order of 1 GeV. Combined with our estimate of the jet formation time, this suggests one has to develop an approach to the jet interactions in the medium and its subsequent hadronization that is i) valid at strong coupling; ii)

describes properly the transformation of partons into the measured hadrons. Within the perturbation theory, the approach to the propagation of the jet in the medium has been developed in [50, 51]; see [52, 53] for reviews. It has been established that the Landau-Pomeranchuk-Migdal (LPM) effect [54–56] – the quantum interference of the radiation processes in the interactions with multiple scattering centers in the medium – is as important in QCD as it was originally found in QED, although the non-Abelian effects modify the radiation pattern. While the LPM effect has been traditionally treated within the perturbation theory, it can be expected to affect the radiation amplitudes also at strong coupling. Indeed, the LPM effect may be viewed as a consequence of quantum mechanics and the low-energy Low theorem that is based only on the symmetries of the theory (gauge invariance and the conservation of vector current) and is valid even when the perturbation theory does not apply.

Recently, the CMS Collaboration presented the data on the modification of the shape of the jets produced in Pb-Pb collisions at the LHC [57]. This data is interesting because it opens a window into the mechanism by which jets lose energy in the quark-gluon plasma (QGP). It is expected that the dominant mechanism of jet energy loss is the induced QCD bremsstrahlung [50–52, 58–60]. This induced gluon radiation would then transform into hadrons and produce an enhancement in the in-medium jet fragmentation function at small values of z, the fraction of the jet's energy carried by the produced hadron, or equivalently, at large values of $\xi = \ln(1/z)$ – see [61] for a recent overview and comparison of various models of energy loss. The data indeed clearly show this enhancement [57]. However, the data also indicate the *suppression* of the fragmentation function at intermediate values of $\xi \simeq 3$. This suppression is surprising because it seems to imply, through the Local Parton Hadron Duality (LPHD) [45], that the radiation of gluons at these intermediate values of ξ is suppressed relative to the in-vacuum fragmentation. This apparent suppression of gluon radiation is hard to reconcile with the expected enhancement due to the induced QCD bremsstrahlung. In this chapter we argue that there is no contradiction between CMS results and the presence of induced QCD radiation.

Describing the fragmentation of a jet into hadrons from first principles requires a theory of confinement, and it is still lacking. Instead, the conventional pQCD approach [8] is based on introducing universal phenomenological fragmentation functions extracted from the experimental data. This practical and useful approach however does not allow to predict how these fragmentation functions would change in the presence of the QCD medium – making such a prediction requires a dynamical theory of fragmentation. While the complete theory of confinement still does not exist, many properties of confining interactions in QCD are known from phenomenology, lattice QCD, and effective theories. One of the properties of QCD with light quarks is the so-called "soft confinement" [33] (for review, see e.g. [34]). For the case of jet fragmentation, "soft confinement" implies that the fragmenting quark polarizes the QCD vacuum and slows down by producing along its trajectory quark-antiquark pairs that later form hadrons – this picture in fact can be considered as the foundation of the phenomenologically successful LPHD hypothesis.

We argued in previous chapters that the massless QED in $1+1$ dimensions (QED_2, also known as the Schwinger model [27–29]) can be used as an effective theory of QCD string breaking and jet hadronization. Indeed, this exactly soluble model captures many properties of quark interactions in QCD – the screening of color charge by light quark-antiquark pairs, the presence of θ-vacuum, and the axial anomaly. QED_2 has previously been applied to the description of hadronic interactions at high energies in Refs. [31, 32].

In $3+1$ dimensions, the typical transverse momentum of mesons is of the order of their mass (in our case $m \simeq 600$ MeV), therefore their longitudinal momentum p is much larger for $p/E_{jet} = z > 0.01$ or $\xi < 5$ for $E_{jet} \sim 120$ GeV. A natural extension [47] of the model presented in the previous chapter is thus to consider N_c copies of the Abelian $U(1)$ gauge group. For the propagation of the quark jet through the medium, this extension allows to consider the rotation of the color orientation of the quark. By using the (1+1) dimensional field theory we neglect the transverse momentum broadening of the jet in the medium; this is a reasonable approximation for the high momentum jets that we consider. Every time the quark exchanges a gluon with the medium, its

color changes; for a medium of length L and the quark mean free path λ, we thus get L/λ sectors bounded by the propagating quark and the exchanged gluons, see Fig. 4.3 and Fig. 4.6. At large N_c, these sectors produce particles independently from each other.

4.1 Landau-Pomeranchuk-Migdal Effect (LPM) in perturbation theory

Later in this chapter we will consider the energy loss of a quark moving in the QCD medium. It is believed that radiative energy loss due to scattering with medium constituents is the dominant energy loss mechanism. We will review some basic facts about radiative energy loss in QCD. We mostly follow [52].

Let's assume that a quark with energy E moves in QCD medium of length L. As the quark moves in this medium it experiences multiple scattering, which induces gluon radiation and in turn the quark loses energy. We assume for now that the scattering centers are static and uncorrelated. The main features of the radiative energy loss can be derived from a heuristic point of view neglecting numerical factors of order $O(1)$, which we will do in the following. Let us recall the formation time of the gluon

$$t_{form} \simeq \frac{\omega}{k_\perp^2}, \tag{4.1}$$

where ω and $k_\perp$ are the gluon's energy and transverse momentum (with respect to the quark) respectively. It is assumed that $\omega >> k_\perp$ and that $k_\perp \simeq \mu$, where μ is a typical scale characterizing the medium (can be thought of as the Debye screening mass in the case of a hot medium). We denote the typical distance between the scattering centers or the mean free path of the quark by λ. When the formation time is much larger than the mean free path, radiation takes place in a coherent way, where many scattering centers act as one. One can define the coherence length

$$l_{coh} \simeq \frac{\omega}{\langle k_\perp^2 \rangle_{coh}}, \tag{4.2}$$

where

$$\langle k_\perp^2 \rangle_{coh} \simeq \frac{l_{coh}}{\lambda}\mu^2 = N_{coh}\mu^2, \tag{4.3}$$

and N_{coh} is the number of coherent scattering centers. We have assumed a random walk expression for the accumulation of the transverse momentum. Substituting (4.3) in (4.2), we can write

$$l_{coh} \simeq \sqrt{\frac{\omega\lambda}{\mu^2}}. \tag{4.4}$$

Using this, we have

$$N_{coh} = \frac{l_{coh}}{\lambda} \simeq \sqrt{\frac{\omega}{\lambda\mu^2}} = \sqrt{\frac{\omega}{E_{LPM}}}, \tag{4.5}$$

where $E_{LPM} = \lambda\mu^2$, and LPM stands for Landau-Pomeranchuk-Migdal.

Let us first consider $\omega \leq E_{LPM}$. In this case, incoherent radiation takes place in L/λ scattering centers. The soft single scattering spectrum is given by [62]

$$\omega\frac{dI}{d\omega} \simeq \frac{\alpha_s}{\pi}N_c, \tag{4.6}$$

where N_c is the number of colors. We can now get the Bethe-Heitler regime for incoherent scattering

$$\omega\frac{dI}{d\omega dz}\Big|_{BH} \simeq \frac{\alpha_s}{\pi}N_c\frac{1}{\lambda}, \tag{4.7}$$

where also $l_{coh} \leq \lambda$. In this case the quark scatters independently with L/λ scattering centers as shown in Fig. 4.1.

The regime of coherent scattering is the case when $\lambda < l_{coh} < L$, keeping in mind that $N_c > 1$, in other words

$$E_{LPM} < \omega < \min\{\omega_{fact}, E\}, \tag{4.8}$$

where $\omega_{fact} \sim \frac{\mu^2}{\lambda}L^2$. We can calculate the spectrum of radiation, but now

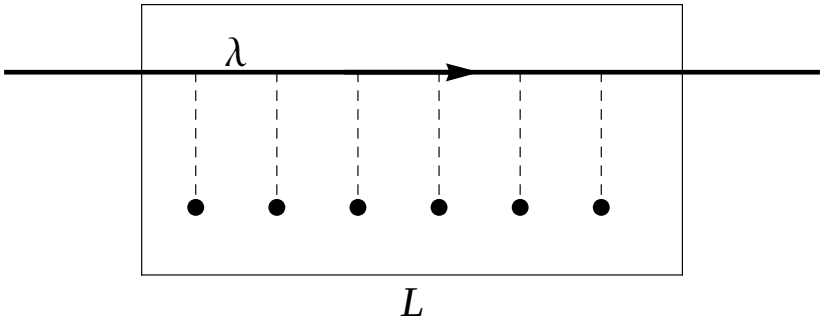

Figure 4.1: Incoherent scattering of the energetic quark with the medium constituents.

keeping in mind that N_{coh} centers act coherently, we get

$$\omega \frac{dI}{d\omega dz}\Big|_{LPM} \simeq \frac{\alpha_s}{\pi} N_c \frac{1}{l_{coh}} \simeq \frac{\alpha_s}{\pi} N_c \sqrt{\frac{\mu^2}{\lambda}\frac{1}{\omega}} = \frac{\alpha_s}{\pi} N_c \frac{1}{\lambda}\sqrt{\frac{E_{LPM}}{\omega}}. \tag{4.9}$$

We see that in this regime, the radiation is suppressed by a factor of $\sqrt{E_{LPM}/\omega}$ compared to the Bethe-Heitler regime. In this regime, many scattering centers act as one, as shown in Fig. 4.2.

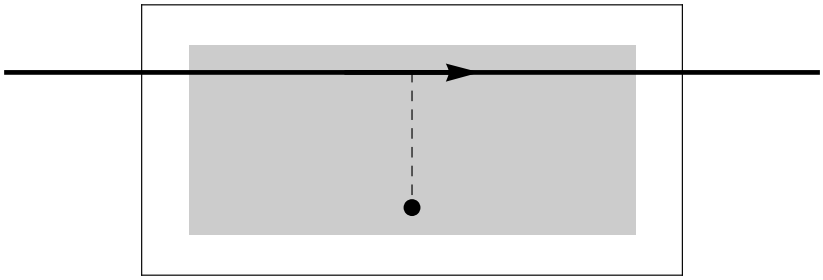

Figure 4.2: Coherent scattering of the quark with medium constituents (LPM regime).

To summarize, we have observed that in the case when $l_{coh} \leq \lambda, \quad \omega < E_{LPM}$, the scattering takes place incoherently and the Bethe-Heitler approximation is valid. On the other hand, when $\lambda \leq l_{coh}, \quad E_{LPM} < \omega$, the radiation is suppressed by a factor $\sqrt{E_{LPM}/\omega}$ compared to the Bethe-Heitler result. By using our model, we will see below that a similar suppression occurs even in

the nonperturbative regime.

4.2 In-medium jet fragmentation without gluon emission

Let us now extend the formalism developed in the previous chapter to the case of a jet propagating through the quark-gluon matter [47, 63]. The quark will exchange color with the matter, rotating in color space and creating in the medium the static color sources located at coordinates $z = z_i$, as in Fig. 4.3. The different sectors in Fig. 4.3 are bounded by the sources with different orientations in color space; each of them is considered as quasi-Abelian, and at large N_c the production of mesons in each sector is independent.

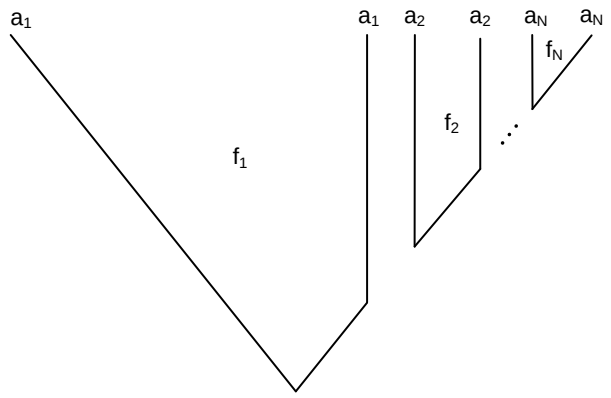

Figure 4.3: The color flow in the jet interactions inside the quark-gluon medium.

We see that there are only three different types of sectors in Fig. 4.3 – the one bounded by the quark escaping from the medium with no interactions (on the left, f_1), the one bounded by the quark that underwent color rotation(s) in the medium (on the right, f_3), and the one bounded on the sides by color static sources in the medium and a propagating quark from below (in the middle,

f_2). We can write the corresponding charge densities

$$\begin{aligned} j_1^0(x) &= -\delta(x+vt)\theta(t) + \delta(x-vt)\left(\theta(t)-\theta(t-t_1)\right) \\ &+ \delta(z-vt_1)\theta(t-t_1), \\ j_2^0(x) &= -\delta(z-vt_1)\theta(t-t_1) + \delta(x-vt)\left(\theta(t-t_1)-\theta(t-t_2)\right) \\ &+ \delta(z-vt_2)\theta(t-t_2), \\ j_3^0(x) &= -\delta(z-vt_2)\theta(t-t_2) + \delta(x-vt)\theta(t-t_2). \end{aligned} \tag{4.10}$$

As in the previous chapter $v = \frac{p_{jet}}{\sqrt{p_{jet}^2+Q_0}}$. p_{jet} is the jet momentum, which we will fix later and $Q_0 \simeq 2$ GeV. By using the methods described above, we get for the corresponding sources (we denote with t_1 and t_2 the time when the first and second scatterings in medium occur respectively)

$$\begin{aligned} \tilde{f}_1(p) &= \frac{-m^2 v\sqrt{\pi}}{E_p - vp}\left[\frac{2}{E_p+vp} - \frac{e^{i(E_p-vp)t_1}}{Ep}\right] \\ \tilde{f}_2(p) &= \frac{m^2 v\sqrt{\pi}}{E_p(E_p-vp)}\left[e^{i(E_p-vp)t_2} - e^{i(E_p-vp)t_1}\right] \\ \tilde{f}_3(p) &= \frac{-m^2 v\sqrt{\pi}}{E_p(E_p-vp)} e^{i(E_p-vp)t_2} \end{aligned} \tag{4.11}$$

We have denoted by $f_i(x) = -m^2\phi_{ext,i}(x)$, where $\phi_{ext,i}(x)$ is calculated from the corresponding charge density $j_i^0(x)$ as in the previous chapter. Summing over the color orientations of different sectors (note that this does not bring in extra powers of N_c in the 't Hooft limit of $N_c \to \infty$, $g^2 N_c$ fixed), we get the hadron spectrum

$$\frac{dN^{med}}{dp} = \frac{1}{2E_p}|\tilde{f}(p)|^2 = \frac{1}{2E_p}(|\tilde{f}_1(p)|^2 + \sum |\tilde{f}_2(p)|^2 + |\tilde{f}_3(p)|^2) \tag{4.12}$$

where we have omitted the interference between different sectors that is suppressed at large N_c. Also, we have to sum over all contours with current f_2 (the times t_1 and t_2 will be different). As an illustration, for the case when we

have only two scatterings, we can write

$$\begin{aligned}\frac{dN^{med}}{dp} &= 4\pi v^2 \frac{m^4}{2E_p}\left\{\frac{1}{(E_p^2-v^2p^2)^2}+\frac{1}{E_p^2(E_p-vp)^2}\right. \\ &- \frac{1}{2}\frac{1}{E_p(E_p-vp)^2}\left[\frac{2\cos(E_p-vp)t_1}{E_p+vp}\right. \\ &+ \left.\left.\frac{\cos[(E_p-vp)(t_2-t_1)]}{E_p}\right]\right\} \end{aligned} \tag{4.13}$$

We want to compare our result to the CMS data [64], so we use the variable $\xi = \ln(1/z)$. Recall that in our case $z = p/p_{jet}$. Since we are interested in evaluating the ratio of the in-medium to in-vacuum fragmentation functions, we also need $dN^{\rm vac}/d\xi$ which has been evaluated already in the previous chapter using as external source

$$j^0(x) = -\delta(z-vt)\theta(-z) + \delta(z+vt)\theta(z), \tag{4.14}$$

where $v = p_{\rm jet}/\sqrt{p_{\rm jet}^2+Q_0^2}$ (same v as in the expressions above) and Q_0 is in the range $1-3$ GeV. Our result for the ratio of in-medium and vacuum fragmentation functions is shown in Fig. 4.4. We put N equally spaced scatterings between t_1 and t_2 (the distance between them corresponds to the mean free path). For large p (small ξ), the measured fragmentation functions of vacuum and in-medium are similar. We call this *Jet Fragmentation Scaling* (JFS). One can see that the observed JFS is well reproduced if the mean free path λ_{mfp} of the quark in the medium is short, $\lambda_{mfp} \leq m^{-1} \simeq 0.3$ fm. It is important to check whether the JFS in our computation stems from the absence of the energy loss – this would contradict the experimental observations [64–67]. The energy loss of the jet in medium is given by

$$\delta E = \int_{m_h}^{E_{jet}} dE_h E_h \left(\frac{dN^{med}}{dE_h} - \frac{dN^{vac}}{dE_h}\right) \tag{4.15}$$

We can use (4.15) to calculate the energy loss δE as a function of jet energy E_{jet}. We plot this in Fig. 4.5; note that our treatment is valid only when

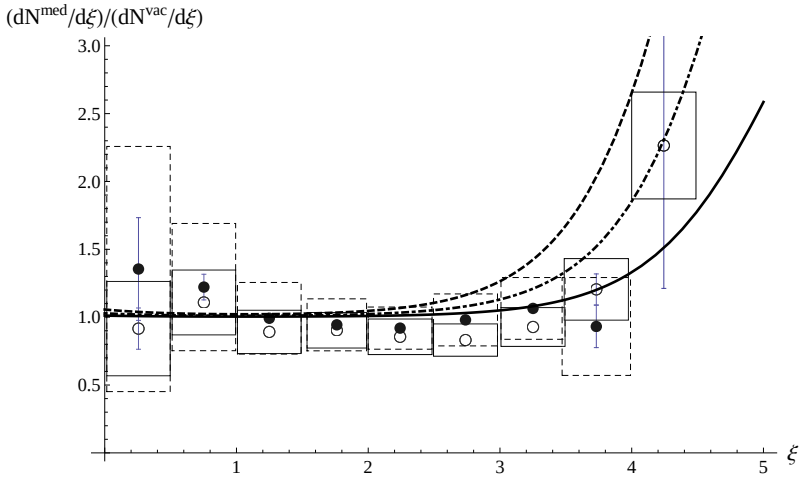

Figure 4.4: Ratio of in-medium to vacuum fragmentation functions. The length of the medium is fixed at 4 fm, the jet energy is $E_{jet} = 100$ GeV. Solid line: the first scattering occurs at $t_1 = 1$ fm (assumed thermalization time), and subsequent scatterings occur with time spacing of $\Delta t = 1/m = 0.3$ fm. Dashed line: double scattering with $t_1 = 2$ fm and $t_2 = 4$ fm ($\Delta t = 2$ fm). Dot-dashed line: four scatterings with $\Delta t = 1$ fm, $t_1 = 1$ fm. Data points are from the CMS Collaboration (see text). Open (filled) circles are for the leading (subleading) jet.

$\delta E \ll E_{jet}$; for short mean free path $\lambda_{mfp} \leq 0.3$ fm this means $E_{jet} \geq 100$ GeV. The energy loss at $\lambda_{mfp} \leq 1$ fm is consistent with the values extracted from the data [64], see [59].

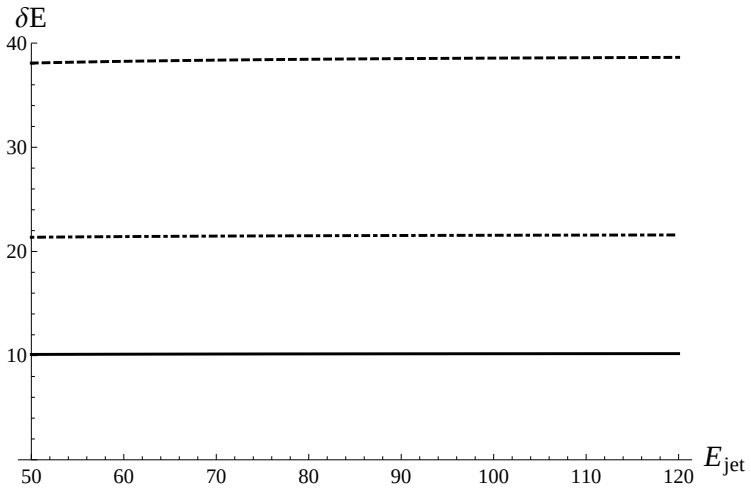

Figure 4.5: Energy loss as a function of jet energy. The lines correspond to the parameters in the caption of Fig. 4.4.

4.3 In-medium fragmentation with non-static sources and gluon emission

In this section we improve on the approach of the previous section (and [47]) by considering the medium-induced perturbative gluon radiation [63]. Compared to the conventional pQCD approaches, we consider also the dynamical modification of the in-medium jet fragmentation due to both the multiple scattering of the jet in the medium and the induced gluon radiation. We also allow for a non-zero momentum transfer from the jet to the medium. Due to this momentum transfer, the scattered particles in the medium are given a kick along the jet momentum and move with some finite velocity after scattering. The typical momentum transfer in medium is of the order of Debye mass m_D, which is also a typical mass of the scattered particles. We can therefore estimate the velocity to be $v_i \sim 1/\sqrt{2}$ $(i = 1, \cdots, n)$. Let us assume first that the

induced radiation is emitted outside of the medium – this process is illustrated in Fig. 4.6; the quark jet scatters n times within the medium prior to emitting a gluon, while the corresponding antiquark jet is assumed to escape without interactions, as would be the case for the surface emission. On the right in Fig. 4.6 we show the corresponding color flow; each color contour at large N_c radiates independently, as explained above. The trajectory of the Abelian charge is given by the boundary of the contour. As in the previous section, there are only three different types of currents we have to consider and they are labeled by j_1, j_2 and j_3. We can write down the charge densities:

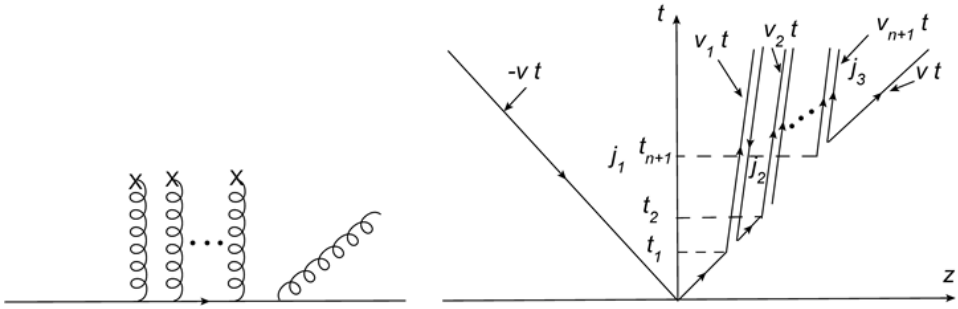

Figure 4.6: In-medium scattering of the jet accompanied by an induced gluon radiation outside of the medium. Left: the Feynman diagram. Right: the corresponding color flow.

$$
\begin{aligned}
j_1^0(x) &= -\delta(z+vt)\theta(-z) + \big\{\delta(z-vt)[\theta(t)-\theta(t-t_1)] \\
&+ \delta[z-vt_1-v_1(t-t_1)]\theta(t-t_1)\big\}\theta(z) \\
j_2^0(x) &= -\delta[z-vt_1-v_1(t-t_1)]\theta(t-t_1) + \delta(z-vt)[\theta(t-t_1)-\theta(t-t_2)] \\
&+ \delta[z-vt_2-v_2(t-t_2)]\theta(t-t_2) \\
j_3^0(x) &= \big[-\delta[z-vt_{n+1}-v_{n+1}(t-t_{n+1})]\theta(t-t_{n+1}) \\
&+ \delta(z-vt)\big]\theta(t-t_{n+1}).
\end{aligned}
\tag{4.16}
$$

The Fourier transform of these charge densities is given by

$$
\tilde{j}_1^0(p) = \frac{ip}{E_P - vp}\Big[\frac{2v}{E_P+vp} - \frac{v-v_1}{E_P-v_1 p}e^{i(E_P-vp)t_1}\Big] \tag{4.17}
$$

$$\tilde{j}_2^0(p) = \frac{-ip}{E_P - vp}\Big[\frac{v - v_2}{E_P - v_2 p}e^{i(E_P - vp)t_2} - \frac{v - v_1}{E_P - v_1 p}e^{i(E_P - vp)t_1}\Big] \tag{4.18}$$

$$\tilde{j}_3^0(p) = \frac{ip}{E_P - vp}\frac{v - v_{n+1}}{E_P - v_{n+1}p}e^{i(E_P - vp)t_{n+1}} \tag{4.19}$$

Similarly as above, we can calculate the corresponding $\tilde{\phi}_{\text{ext}}(p)$ to compute the distribution of hadrons. We again assume no interference between contours, therefore the hadron distribution is given by

$$\frac{dN^{med}}{dp} = \frac{m^4}{2E_P}(|\tilde{\phi}_{1,\text{ext}}(p)|^2 + \sum |\tilde{\phi}_{2,\text{ext}}(p)|^2 + |\tilde{\phi}_{3,\text{ext}}(p)|^2), \tag{4.20}$$

where $\tilde{\phi}_{2,\text{ext}}(p)$ is calculated from $j_2^0(x)$ and we have to sum over all of contours of this type. We define in the same way as above $z = p/p_{\text{jet}}$, where p is the momentum of the final-state hadron and p_{jet} is the jet momentum. In order to compare with the data, we again use $\xi = \ln(1/z)$.

We are now in a position to compute $dN^{\text{med}}/d\xi$. The ratio of fragmentation functions of in-medium and vacuum, as a function of $\xi = \ln\frac{1}{z}$, is shown in Fig. 4.7. The result is plotted for different mean free paths, i.e. the different distances between scattering centers in Fig. 4.6 and is compared to data taken from [57]. As mentioned above and as it was shown already in [47], the enhancement for large ξ results from the radiation coming from the medium-induced color contours of type j_2. On the other hand, it can be seen that the suppression for intermediate ξ comes from the contour of (4.19). The underlying physics is the partial screening of the color charge of the jet by a comoving medium-induced gluon. A similar effect due to coherent parton branching has recently been considered in [68]. When v_{n+1} approaches v, where v_{n+1} is the velocity of the final state gluon, we get a suppression in the fragmentation function. The final state gluon is typically emitted at the rapidity interval $\Delta\eta \sim 1/\alpha_s \simeq 2$ away from the leading parton in the jet; this is the value that was assumed in the plot in Fig. 4.7. We have also considered

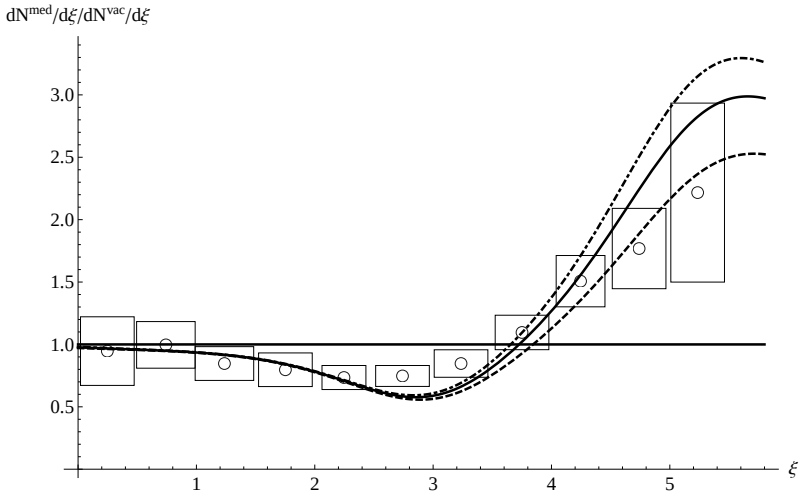

Figure 4.7: The ratio of in-medium and vacuum fragmentation functions for $p_{\text{jet}} = 120$ GeV. The first scattering occurs at $t_1 \simeq 1$ fm, which is the assumed thermalization time. The length of the medium is $L = 5$ fm. The curves correspond to mean free paths of $\lambda = 0.57$, 0.4 and 0.2 fm from top to bottom respectively. The data points are from the CMS Collaboration.

the case when a gluon is radiated from the original jet and then interacts within the medium as shown in Fig. 4.8 – this is the dominant diagram in the BDMPS [50, 51] approach. We have found that for the same values of parameters this case leads to the ratio of fragmentation functions that is very similar to the one presented in Fig. 4.7.

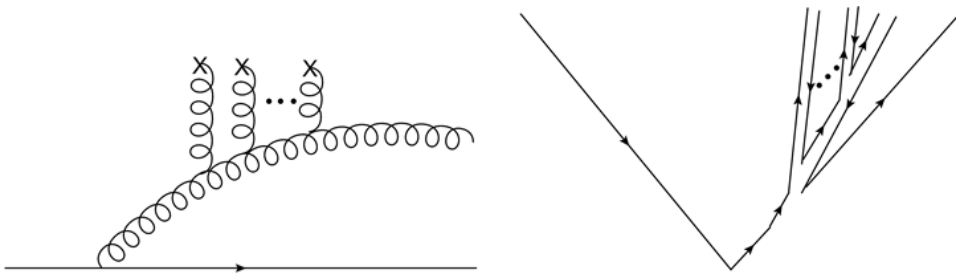

Figure 4.8: In-medium scattering of a gluon radiated from the original jet.

4.4 Transverse-momentum difference between Au+Au and p+p

Let us note that even though the energy cannot be transferred outside the jet cone in our $1+1$ model, it is transferred from the high energy jet to low energy hadrons. Below a certain experimental cutoff, these soft hadrons are not counted as a part of the jet, and therefore this leads to an effective energy loss. To illustrate this, we compute within our model the quantity defined in the STAR Collaboration publication [69] that measures the difference in momentum distributions of the hadrons produced in jet fragmentation in AA and pp collisions[1]:

$$D_{AA}(p) = Y_{Au-Au}(p)\,\langle p\rangle_{Au-Au} - Y_{p-p}(p)\,\langle p\rangle_{p-p}\,, \tag{4.21}$$

where $Y(p)$ is the yield in a given bin with average $\langle p\rangle$,

$$Y(p) = \int_{\text{bin with average }\langle \text{p}\rangle} dp' \frac{dN}{dp'}, \tag{4.22}$$

leading to

$$D_{AA}(p) = \langle p\rangle \int_{\text{bin with average }\langle p\rangle} dp' \frac{dN^{\text{med}}}{dp'} - \langle p\rangle \int_{\text{bin with average }\langle p\rangle} dp' \frac{dN^{\text{vac}}}{dp'}. \tag{4.23}$$

We have plotted the results in Fig. 4.9, where we compare our calculation with the measurements presented in [69]; we have used the mean free path of $\lambda = 0.4$ fm. The fluctuations around $p = 1$ GeV and $p = 5$ GeV seem to be due to the sensitivity of D_{AA} to the boundaries of the bin. The agreement with the data suggests that our simple model adequately captures the dynamics of the jet energy redistribution in the longitudinal direction.

[1] in $1+1$ dimensions there is only one spatial direction, so $p_T = p$.

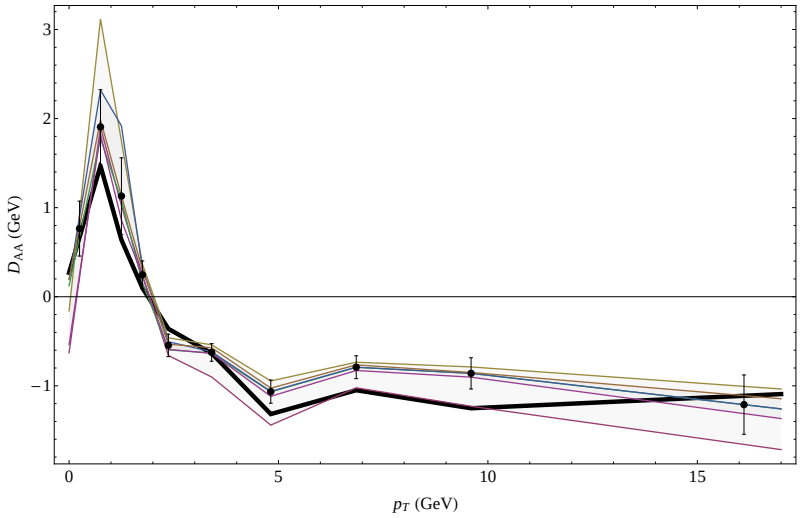

Figure 4.9: D_{AA} defined in (4.21) and (4.23) for jet energy of $20 < p_{jet} < 40$ GeV. Black dots and shaded areas show experimenal data, jet energy scale, v2/v3 and detector uncertainties respectively, taken from the STAR Collaboration paper (see text); solid line interpolates between calculated values of D_{AA} from (4.23).

4.5 Discussion

To summarize, we have used the effective $1+1$ dimensional Abelian model, introduced in the previous chapter, to describe the dynamical modification of jet fragmentation in the QCD medium. We have found that this approach describes well the suppression of the in-medium fragmentation at intermediate values of $\xi = \ln(1/z)$ observed by the CMS Collaboration, and there is thus no contradiction between the LHC results and the picture of QCD radiation induced by the scattering of the jet. The physics that underlies the suppression of the in-medium fragmentation function is the partial screening of the color charge of the jet by the comoving medium-induced gluon. It would be interesting to develop a hybrid approach to jet fragmentation combining the full DGLAP perturbative evolution down to the scale of $Q_0 \sim 1-2$ GeV, induced gluon radiation, and the non-perturbative dynamical fragmentation as modeled above.

Chapter 5

Anomalous soft photon production

The production of soft photons in hadron collisions is governed by the Low theorem [70] that is based on very general properties of QED as a vector gauge theory. In hadron collisions, the Low theorem states that soft photons are produced by the bremsstrahlung off the charged hadrons [71], and relates the soft photon yield to the measured hadron spectrum. This allows to make predictions that can be tested experimentally. Surprisingly, nearly every experiment that studied the production of soft photons in high energy hadron collisions found a dramatic (by factor of $2 \div 5$) enhancement above the Low theorem's predictions, see e.g. [72–77] – this is the long-standing puzzle of the "anomalous photon production." Many theoretical models have been proposed to explain the anomalous photon production (for a review, see e.g. [78]); some of them are based on collective effects in produced hadronic matter [79–81], including the effects of anomalies [82–86]; other invoke the synchrotoron radiation in the QCD vacuum [87], new light bound states [88] or strong coupling phenomena treated within holography [89] – however none of them explains all features of the observed phenomenon.

A particularly striking recent result is the measurement of the direct soft photon yield in hadronic decays of the Z^0 boson by the DELPHI Collaboration [90, 91]. The data recorded during the operation of the LEP e^+e^-

collider at CERN show the photon spectrum similar to the one expected from bremsstrahlung, but with a magnitude about *four times* higher than the prediction of the Low theorem based on the measured charged hadron yields. Contrary to processes with hadronic final states, the DELPHI measurement [92] of photons produced in the $e^+e^- \to Z^0 \to \mu^+\mu^- + n\gamma$ channel is in good agreement with the theoretical expectation based on muon inner bremsstrahlung – so the puzzle of the anomalous soft photons seems to be specific to the production of hadronic final states. Remarkably, the soft photon yield was found [90] to be more sensitive to the neutral hadron multiplicity than to the charged one that is expected to govern the photon bremsstrahlung.

The anomalous soft photons present a challenge to the foundations of theory. Moreover, this puzzle is an obstacle to using soft photons for diagnosing quark-gluon plasma, as we need to understand the "background" - the mechanism of photon production in elementary collisions. To be specific, in this chapter we concentrate on the direct soft photon production in hadronic decays of Z^0 that are dominated by the fragmentation of the quark jets produced in the $Z^0 \to q\bar{q}$ process. The direct (i.e. not originating from hadron decays) soft photon emission by the fragmenting quark and antiquark within the perturbative framework was found [90] insufficient to explain the data. Since the bremsstrahlung of final state charged hadrons also does not describe the yield, one is naturally led to a possible nonperturbative mechanism of photon emission in the quark fragmentation process. Because of this, it is important to re-examine the problem by putting emphasis on the possible non-perturbative QCD effects on soft photon production.

The quark propagating through the confining QCD vacuum pulls from the Dirac sea the quark-antiquark pairs that later form hadrons; even if these hadrons are neutral, all quarks possess electric charge and can radiate photons. It is clear that such a mechanism involves QCD dynamics at large distances, where the coupling is strong and we have to rely on an effective theory. We will use the model of jet fragmentation we saw in previous chapters (see also [47, 63]) to describe the real-time dynamics of jet fragmentation and soft photon production [93]. An important property of this theory is that the particle

production is determined by the axial anomaly as we saw before and will make use of it below. But, first, we review very shortly the Low theorem and its consequences in soft photon production in high energy scattering experiments.

5.1 Review of Low theorem

At very low photon momentum ($k \to 0$), the amplitude for photon production is dominated by the Bremsstrahlung off incoming and outgoing charged particles [70]. In order to illustrate this fact, let us consider diagrams in Fig. 5.1 which show the scattering between a charged particle (solid line) with a neutral one (dashed line). The radiated photon can be emitted either from the incoming, outgoing or the intermediate charged particle propagator. When the photon is attached in the incoming line, then we get an intermediate charged propagator with denominator $(p-k)^2 - m^2$. Both the incoming charged particle and the photon are on mass shell, therefore $p^2 - m^2 = 0$ and $k^2 = 0$. This means that the propagator is proportional to $1/p \cdot k$, which is singular for $k \to 0$. The same singularity is found if the photon is attached to the outgoing charged particle line. In the case when the photon is attached in the intermediate (virtual) line the situation is different. The virtual line is not on mass shell, therefore there is no singularity. This means that the amplitude is dominated by the Bremsstrahlung off incoming and outgoing charged particles. Using this argument, the soft photon can be computed from the charged hadronic spectrum as follows

$$\omega \frac{dN^\gamma}{d^3k} = \frac{\alpha}{(2\pi)^2} \sum_n \int d^3p_1 \cdots d^3p_n \sum_{i,j} \frac{-Q_i Q_j (p_i \cdot p_j)}{(p_i \cdot k)(p_j \cdot k)} \frac{dN^{hadr}}{d^3p_1 \cdots d^3p_n}. \tag{5.1}$$

DELPHI data mentioned above cannot be described by this expression as we will see below.

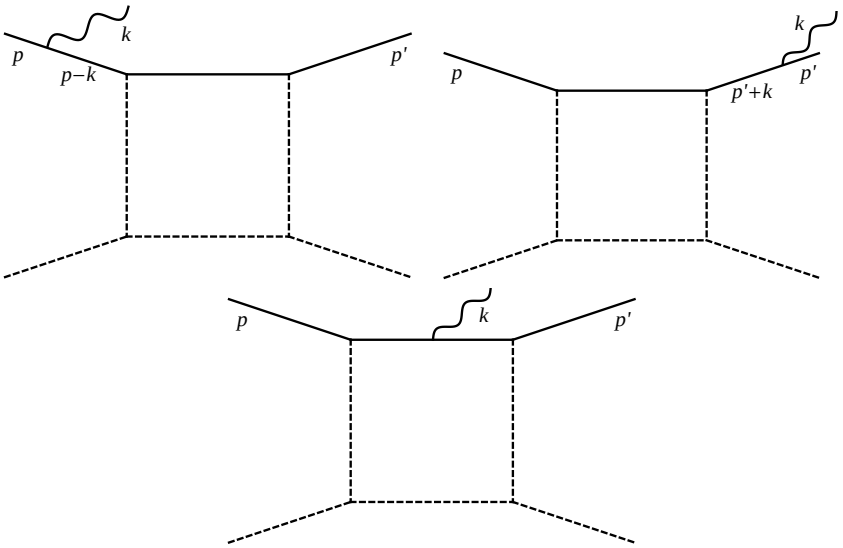

Figure 5.1: Scattering of a charged (solid line) and a neutral (dashed line) particle.

5.2 Oscillations of electric and axial charge in quark fragmentation

The production of quark-antiquark pairs in the fragmentation of the quark allows interpretation in terms of topology of the gauge field and chirality of the quarks. In this section, we will illustrate this using the example of the $1+1$ dimensionally reduced theory. We will assume that the dynamics of pair production along the jet axis can be modeled by massless Quantum Electrodynamics in $1+1$ dimensions or QED_2:

$$\mathcal{L} = -\frac{1}{4} G_{\mu\nu} G^{\mu\nu} + \bar{\psi} i \gamma^\mu \partial_\mu \psi - g \bar{\psi} \gamma^\mu \psi B_\mu - g j^\mu_{ext} B_\mu \tag{5.2}$$

where $\mu = 0, 1$, B_μ is the gauge field, $G_{\mu\nu} = \partial_\mu B_\nu - \partial_\nu B_\mu$ is the field strength and j^μ_{ext} is an external current. We have denoted the $1+1$ dimensional gauge field by B_μ, because we reserve the notation A_μ for the electromagnetic gauge potential, which we will couple to the $1+1$ dimensional theory. As in the previous chapters, the leading quarks of the jets are introduced through an external current composed by the fermion and the anti-fermion moving back-

to-back with equal velocities v (see Fig.5.2):

$$j^0_{ext}(x) = \delta(z - vt)\theta(z) - \delta(z + vt)\theta(-z) \tag{5.3}$$

where $x^\mu = (t, z)$ and

$$v = \frac{p_{jet}}{\sqrt{p^2_{jet} + Q^2_0}} \tag{5.4}$$

where p_{jet} is the jet momentum and $Q_0 \sim 2$ GeV is the time-like virtuality scale at which the pQCD DGLAP cascade stops, and the effects of confinement described by our effective theory begin to operate. We have not considered here the emissions of the additional partons in the DGLAP cascade. These emissions would modify the external current, but because of the color coherence in the perturbative cascade their effect should be diminished by destructive interference.

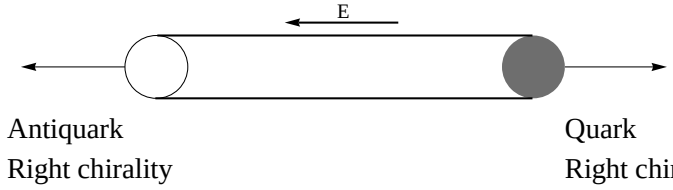

Figure 5.2: Fermion and antifermion moving back-to-back.

Recall the bosonization relation for the vector current

$$j^\mu(x) = \bar{\psi}(x)\gamma^\mu\psi(x) = -\frac{1}{\sqrt{\pi}}\epsilon^{\mu\nu}\partial_\nu\phi(x) \tag{5.5}$$

where ϕ is a real scalar field; note that with (5.5) the conservation of vector current is automatic. The axial current, we saw above, can be written as

$$j^\mu_5(x) = \bar{\psi}(x)\gamma^\mu\gamma^5\psi(x) = \frac{1}{\sqrt{\pi}}\partial^\mu\phi(x). \tag{5.6}$$

The equation of motion for the scalar field is

$$(\Box + m^2)\phi(x) = -m^2\phi_{ext}(x) \tag{5.7}$$

where $\Box \equiv \partial_t^2 - \partial_z^2$ and $m^2 = g^2/\pi$ and ϕ_{ext} can be computed using (2.72).

The coupling to a classical source results in particle creation. The produced particles (that after bosonization become the quanta of the ϕ field) can be interpreted as neutral mesons produced in the fragmentation of the string stretched between the original quark and antiquark. Let us for a moment consider the ultra-relativistic limit $v \to 1$ in which the problem becomes somewhat simpler. Due to the Lorentz invariance, we can write the equation of motion in terms of the proper time τ and rapidity y:

$$\begin{aligned} \tau &= \sqrt{t^2 - z^2} \\ y &= \frac{1}{2} \ln \frac{t+z}{t-z}. \end{aligned} \tag{5.8}$$

The equation of motion (5.7) in the $v \to 1$ limit is independent of rapidity and can be written as

$$(\Box + m^2)\phi(m\tau) = -m^2 \phi_{ext}(m\tau), \tag{5.9}$$

which is an ordinary differential equation in the proper time:

$$(\Box + m^2)\phi(m\tau) = m\frac{1}{\tau}\phi'(m\tau) + m^2\phi''(m\tau) + m^2\phi(m\tau) = -m^2\phi_{ext}(m\tau), \tag{5.10}$$

where the prime denotes differentiation with respect to $m\tau$. On the other hand,

$$\begin{aligned} \phi_{ext}(m\tau) &= -\sqrt{\pi}\int^z dz'[-\delta(z+t)\theta(-z) + \delta(z-t)\theta(z)] \\ &= \sqrt{\pi}\theta(t^2 - z^2) = \sqrt{\pi}\theta(\tau^2); \end{aligned} \tag{5.11}$$

we therefore have to solve

$$\phi''(m\tau) + \frac{1}{m\tau}\phi'(m\tau) + \phi(m\tau) = -\sqrt{\pi}\theta(m^2\tau^2). \tag{5.12}$$

We encountered this equation before the solution can be written as

$$\phi(m\tau) = -\sqrt{\pi}\theta(m^2\tau^2)(1 - J_0(m\tau)), \tag{5.13}$$

where J_0 is the Bessel function. The equations (5.13) and (5.5) show that the evolution in proper time gives rise to oscillation in the vector (electric) charge density

$$\begin{aligned} j^0(\tau, y) &= \frac{1}{\sqrt{\pi}}\partial_z(\sqrt{\pi}\theta(m^2\tau^2)(1 - J_0(m\tau))) = -\partial_z J_0(m\tau) \\ &= -(-m\sinh y(-J_1(m\tau))) = -m\sinh y J_1(m\tau). \end{aligned} \tag{5.14}$$

It is this oscillation of electric charge that will be responsible for the enhancement of the soft photon yield once we introduce the coupling to the dynamical $(3+1)$ dimensional electromagnetic field.

Since the oscillation of electric charge is crucial for our interpretation of the anomalous soft photon production, it is worthwhile to discuss this phenomenon in more detail. We will now show that the oscillation of electric charge is induced by the axial anomaly in the presence of chirality imbalance [1]. In $(1+1)$ dimensions, the helicity of a fermion is determined simply by the direction of its motion – the fermion moving to the right is right-handed, and the fermion moving to the left is left-handed. For an antifermion, just like in $(3+1)$ dimensions, chirality and helicity have the opposite signs - so the antifermion moving to the left has right-handed chirality. Our original configuration of a fermion-antifermion pair moving back-to-back therefore has two units of chirality, see Fig. 5.2.

The index theorem in two dimensions is given by

$$\Delta Q_5 = N_R - N_L = \frac{g}{\pi}\int d^2x F_{01} \tag{5.15}$$

where $N_{R,L}$ is the number of left/right movers. We can see that a nonzero axial charge gives rise to an electric field. This has a simple physical interpretation – the presence of electric field due to the Lorentz force creates an asymmetry between the left- and right-moving charged fermions. Using bosonization relations and requiring that the fields vanish at infinity, we can find the electric

[1] In $(3+1)$ dimensions, these are the crucial ingredients of the Chiral Magnetic Effect [94–97].

field induced by the pairs created by the original external source:

$$F_{01}^{ind} = -\frac{g}{\sqrt{\pi}}\phi. \tag{5.16}$$

Let us now show that the axial charge ΔQ_5 oscillates as a function of time. To do this, we will use (5.15), where $F_{01}^{tot} = F_{01}^{ind} + F_{01}^{ext}$ will be the sum of the electric field (5.16) induced by the pair creation and the field created by the external source:

$$F_{01}^{ext} = -g[\theta(z+t) - \theta(z-t)] = -g\theta(t^2 - z^2). \tag{5.17}$$

The total axial charge as a function of time is thus given by

$$\begin{aligned}
\Delta Q_5 &= \frac{g}{\pi}\int d^2x F_{01}^{tot} = \frac{g}{\pi}\int d^2x \left(-g\theta(m^2\tau^2) + g\theta(m^2\tau^2)(1 - J_0(m\tau))\right) \\
&= -\frac{g^2}{\pi}\int_0^t dt' \int_{-t'}^{t'} dz J_0(m\sqrt{t'^2 - z^2}) \\
&= -2m^2 \int_0^t dt' \int_0^{t'} dz J_0(m\sqrt{t'^2 - z^2}) \\
&= 2m\int_0^t dt' \sin(mt') = 2[\cos(mt) - 1]
\end{aligned} \tag{5.18}$$

The axial charge thus indeed oscillates with the period $T = 2\pi/m$ – the appearance of m of course is not surprising since it is the only scale in the theory. However, the oscillation of the axial charge is a non-trivial consequence of i) the periodicity of the θ-vacuum of the Schwinger model, and ii) non-equilibrium nature of our process. The chiral charge of the original quark-antiquark pair with time is screened by the electric field, which then consequently decays producing additional chiral quark-antiquark pairs – because the set-up describing the separating quark and antiquark jets is far from equlibrium, the axial charge keeps oscillating around its equilibrium value of $\Delta Q_5 = 0$. Because the axial anomaly in $(1+1)$ dimensions couples the axial and vector currents, as indicated by (5.5) and (5.6), the oscillations of axial charge translate into the

oscillations of electric current[2]. We will now couple our theory to the $(3+1)$ dimensional electromagnetic field, and show that the fluctuations of electric current induced by the anomaly indeed source the soft photon production.

5.3 The soft photon production due to the axial anomaly

In the previous section we have considered the sources moving along the light-cone, and have demonstrated that the axial anomaly leads to the undamped axial charge oscillations with frequency m (the mass of the scalar meson). Let us now consider a more realistic case when the sources move with velocity $v < 1$ given by (5.4). We will solve equation (5.7) and using the bosonization relation (5.5) get the total electric current induced by the quark-antiquark pairs. We then couple this current to $(3+1)$ electromagnetic field and compute the rate of the soft photon bremsstrahlung.

The general solution to the equation of motion (5.7) is given by

$$\phi(x) = \phi_0(x) + i \int d^2x' D_R(x - x')(-m^2 \phi_{ext}(x')), \tag{5.19}$$

where $D_R(x)$ is the retarded scalar field propagator and $\phi_0(x)$ satisfies the Klein-Gordon equation (see A.2). Taking the Fourier transform of (2.72)

$$\tilde{j}^{\mu}_{ext}(p) = -\frac{1}{\sqrt{\pi}} \epsilon^{\mu\nu}(-ip_\nu)\tilde{\phi}_{ext}(p), \tag{5.20}$$

we can solve for $\tilde{\phi}_{ext}(p)$

$$\tilde{j}^{0}_{ext}(p) = -\frac{1}{\sqrt{\pi}}(-ip_1)\tilde{\phi}_{ext}(p) \Rightarrow \tilde{\phi}_{ext}(p) = -i\frac{\sqrt{\pi}}{p_1}\tilde{j}^{0}_{ext}(p). \tag{5.21}$$

Let us recall that the direction of p^1 is along the jet axis, which we choose to be the z direction, therefore $p^1 = -p_1 \equiv p_z$. We are only interested in the

[2]This is the $(1+1)$ analog of the Chiral Magnetic Wave [98] – a gapless collective mode induced by the axial anomaly in $(3+1)$ dimensional hydrodynamics.

contribution to (5.19) which is induced by the interaction with the external source; therefore we can write the solution in momentum space as

$$\tilde{\phi}(p) = \frac{-m^2\tilde{\phi}_{ext}(p)}{-p_\mu p^\mu + m^2} = -m^2\left(i\frac{\sqrt{\pi}}{p_z}\tilde{j}^0_{ext}(p)\right)\frac{1}{-p_\mu p^\mu + m^2}; \tag{5.22}$$

this is the scalar field induced by the external source. We will need the Fourier transform of (5.3) and it is given by

$$\tilde{j}^0_{ext}(p) = i\frac{2vp_z}{p_0^2 - v^2p_z^2}. \tag{5.23}$$

We also need j^1_{ext}, which can be computed using the conservation equation $\partial_0 j^0_{ext} = -\partial_1 j^1_{ext}$:

$$\tilde{j}^1_{ext}(p) = -\frac{p^0}{p_1}\tilde{j}^0_{ext}(p) = i\frac{2vp^0}{p_0^2 - v^2p_z^2}. \tag{5.24}$$

The induced meson field in momentum space can now be writen down as

$$\tilde{\phi}(p) = \frac{-1}{p_\mu p^\mu - m^2}\frac{2\sqrt{\pi}m^2v}{p_0^2 - v^2p_z^2}. \tag{5.25}$$

By taking the inverse Fourier transform of (5.25) and using the bosonization relation (5.5), we can compute the induced vector current $j^\mu(x)$.

So far we have been considering only the strong interaction dynamics that within a jet was modeled by a $(1+1)$ dimensionally reduced effective theory. Since we know that all quarks possess in addition to color also the electric charge, they couple to electromagnetic fields, with a different coupling constant $\sim e$. The electromagnetic field of course is not confined within a string (unlike the gauge field B_μ that we considered so far) and so can propagate in $(3+1)$ dimensions. Therefore we have to couple the total current j_{tot} of the $(1+1)$ quarks to the $(3+1)$ dimensional electromagnetic gauge field A_μ. Our system thus resembles a quantum wire where the charges propagate only along the wire but can radiate photons in $(3+1)$ dimensions. We illustrate this in Fig. 5.3

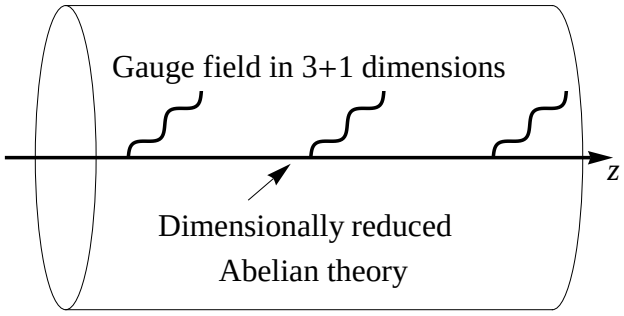

Figure 5.3: Electrically charged $1+1$ current, resembling a quantum wire, coupled to a $3+1$ dimensional electromagnetic field.

The resulting theory has a familiar form

$$\mathcal{L} = -\frac{1}{4}F_{\mu\nu}F^{\mu\nu} + j^{\mu}_{tot}A_{\mu}. \tag{5.26}$$

The photon bremsstrahlung spectrum can now be evaluated using the standard formula

$$\frac{dN_\gamma}{d^3p} = \frac{1}{(2\pi)^3}\frac{1}{2p^0}|\tilde{j}^{\mu}_{tot}(p)\tilde{j}^{*}_{tot,\mu}(p)|, \tag{5.27}$$

where $\tilde{j}_{tot}$ is the Fourier transform of the current. In $3+1$ dimensions, the photon distribution will depend on the (3+1) Fourier transform of the current, therefore we make the identification $p_\mu p^\mu = p_0^2 - p_z^2 = p_\perp^2$. The contribution from the sea quarks (i.e. the quarks produced from the vacuum by the external source) is given by

$$\tilde{j}^{\mu}_{\rm sea}(p) = -eQ_f\frac{1}{\sqrt{\pi}}\epsilon^{\mu\nu}(-ip_\nu)\tilde{\phi}(p) = -ieQ_f\frac{\epsilon^{\mu\nu}p_\nu}{p_\perp^2 - m^2}\frac{2m^2 v}{p_0^2 - v^2p_z^2} \tag{5.28}$$

where Q_f is the fraction of the electric charge for a given quark flavor. Note that the spatial component is now in the z direction, so in (5.28) we should take $\epsilon^{03} = -\epsilon^{30}$=1. We should also add to (5.28) the contribution from valence quarks – the original quark and antiquark moving back-to-back along the z

direction with velocities v. Their current is given by

$$\begin{aligned} j^0_{\rm val}(x) &= eQ_f\delta(x)\delta(y)[\delta(z-vt)\theta(z)-\delta(z+vt)\theta(-z)] \\ j^3_{\rm val}(x) &= eQ_f\delta(x)\delta(y)[v\delta(z-vt)\theta(z)+v\delta(z+vt)\theta(-z)] \end{aligned} \tag{5.29}$$

We now take the Fourier transform

$$\begin{aligned} \tilde{j}^0_{\rm val}(p) &= e\int d^4x e^{ip\cdot x} j^0_{\rm val}(x) =^{\epsilon\to 0} e\int_0^\infty dt e^{ip^0t-\epsilon t}\left(e^{-ip_zvt}-e^{ip_zvt}\right) \\ &= ieQ_f\frac{2vp_z}{p_0^2-v^2p_z^2}. \end{aligned} \tag{5.30}$$

Similarly,

$$\tilde{j}^3_{\rm val}(p) = ie\frac{2vp^0}{p_0^2-v^2p_z^2}. \tag{5.31}$$

The total current that contributes to the photon production is given by the sum of the sea and valence contributions:

$$\tilde{j}^\mu_{\rm tot}(p) = \tilde{j}^\mu_{\rm sea}(p)+\tilde{j}^\mu_{\rm val}(p). \tag{5.32}$$

From (5.27) and (5.32), we can now compute the photon spectrum. Let us consider the case of Z_0 decay to quarks; to do so we have to introduce the probability for Z_0 to decay to a certain flavor of quark. The final formula for the photon spectrum is given by

$$\begin{aligned} \frac{dN_\gamma}{d^3p} &= \left(\frac{\Gamma_{uu}+\Gamma_{cc}}{\Gamma_{\rm hadron}}\left(\frac{2}{3}\right)^2+\frac{\Gamma_{dd}+\Gamma_{ss}+\Gamma_{bb}}{\Gamma_{\rm hadron}}\left(\frac{1}{3}\right)^2\right) \\ &\cdot\ \frac{1}{(2\pi)^3}\frac{1}{2p^0}e^2\frac{4v^2}{(p_0^2-v^2p_z^2)^2}p_\perp^2\left(1+\frac{m^2}{p_\perp^2-m^2}\right)^2 \\ &= \left(B_{2/3}\left(\frac{2}{3}\right)^2+B_{1/3}\left(\frac{1}{3}\right)^2\right)\frac{1}{(2\pi)^3}\frac{1}{2p^0}e^2\frac{4v^2}{(p_0^2-v^2p_z^2)^2}p_\perp^2 \\ &\cdot\ \left(1+\frac{m^2}{p_\perp^2-m^2}\right)^2 \end{aligned} \tag{5.33}$$

where Γ_{ff} is the decay width of Z_0 to quark-antiquark of flavor f and $\Gamma_{\rm hadron}$

is the total decay width of Z_0 to hadrons; the Particle Data Group [99] gives the values $B_{2/3} = 0.331$ and $B_{1/3} = 0.669$.

The formula (5.33) is the main result of this chapter. Without the second term in the parenthesis, it is just the usual formula for the bremsstrahlung radiation off the original quark and antiquark produced by the Z_0 decay. The second term in the parenthesis is the contribution of the quantum back-reaction of the vacuum – in other words, this term represents the photons produced by the transient quark-antiquarks pairs created in the fragmentation of the string. This term originates from the scalar propagator of the field ϕ which in our model is stable, so we get a spectral density of an infinitely narrow resonance – so there is a sharp resonance in photon production at $p_\perp = m$, the frequency of the vacuum current oscillation. It is important to note that in the soft photon limit of $p_\perp \to 0$, the two terms in the parenthesis cancel each other – this is in accord with the Low theorem stating that the very soft photons can be produced only by the asymptotic states – the charged mesons. In our case, the transient quarks and antiquarks are ultimately bound into neutral mesons and so are not allowed to contribute to the photon spectrum in the $p_\perp \to 0$ limit.

5.4 Phenomenology of soft photon production

It is clear that our model is unrealistic in assuming the zero width of the meson ϕ – all mesons that exist in the hadron spectrum possess non-zero width. Moreover, the mass m in reality cannot be a fixed number, as the scalar meson of our effective theory represents the entire hadron spectrum. To make our model more realistic we thus have to i) consider a distribution in m and ii) to account for a finite width of the mesons. To reach the objective i), let us first consider the potential acting between the static fermions in the Schwinger model that we use. For a fermion-antifermion pair separated by the distance r, the potential is given by (see (2.102))

$$V(r) = \frac{g\sqrt{\pi}}{2}\left(1 - e^{-\frac{g}{\sqrt{\pi}}r}\right). \tag{5.34}$$

At large distances, the potential is screened by the produced pairs, but at short distances $r \ll m^{-1}$ the potential is linear,

$$V(r) \simeq \frac{g\sqrt{\pi}}{2}\frac{g}{\sqrt{\pi}}r = \frac{g^2}{2}r = \frac{\pi}{2}m^2 r, \quad r \ll m^{-1}, \tag{5.35}$$

with the string tension $\kappa^2 = \frac{\pi}{2}m^2$. To introduce a distribution in m, let us assume that the string tension fluctuates with a Gaussian probability distribution [100]

$$P(\kappa^2) = \sqrt{\frac{2}{\pi < \kappa^2 >}}e^{-\frac{\kappa^2}{2<\kappa^2>}}, \tag{5.36}$$

where

$$< \kappa^2 >= \int_0^\infty d\kappa P(\kappa^2)\kappa^2. \tag{5.37}$$

We use the mean value of the string tension $< \kappa^2 >= 0.9$ GeV/fm suggested by the lattice studies and Regge phenomenology.

To account for a finite decay width of the meson, we write the propagator as

$$\frac{1}{p_\perp^2 - m^2} \to \frac{1}{p_\perp^2 - m^2 + i\gamma^2} \tag{5.38}$$

where γ is an effective width. From (5.33) it is clear that the soft photon production will be dominated by the longest living resonances. Using the PDG [99] values for the masses and widths of the neutral isoscalar resonances, we find the values of $\gamma = \sqrt{m\Gamma}$ in the range of $\gamma \simeq 8 \times 10^{-4}$ GeV for the η meson, and $\gamma \simeq 8 \times 10^{-2}$ GeV for the ω meson. We will see that the value of γ extracted from the fit to the DELPHI data on soft photon production falls in this range.

The DELPHI Collaboration [90] measured the photons with transverse momenta $p_\perp < 80$ MeV and total energies within $0.2 < E_\gamma < 1$ GeV. We thus substitute (5.38) in (5.33) and compute the total number of photons in this kinematic domain

$$N_\gamma = \int dm \sqrt{\frac{\pi}{2}}\, P(\frac{\pi}{2}m^2) \left(\int d^3p \frac{dN}{d^3p}\right) \tag{5.39}$$

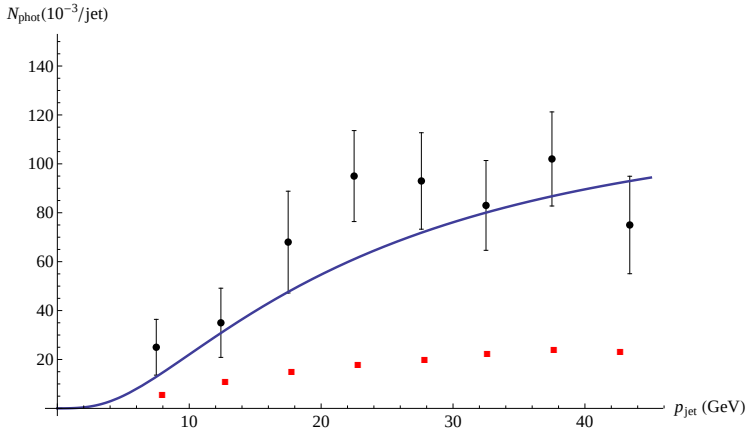

Figure 5.4: The soft photon yield as a function of the jet momentum. The circles are the DELPHI Collaboration data (see text), and the squares represent the calculations of soft photon production based on the Low theorem (see (5.1)). The solid line is our result.

by integrating over the appropriate range of transverse momentum and energy. Since γ is small, we can use

$$\delta(x) = \lim_{\epsilon \to 0} \frac{1}{\pi} \frac{\epsilon}{x^2 + \epsilon^2} \tag{5.40}$$

and write

$$\left| 1 + \frac{m^2}{p_\perp^2 - m^2 + i\gamma^2} \right|^2 = \frac{p_\perp^4 + \gamma^4}{(p_\perp^2 - m^2)^2 + \gamma^4} \to \left(1 + \frac{p_\perp^4}{\gamma^4} \right) \left(\gamma^2 \frac{\pi}{2m} \right) \delta(p_\perp - m) \tag{5.41}$$

We use the delta function to eliminate the integral over $p_\perp$ in (5.39). We use the standard value of the string tension $< \kappa^2 >= 0.9$ GeV/fm and extract the value of the parameter $\gamma = 0.003$ GeV by fitting to the measured experimental photon yield. In Fig. 5.4 we show the result as compared to the DELPHI data on the total number of photons as a function of the jet momentum [90]. One can see that our mechanism describes the observed enhancement reasonably well, with the fitted value of the parameter $\gamma = 0.003$ GeV within a reasonable range expected for neutral isoscalar resonances.

5.5 Discussion

We have modeled the propagation of a high energy quark through the confining QCD vacuum by using an exactly soluble $1+1$ dimensional massless Abelian gauge model motivated and used in previous chapters. In this theory, we have established the phenomenon of coherent oscillations of the axial and vector (electric) charges coupled by the axial anomaly and induced by the propagating high energy quark. These oscillations originate from the continuous production of quark-antiquark pairs pulled from the vacuum to screen the axial and electric charges of the external source. We have found that soft photons provide an important signature of this mechanism, as it leads to a strong enhancement of the soft photon yield. At the cost of introducing an adjustable parameter, our model can then describe the DELPHI data on the soft photon production.

We readily admit that the use of a $1+1$ model, and the procedure we use to compare our results to the experimental data can be questioned. Moreover, our numerical result depends on an adjustable parameter that cannot be determined within our model (even though its value appears reasonable). Nevertheless, we hope that the described mechanism of string fragmentation may be close to the one in real $(3+1)$ QCD. It would be interesting to generalize our study to a $(3+1)$ model as it would allow, for example, to address the effects of spin and chirality on the fragmentation of a polarized quark (see [101] for an attempt in this direction).

Chapter 6

Further applications

One of the most important indications that an electric flux tube exists between color charges comes from lattice studies. This presents a clear indication of confinement. On the other hand, it has been observed that the transverse profile of the electric field resembles that of the ANO vortex [102, 103]. This supports further the assumption we presented above and which is known for a long time, that the QCD string is Abelian. In previous chapters we assumed that the Schwinger model describes the dynamics of fermions along the QCD string when the endpoints move with relativistic speeds. We will argue however, based on the arguments given above in 2.2 that the dynamics of massless fermions along the string is described in a similar way even for static endpoints.

Recently a measurement of the chiral condensate in the presence of static color charges was performed [104]. The chiral condensate was found to be suppressed around the string, which indicates a partial restoration of chiral symmetry in the confining background. Using a probabilistic model of the fluctuating "thin" string [105] (the "thin" string is 1+1 dimensional, described by the Schwinger model) we can describe reasonably well the result in [104].

6.1 Probabilistic fluctuation of the thin string

We will argue that the partial restoration of chiral symmetry observed in the lattice study mentioned above, can be described if one assumes the presence

of a "thin" $(1+1)$ dimensional string with its position fluctuating in the transverse plane as shown in Fig. 6.1. Let us denote the physical $(3+1)$

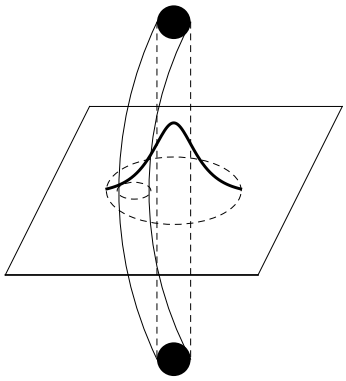

Figure 6.1: Thin string fluctuating in the transverse plane.

dimensional electric field measured on the lattice by $E^{3+1}_{phys}(x_t)$, where x_t is the transverse coordinate, and the electric field along the thin string in the $(1+1)$ description by E^{1+1}. We assume that both descriptions of the string should yield the same string tension, so the energy per unit length of the string should be equal:

$$\frac{1}{2}\int d^2x_t (E^{3+1}_{phys}(x_t))^2 = \frac{1}{2}(E^{1+1})^2 \tag{6.1}$$

Let us now assume that $P(x_t)$ is the probability for finding the thin string in the transverse plane at a position x_t. From the condition (6.1), we can constrain this probability distribution:

$$(E^{3+1}_{phys}(x_t))^2 = (E^{1+1})^2 P(x_t). \tag{6.2}$$

Since

$$\int d^2x_t P(x_t) = 1, \tag{6.3}$$

the requirement (6.1) is fulfilled.

6.2 Chiral symmetry restoration

Now we can use the lattice data on the distribution of electric field to extract the probability distribution (6.2). The knowledge of the dependence of the chiral condensate in the $1+1$ dimensional theory on the electric field together with the probability distribution will then allow us to predict the distribution of the chiral condensate around the confining flux tube. Recall the bosonization relation

$$\bar{\psi}\psi = -\frac{ge^{\gamma}}{2\pi^{3/2}}\cos(2\sqrt{\pi}\phi), \tag{6.4}$$

where $\gamma \approx 0.5772$ is the Euler number.

The chiral condensate can be evaluated through the Feynman-Hellmann theorem by differentiating the energy of the ground state in the presence of an electric field E^{1+1} with respect to the fermion mass m, in the chiral limit $m = 0$ [43] (see (2.91)):

$$\left\langle \bar{\psi}\psi(x) \right\rangle_{E^{1+1}} = -\frac{ge^{\gamma}}{2\pi^{3/2}}\cos\left(\frac{2\pi E^{1+1}}{g}\right). \tag{6.5}$$

where x is the longitudinal coordinate. We see that the value of the condensate is constant along the string and depends only on the value of the background electric field.

Let us now assume that the thin string fluctuates in the transverse plane (see Fig. 1), and the corresponding probability distribution is $P(x_t)$ normalized by (6.3). If the effective radius of the string is a, then the probability to find a string at a given transverse position is given by the integral of $P(x_t)$ over the string area, i.e. $\pi a^2 P(x_t)$. If the string with its electric field is present at a given x_t, it will modify the value of the chiral condensate according to (6.5). If not, then there will be no electric field and the chiral condensate will not be modified, so within the Schwinger model it would be given by

$$\left\langle \bar{\psi}\psi \right\rangle (E^{1+1} = 0) \equiv \left\langle \bar{\psi}\psi \right\rangle_0 .$$

Therefore in this picture the chiral condensate in the transverse plane can be

computed as

$$\begin{aligned} \left\langle \bar{\psi}\psi(x_t) \right\rangle &= \left(1 - \pi a^2 P(x_t)\right) \left\langle \bar{\psi}\psi \right\rangle_0 \\ &+ \pi a^2 P(x_t) \left\langle \bar{\psi}\psi \right\rangle_{E^{1+1}} . \end{aligned} \tag{6.6}$$

We will see below that from the fit to the lattice data the value of the effective radius of the string a appears comparable to the lattice spacing, i.e. the string is indeed "thin."

In [104], the authors compute on the lattice the following observable that quantifies the effect of confining flux tube on the chiral condensate:

$$r(x_t) = \frac{\langle \bar{q}q(x_t) W \rangle}{\langle \bar{q}q \rangle \langle W \rangle}, \tag{6.7}$$

where W is the Wilson loop operator of the static quarks. In our model, this quantity is given by

$$r(x_t) = \frac{\left\langle \bar{\psi}\psi(x_t) \right\rangle}{\left\langle \bar{\psi}\psi \right\rangle_0}. \tag{6.8}$$

The suppression of the chiral condensate has been described recently in terms of the σ meson cloud surrounding the string [106]. To evaluate this quantity from (6.6), we now need an independent information on the probability distribution $P(x_t)$. Since $P(x_t)$ is the probability to find a longitudinal chromoelectric field at a given point x_t, the most direct source of information about it is the profile of chromoelectric field in the confining flux tube. There have been many lattice studies of the profile of the chromoelectric field between two static color charges. Here we use the recent lattice results of [103] (see also [107]). The measured chromoelectric field, as a function of the transverse coordinate, was shown to be described well by the following parameterization:

$$E(x_t) = \frac{\phi}{2\pi} \frac{\mu^2}{\alpha} \frac{K_0[(\mu^2 x_t^2 + \alpha^2)^{1/2}]}{K_1(\alpha)}, \tag{6.9}$$

where the values of the parameters above depend on the lattice coupling constant $\beta = 2N/g^2$ and the number of "cooling steps" used to remove the short wavelength fluctuations. In [103], the parameters μ, ϕ and α were computed

for four values of the coupling. In Fig. 6.2, we plot the profile of the electric field as a function of the transverse coordinate, computed at $\beta = 6.01$ with 10 cooling steps in [103]. We still have to fix the value of a in order to compare

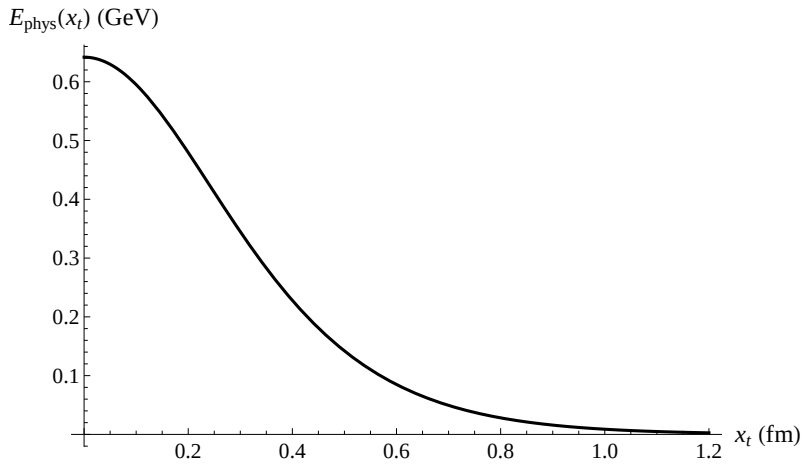

Figure 6.2: The longitudinal chromoelectric field between two static charges as given by (6.9).

with data. By choosing the same values of parameters as above and by fitting to the lattice data [104], as shown in Fig. 6.3, we get $a = 1.12 a_{latt}$. a_{latt} is the lattice spacing which also depends on the coupling. We have chosen the value of β which gives the best fit and smallest a.

6.3 Anomaly inflow

Anomaly inflow was introduced by Callan and Harvey [108]. Let's consider a complex scalar field

$$\phi(x) = \phi_1(x) + i\phi_2(x) = f(x)e^{i\theta(x)}, \tag{6.10}$$

with vacuum expectation value $\langle\phi\rangle = \mu \neq 0$. This is similar to the Abrikosov-Nielsen-Olesen string considered above, in 2.2. We assume that the string axis is along the z direction. We work in cylindrical coordinates (ρ, ϕ, z). Due to the symmetry of the problem, we assume that $f = f(\rho)$. In four dimensions,

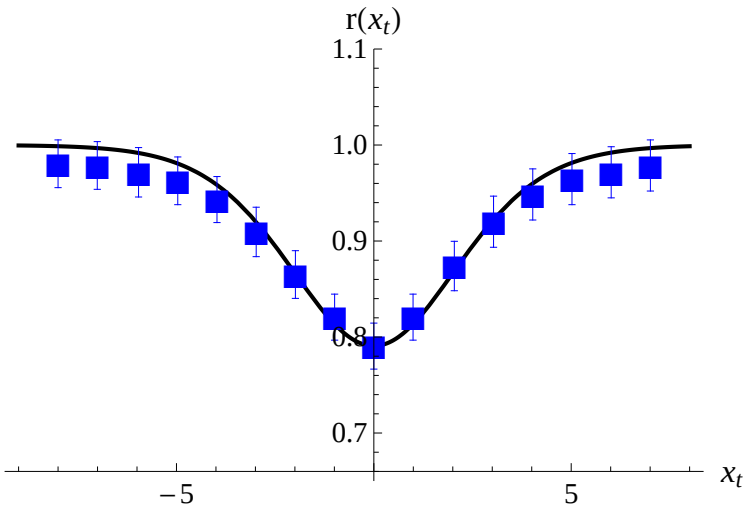

Figure 6.3: The chiral condensate around a confining flux tube as a function of the transverse distance. The solid line is the result of our model based on (6.8). The squares are the lattice data (see text).

the boundary conditions are still the same as above, namely

$$f(\rho) \underset{\rho\to 0}{\to} 0, \;\; f(\rho) \underset{\rho\to\infty}{\to} \mu, \;\; \theta \underset{\rho\to\infty}{\to} n\phi. \tag{6.11}$$

We in turn assume the following coupling between the scalar and fermions

$$\mathcal{L}_f = \bar{\psi} i\partial\!\!\!/ \psi - \bar{\psi} f(\rho) e^{i\gamma^5\theta}\psi. \tag{6.12}$$

From an index theorem [109], the Dirac equation has $|n|$ chiral zero modes, which move along the string (along $-z$ direction for $n > 0$ and $+z$ direction for $n < 0$). In [108] an explicit solution of these zero modes was given and it was shown that their wavefunction falls off exponentially away from the string in the transverse direction. The solution is similar to (2.43). This can be understood heuristically to be a result of fermions acquiring mass outside the string, but they remain massless inside. We can write the effective action for these zero modes

$$S = \int d^2x \; \bar{\psi}\gamma^\mu (i\partial_\mu - gA_\mu)\frac{1-\bar{\gamma}}{2}\psi, \tag{6.13}$$

where $\bar{\gamma} = \gamma^0\gamma^3$ and g is the coupling constant. The theory in (6.13) is anomalous with consistent anomaly given by[1]

$$\partial_\mu J^\mu = \frac{g}{4\pi}\epsilon^{\mu\nu}\partial_\mu A_\nu. \tag{6.14}$$

The indices μ, ν take values $0, 3$. We will only consider the Abelian case in the following. By consistent here we denote currents which are obtained by varying the action with respect to the gauge field.

The anomaly we mentioned above breaks conservation of charge along the string. The theory in the bulk has to be gauge invariant and this is achieved by the so called *anomaly inflow*. In order for the charge to be conserved, there should be an inflow of charge from the bulk to the string. The diagram in Fig. 6.4 contributes to such a process and it can be shown to give the following inflow current [108, 110, 111]

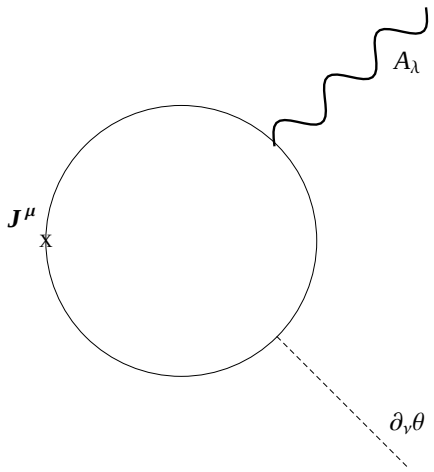

Figure 6.4: Feynman diagram contributing to the vacuum current.

$$\langle J^\mu \rangle = \frac{g}{8\pi^2}\epsilon^{\mu\nu\kappa\lambda}\partial_\nu\theta F_{\kappa\lambda}. \tag{6.15}$$

(In the case of a non-Abelian gauge group, we have to consider diagrams with two gauge field external lines. See [111] for an explicit calculation.) The

[1]the theory also has gravitational anomalies, but we don't consider them here

anomaly equation (6.14) is derived by requiring

$$[\partial_x, \partial_y]\theta = 2\pi\delta(x)\delta(y), \tag{6.16}$$

(in our conventions $\epsilon^{0123} = \epsilon^{03} = 1$) and the solution is $\theta = \phi$.

6.4 Electric charge distribution of the jet

If the QCD string has the form of an axionic string, as proposed for example in [112, 113], there could be interesting consequences. The existence of the inflow current (6.15), could result in transverse modification of charge distribution of jets for example. Let us consider again the case of quark di-jet, where fast moving quark-antiquark in the z-direction, have charge g and velocity v (see Fig. 6.5). We work in cylindrical coordinates (ρ, ϕ, z). The fields as a function

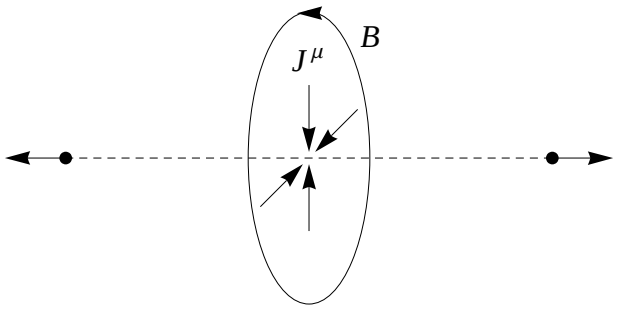

Figure 6.5: Inflow current in the di-jet event.

of time, distance ρ from the string, are given by [114] (for one charge)

$$\begin{aligned} E_1(t) &= g\frac{\gamma\rho}{(\rho^2+\gamma^2v^2t^2)^{3/2}}, \\ B_2(t) &= vE_2(t), \\ E_3(t) &= -g\frac{\gamma vt}{(\rho^2+\gamma^2v^2t^2)^{3/2}}, \end{aligned} \tag{6.17}$$

where $\gamma = (1-v^2)^{-1}$. We choose $t = 0$, the time when the charge density in the transverse plane of the string is observed. We see that the only component of the field strength that contributes is $F_{\rho z} = -B_2\cos\phi$. Using (6.15), one

might expect

$$j^0 = -\frac{g}{8\pi^2}\frac{1}{\rho}\left(-\cos\phi B_2(t=0)\right) = \frac{v\gamma g^2}{8\pi^2}\frac{1}{\rho^3}\cos\phi. \tag{6.18}$$

It should be noted that the way we have defined the coupling constant g, it will be proportional to the electromagnetic coupling e (this is not the two dimensional coupling we showed in the previous chapters). Therefore, the effect in (6.18) will be suppressed as $\sim e^2$.

6.5 Discussion

From Fig. 6.3, one can see that our simple model of fluctuating thin string describes the lattice results quite well. This lends additional support to the dual Meissner mechanism of confinement, and suggests that the longitudinal dynamics along the core of the string can be adequately described by the dimensionally reduced $(1+1)$ dimensional model. In the future, it would be interesting to extend this approach to nonabelian strings.

Another promising direction is to apply our findings to the phenomenology of nonperturbative jet fragmentation. We have already observed that the longitudinal momentum distributions within a jet are adequately described by the $(1+1)$ string model (see chapters 3, 4 and 5). The Fourier transform of the transverse coordinate distribution of the "thin string" extracted from the lattice may allow to describe also the nonperturbative transverse momentum distribution inside the jet; this introduces the "intrinsic" transverse momentum $k_t \sim 1$ GeV as required by the data.

It would also be interesting for experimentalists and lattice QCD experts to study the current inflow in the presence of the QCD string. This could lend more support on the claim that the string is axionic.

Chapter 7

Conclusion

In this thesis we have revisited a very well known model, the Schwinger model, in order to study the real-time dynamics of the QCD string, multi-particle production, parton to hadron transition (hadronization) and the connection between confinement and chiral symmetry breaking. Our motivation for using this model is not only the fact that it shares with QCD many important features such as confinement, θ-vacuum, etc. We motivate it further by accepting a specific model of the QCD vacuum, the dual superconductor theory. Using the procedure of Abelian projection the QCD string can be shown to be Abelian. Dimensional reduction is justified from the localization of fermionic zero modes along the string and also from the consideration of very energetic jets.

In chapter 3 we saw, in coordinate space, that the scenario of quark-antiquark moving back to back, results in the string stretching between them to break. From the index theorem in $1+1$ dimensions, we observed that particle creation, or the form of the string, is determined by the anomaly. In order to make contact to the experimental data, we introduced two parameters to the theory, an infrared scale Q_0 assumed to be the scale where the pQCD cascade stops and the mass of the final hadrons m. The result agrees reasonably well with experiment for physically justified values of these parameters.

One of the main motivations for developing a dynamical model of string fragmentation is its applicability in heavy ion physics. An important tool for

studying the properties of the quark-gluon plasma is the effect the medium has in hard probes. In the simplest example of the medium consisting of static color sources (see chapter 4), we were able to explain some aspects of the modification of fragmentation functions of jets, measured by CMS collaboration. It was shown that the Landau-Pomeranchuk-Migdal effect can also be derived nonperturbatively. Also, the nonperturbative aspect of final gluon radiation could be important in explaining the suppression of intermediate transverse momentum hadrons.

Using this model, in chapter 5, we were able to address a long lasting puzzle in hardon physics - the soft photon yield in high energy processes, with hadrons in the final state, is much higher than expected from Low theorem. As the quark fragments, an electromagnetic current is created from the vacuum, which serves as a source of soft photons. We showed that this source, by considering the fluctuations of the string tension, can be one of the mechanisms giving the excess of observed photons.

We also studied the recently observed phenomenon in lattice QCD of the fact that the chiral symmetry is partially restored along the QCD string. The transverse spread of the chromoelectric field between static quarks is viewed as defining the probability distribution for the string's transverse location. We get the probability distribution from measurements on the lattice of the electric field profile between static quark-antiquark pair and we calculate the chiral condensate. The result agrees well with data if we assume the effective width of the string to be of the order of lattice spacing. We also speculated on the possibility that the QCD string may resemble an axionic string and this could lead to observable effects on electric charge distribution of jets.

It would be interesting in the future to have a hybrid approach, where the DGLAP evolution, together with induced radiation and the dynamical string fragmentation are included. It would also be interesting to systematically derive the dimensionally reduced theory. One could then describe the nonpertrubative contribution to the transverse momentum of the jet. Another application would be for example the effects of spin and chirality on the fragmentation of a polarized quark.

Appendix A

Conventions and solution of equation of motion

A.1 Conventions

We denote the coordinate 2-vector as

$$x^\mu = (x^0, x^1) = (t, x). \tag{A.1}$$

The metric in Minkowski space has the following signature

$$g_{\mu\nu} = \text{diag}(-1, 1). \tag{A.2}$$

We make the following choice of the gamma matrices

$$\gamma^0 = \sigma_2, \quad \gamma^1 = i\sigma_1, \quad \gamma^5 = \gamma^0\gamma^1 = \sigma_3, \tag{A.3}$$

where σ_i are the Pauli matrices, defined in the usual way

$$\sigma_1 = \begin{pmatrix} 0 & 1 \\ 1 & 0 \end{pmatrix}, \ \sigma_2 = \begin{pmatrix} 0 & -i \\ i & 0 \end{pmatrix}, \ \sigma_3 = \begin{pmatrix} 1 & 0 \\ 0 & -1 \end{pmatrix} \tag{A.4}$$

Dirac spinors are denoted as

$$\psi_L = \begin{pmatrix} \psi_1 \\ 0 \end{pmatrix}, \quad \psi_R = \begin{pmatrix} 0 \\ \psi_2 \end{pmatrix} \tag{A.5}$$

Where L, R means left and right chirality, which follows from

$$\gamma^5 \psi_{L,R} = \pm \psi_{L,R}. \tag{A.6}$$

A.2 Green's function

We consider the Klein-Gordon equation with a source

$$(\Box + m^2)\phi(x) = j(x) \tag{A.7}$$

The solution of (A.7) can be constructed by first computing the Green's function (retarded propagator) D_R, which satisfies

$$(\Box + m^2)D_R(x) = -i\delta^{(2)}(x). \tag{A.8}$$

The general solution of (A.7) is then given by

$$\phi(x) = \phi_0(x) + i \int d^2x' D_R(x - x') j(x'), \tag{A.9}$$

where $(\Box + m^2)\phi_0(x) = 0$. In momentum space, the retarded propagator is given by

$$\tilde{D}_R(p) = \frac{i}{p^2 - m^2}. \tag{A.10}$$

In coordinate space

$$\begin{aligned} D_R(x) &= \int \frac{d^2p}{(2\pi)^2} e^{-ip\cdot x} \frac{i}{p^2 - m^2} \\ &= \int_{-\infty}^{\infty} \frac{dp}{2\pi} e^{ipx} \int_{-\infty}^{\infty} \frac{dp^0}{2\pi i} \frac{-1}{(p^0 - E_p)(p^0 + E_p)} e^{-ip^0 x^0}, \end{aligned} \tag{A.11}$$

where we denote the spatial component of the momentum $p^1 = p$ and $E_p \equiv \sqrt{p^2 + m^2}$. We perform the contour integral over p^0, using the usual prescription

$$D_R(x) = \int_{-\infty}^{\infty} \frac{dp}{2\pi} e^{ipx} \frac{1}{2E_p} \left(-e^{iE_p x^0} + e^{-iE_p x^0} \right). \tag{A.12}$$

We make the change of variables $p = m \cosh y$,

$$D_R(x) = -\int_{-\infty}^{\infty} \frac{dy}{4\pi} \left[e^{im(x \sinh y + x^0 \cosh y)} - e^{im(x \sinh y - x^0 \cosh y)} \right]. \tag{A.13}$$

For $(x^0)^2 - x^2 > 0$ we can write

$$x \sinh y \pm x^0 \cosh y = \pm \sqrt{(x^0)^2 - x^2} \cosh \left(y \pm \tanh^{-1} \frac{x}{x^0} \right), \tag{A.14}$$

therefore,

$$D_R(x) = -\int_{-\infty}^{\infty} \frac{dy}{4\pi} \Bigg[\quad e^{im\sqrt{(x^0)^2 - x^2} \cosh y} \\ - e^{-im\sqrt{(x^0)^2 - x^2} \cosh y} \Bigg] \theta((x^0)^2 - x^2). \tag{A.15}$$

We have made the change of variables $y \pm \tanh^{-1} \frac{x}{x^0} \to y$. The result (A.15) can be written as

$$D_R(x) = -i \int_0^{\infty} \frac{dy}{\pi} \sin[m\sqrt{(x^0)^2 - x^2} \cosh y] \theta((x^0)^2 - x^2). \tag{A.16}$$

Using identity 8.411, number 11 in [115], we get

$$D_R(x) = -\frac{i}{2} J_0(m\sqrt{(x^0)^2 - x^2}) \theta((x^0)^2 - x^2) \theta(x^0). \tag{A.17}$$

Outside the lightcone, $(x^0)^2 - x^2 < 0$, the Green's function is proportional to $K_0(m\sqrt{x^2 - (x^0)^2})$.

A.3 Solution of inhomogeneous Bessel equation

We will solve (3.13) assuming Lorentz invariance. Let's define

$$\tau = \sqrt{t^2 - x^2} \tag{A.18}$$

We then have $\phi = \phi(\tau)$. The equation (3.13) becomes

$$\phi'' + \frac{1}{m\tau}\phi' + \phi = -\phi_{ext}, \tag{A.19}$$

where the primes indicate derivatives with respect to $m\tau$. This equation is just an inhomogeneous Bessel equation of order zero. The particular solution of this equation is

$$\phi_p(x) = \frac{\pi}{2}\int_0^{m\tau} d\xi\ \xi\left[J_0(\xi)Y_0(m\tau) - J_0(m\tau)Y_0(\xi)\right](-\phi_{ext}(\xi)). \tag{A.20}$$

In the case of quark-antiquark moving back to back in the lightcone, in the region $t^2 - z^2 > 0$, $\phi_{ext} = -\sqrt{\pi}$, therefore

$$\phi_p(x) = \sqrt{\pi}\frac{\pi}{2}\left\{m\tau J_1(m\tau)Y_0(m\tau) - J_0(m\tau)\left[\frac{2}{\pi} + m\tau Y_1(m\tau)\right]\right\} \tag{A.21}$$

using

$$J_n(x)\frac{dY_n}{dx} - \frac{dJ_n}{dx}Y_n(x) = \frac{2}{\pi}\frac{1}{x}, \tag{A.22}$$

we can write

$$\phi_p(x) = \sqrt{\pi}\frac{\pi}{2}\left\{-\frac{2}{\pi}J_0(m\tau) + m\tau\frac{1}{m\tau}\frac{2}{\pi}\right\} = \sqrt{\pi}[1 - J_0(m\tau)]. \tag{A.23}$$

A.4 Compactness of the scalar field

In this section, following [116], we will see that the scalar field ϕ is compact. Using the expression for the axial charge and bosonization relations, we can

write

$$Q_5 = \int dx\ j_5^0 = \int dx\ \psi^\dagger \gamma^5 \psi = \frac{1}{\sqrt{\pi}} \int dx\ \partial_0 \phi. \tag{A.24}$$

The conjugate momentum of the field ϕ is

$$\Pi_\phi = \partial_0 \phi, \tag{A.25}$$

and from the usual equal time commutation relation between the field and its momentum

$$[\phi(x^0, x), \Pi_\phi(x^0, y)] = i\delta(x - y), \tag{A.26}$$

we get

$$[\phi(x), Q_5] = \frac{i}{\sqrt{\pi}}. \tag{A.27}$$

This means that the axial charge is a generator of translations of the field ϕ, namely

$$e^{i\alpha\sqrt{\pi}Q_5} \phi e^{-i\alpha\sqrt{\pi}Q_5} = \phi + \alpha, \tag{A.28}$$

for some given α. The action of $\exp(in\pi Q_5)$, for n integer, on a fermion leaves it unchanged (up to an unphysical sign). This means that the physically distinct states for the bosonic fields are only those in the interval $\phi \in [0, \sqrt{\pi}]$, what we had to show.

Appendix B

$U(1)$ magnetic monopoles

In this appendix we briefly review the concept of the Abelian magnetic monopoles, mostly following [26, 117].

Let's first consider the source free Maxwell equations. They can be combined into two complex equations

$$\begin{aligned} \boldsymbol{\nabla} \times (\boldsymbol{E} + i\boldsymbol{B}) - i\frac{\partial}{\partial t}(\boldsymbol{E} + i\boldsymbol{B}) &= 0, \\ \boldsymbol{\nabla} \cdot (\boldsymbol{E} + i\boldsymbol{B}) &= 0. \end{aligned} \tag{B.1}$$

These equations are invariant under the following transformations

$$\boldsymbol{E} + i\boldsymbol{B} \to \boldsymbol{E}' + i\boldsymbol{B}' = e^{i\alpha}(\boldsymbol{E} + i\boldsymbol{B}). \tag{B.2}$$

If we introduce electric sources to Maxwell's equations, the above symmetry is broken. This symmetry is restored however if we assume that there are magnetic sources as well. The charged object giving rise to these sources, in analogy with its electric counterpart, is called a magnetic monopole and gives rise to a Coulomb like magnetic field

$$\boldsymbol{B} = \frac{Q_M}{4\pi r^2}\hat{\boldsymbol{r}} = \frac{g}{r^2}\hat{\boldsymbol{r}}. \tag{B.3}$$

We have denoted the magnetic charge by g and $\hat{\boldsymbol{r}} \equiv \boldsymbol{r}/|\boldsymbol{r}|$ is the unit vector along the radial direction. We write the electric field of the electric monopole

as

$$\boldsymbol{E} = \frac{Q_E}{4\pi r^2}\hat{\boldsymbol{r}} = \frac{e}{r^2}\hat{\boldsymbol{r}}, \tag{B.4}$$

where e is the electric charge.

Let's assume that there is a point-like magnetic monopole at the origin of the coordinate system

$$\rho_M = 4\pi g \delta^{(3)}(\boldsymbol{x}). \tag{B.5}$$

The magnetic field, away from the sources can still be written as curl of the vector potential, $\boldsymbol{B} = \boldsymbol{\nabla} \times \boldsymbol{A}$. Let's consider the following gauge potential in spherical coordinates[1],

$$\boldsymbol{A} = g\frac{1-\cos\theta}{r\sin\theta}\hat{\boldsymbol{\phi}}. \tag{B.7}$$

It gives rise to the magnetic field

$$\begin{aligned}
\boldsymbol{B} = \boldsymbol{\nabla} \times \boldsymbol{A} &= \frac{1}{r\sin\theta}\left[\frac{\partial}{\partial\theta}(\sin\theta A_\phi) - \frac{\partial A_\theta}{\partial\phi}\right]\hat{\boldsymbol{r}} + \frac{1}{r}\left[\frac{1}{\sin\theta}\frac{\partial A_r}{\partial\phi} - \frac{\partial}{\partial r}(rA_\phi)\right]\hat{\boldsymbol{\theta}} \\
&+ \frac{1}{r}\left[\frac{\partial}{\partial r}(rA_\theta) - \frac{\partial A_r}{\partial\theta}\right]\hat{\boldsymbol{\phi}} \\
&= \frac{1}{r\sin\theta}\left[\frac{\partial}{\partial\theta}(\sin\theta A_\phi)\right]\hat{\boldsymbol{r}} = g\frac{\hat{\boldsymbol{r}}}{r^2},
\end{aligned} \tag{B.8}$$

which is the field of the monopole. We notice that the gauge potential (B.7) is singular at the negative z axis (or $\theta = \pi$), therefore it is not defined there. By choosing different coordinates, the singularity can be shifted at different positions, but we cannot construct a singularity free field everywhere in $\mathbb{R}^3 \setminus \{0\}$. This can be easily shown in the following way. If we integrate the magnetic field over a closed sphere S^2 with the monopole at the center, using Gauss' law, we get

$$\int_{S^2} d\boldsymbol{S}\cdot\boldsymbol{B} = \int_{B^2} d^3x\ \boldsymbol{\nabla}\cdot\boldsymbol{B} = \int_{B^2} d^3x\ \rho_M(\boldsymbol{x}) = 4\pi g, \tag{B.9}$$

[1]The spherical coordinates (r, ϕ, θ) are given in terms of Cartesian coordinates

$$x = r\sin\theta\cos\phi, \quad y = r\sin\theta\sin\phi, \quad z = r\cos\theta. \tag{B.6}$$

where $\partial B^2 = S^2$. On the other hand, using Stokes' theorem

$$\int_{S^2} d\boldsymbol{S} \cdot \boldsymbol{B} = \int_{S^2} d\boldsymbol{S} \cdot (\boldsymbol{\nabla} \times \boldsymbol{A}) = \int_{\partial S^2} d\boldsymbol{x} \cdot \boldsymbol{A} = 0, \tag{B.10}$$

because $\partial S^2 = \emptyset$. This is in contradiction with the above result, which means that $\boldsymbol{A}$ must be singular. Since the potential we chose above is not defined everywhere, we need at least two expressions of the gauge potential at different patches of space. We consider

$$\begin{aligned} \boldsymbol{A}_+ &= g\frac{1-\cos\theta}{r\sin\theta}\hat{\boldsymbol{\phi}}, \quad \theta < \pi - \epsilon : U_+ \\ \boldsymbol{A}_- &= g\frac{-1-\cos\theta}{r\sin\theta}\hat{\boldsymbol{\phi}}, \quad \theta > \epsilon : U_-. \end{aligned} \tag{B.11}$$

The patches $U_\pm$ are shown in Fig. B.1. Potentials $\boldsymbol{A}_\pm$ are well defined in $U_\pm$.

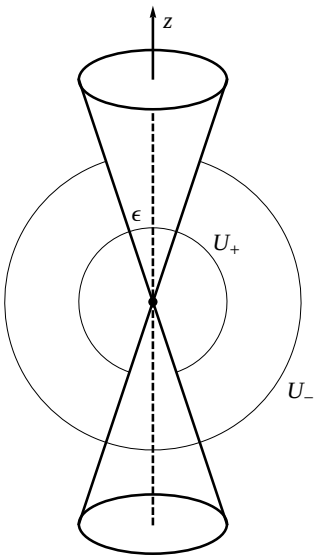

Figure B.1: The choice of the gauge potential in different patches of space.

In the overlap region $U_+ \cap U_-$ both potentials are valid. Since they give the same magnetic field, they should be related by a gauge transformation

$$\boldsymbol{A}_- = \boldsymbol{A}_+ + \boldsymbol{\nabla}\Lambda. \tag{B.12}$$

By using the explicit expressions (B.11), we get

$$\boldsymbol{A}_- - \boldsymbol{A}_+ = \boldsymbol{\nabla}\Lambda. \tag{B.13}$$

In other words,

$$\frac{-2g}{r\sin\theta} = \frac{1}{r\sin\theta}\frac{\partial\Lambda}{\partial\phi}, \tag{B.14}$$

which gives,

$$\Lambda = -2g\phi. \tag{B.15}$$

Let's consider a particle with charge e, coupled to the gauge field. Quantum mechanically, the particle is described by wavefunctions $\psi_\pm$ in regions $U_\pm$ respectively. Similarly as for the gauge field, the wavefunctions in two different patches are related by the gauge transformation

$$\psi_- = e^{ie\Lambda}\psi_+. \tag{B.16}$$

Since the patches intersect along the equator, both wavefuctions apply. Going around the equator

$$\begin{aligned} \phi = 0 \quad &: \quad \psi_- = \psi_+, \\ \phi = 2\pi \quad &: \quad \psi_- = e^{-i2eg2\pi}\psi_+, \end{aligned} \tag{B.17}$$

and requiring that the wavefunction be singlevalued, we get the condition

$$2eg = n, \quad n = 0, \pm 1, \pm 2, \ldots. \tag{B.18}$$

This is the well known Dirac quantization condition.

Bibliography

[1] David J. Gross and Frank Wilczek. Ultraviolet Behavior of Nonabelian Gauge Theories. *Phys.Rev.Lett.*, 30:1343–1346, 1973.

[2] H. David Politzer. Reliable Perturbative Results for Strong Interactions? *Phys.Rev.Lett.*, 30:1346–1349, 1973.

[3] Kenneth G. Wilson. Confinement of Quarks. *Phys.Rev.*, D10:2445–2459, 1974.

[4] J. Goldstone. Field Theories with Superconductor Solutions. *Nuovo Cim.*, 19:154–164, 1961.

[5] Murray Gell-Mann, R.J. Oakes, and B. Renner. Behavior of current divergences under SU(3) x SU(3). *Phys.Rev.*, 175:2195–2199, 1968.

[6] Boris Lazarevich Ioffe, Victor Sergeevich Fadin, and Lev Nikolaevich Lipatov. Quantum chromodynamics: Perturbative and nonperturbative aspects. 2010.

[7] Mikhail A. Shifman, A.I. Vainshtein, and Valentin I. Zakharov. QCD and Resonance Physics. Sum Rules. *Nucl.Phys.*, B147:385–447, 1979.

[8] John C. Collins, Davison E. Soper, and George F. Sterman. Factorization of Hard Processes in QCD. *Adv.Ser.Direct.High Energy Phys.*, 5:1–91, 1988, hep-ph/0409313.

[9] Yakov I. Azimov, Yuri L. Dokshitzer, Valery A. Khoze, and S.I. Troyan. Similarity of Parton and Hadron Spectra in QCD Jets. *Z.Phys.*, C27:65–72, 1985.

[10] Bo Andersson. The Lund model. *Camb.Monogr.Part.Phys.Nucl.Phys.Cosmol.*, 7:1–471, 1997.

[11] Peter Skands. Introduction to QCD. 2012, 1207.2389.

[12] Andy Buckley, Jonathan Butterworth, Stefan Gieseke, David Grellscheid, Stefan Hoche, et al. General-purpose event generators for LHC physics. *Phys.Rept.*, 504:145–233, 2011, 1101.2599.

[13] Consequences of Dirac's Theory of Positrons. *Z. Phys.*, 98:714, 1936, English translation at arXiv:physics/0605038.

[14] Gerald V. Dunne. Heisenberg-Euler effective Lagrangians: Basics and extensions. 2004, hep-th/0406216.

[15] David d'Enterria, Ralph Engel, Tanguy Pierog, Sergey Ostapchenko, and Klaus Werner. Constraints from the first LHC data on hadronic event generators for ultra-high energy cosmic-ray physics. *Astropart.Phys.*, 35:98–113, 2011, 1101.5596.

[16] Yoichiro Nambu. Strings, Monopoles and Gauge Fields. *Phys.Rev.*, D10:4262, 1974.

[17] G. 't Hooft. . *High Energy Physics*, 1975.

[18] S. Mandelstam. Vortices and Quark Confinement in Nonabelian Gauge Theories. *Phys.Rept.*, 23:245–249, 1976.

[19] Alexander M. Polyakov. Particle Spectrum in the Quantum Field Theory. *JETP Lett.*, 20:194–195, 1974.

[20] Gerard 't Hooft. Magnetic Monopoles in Unified Gauge Theories. *Nucl.Phys.*, B79:276–284, 1974.

[21] Gerard 't Hooft. Topology of the Gauge Condition and New Confinement Phases in Nonabelian Gauge Theories. *Nucl.Phys.*, B190:455, 1981.

[22] Gerard 't Hooft. Monopoles, instantons and confinement. 1999, hep-th/0010225.

[23] Georges Ripka. Dual superconductor models of color confinement. 2003, hep-ph/0310102.

[24] A.A. Abrikosov. On the Magnetic properties of superconductors of the second group. *Sov.Phys.JETP*, 5:1174–1182, 1957.

[25] Holger Bech Nielsen and P. Olesen. Vortex Line Models for Dual Strings. *Nucl.Phys.*, B61:45–61, 1973.

[26] Erick J. Weinberg. Classical solutions in quantum field theory. 2012.

[27] Julian S. Schwinger. Gauge Invariance and Mass. 2. *Phys.Rev.*, 128:2425–2429, 1962.

[28] J.H. Lowenstein and J.A. Swieca. Quantum electrodynamics in two-dimensions. *Annals Phys.*, 68:172–195, 1971.

[29] Sidney R. Coleman, R. Jackiw, and Leonard Susskind. Charge Shielding and Quark Confinement in the Massive Schwinger Model. *Annals Phys.*, 93:267, 1975.

[30] A. Casher, John B. Kogut, and Leonard Susskind. Vacuum polarization and the absence of free quarks. *Phys.Rev.*, D10:732–745, 1974.

[31] T. Fujita and J. Hufner. Quark Fragmentation Function in the Schwinger Model. *Phys.Rev.*, D40:604–606, 1989.

[32] C.Y. Wong, Ren-Chuan Wang, and C.C. Shih. Study of particle production using two-dimensional bosonized QED. *Phys.Rev.*, D44:257–262, 1991.

[33] V.N. Gribov. The Theory of quark confinement. *Eur.Phys.J.*, C10:91–105, 1999, hep-ph/9902279.

[34] Yuri L. Dokshitzer and Dmitri E. Kharzeev. The Gribov conception of quantum chromodynamics. *Ann.Rev.Nucl.Part.Sci.*, 54:487–524, 2004, hep-ph/0404216.

[35] Andrea Beraudo, Jose Guilherme Milhano, and Urs Achim Wiedemann. Medium-induced color flow softens hadronization. *Phys.Rev.*, C85:031901, 2012, 1109.5025.

[36] Holger Bech Nielsen and Masao Ninomiya. ADLER-BELL-JACKIW ANOMALY AND WEYL FERMIONS IN CRYSTAL. *Phys.Lett.*, B130:389, 1983.

[37] N.S. Manton. The Schwinger Model and Its Axial Anomaly. *Annals Phys.*, 159:220–251, 1985.

[38] Mikhail A. Shifman. Anomalies and Low-Energy Theorems of Quantum Chromodynamics. *Phys.Rept.*, 209:341–378, 1991.

[39] Holger Bech Nielsen and Masao Ninomiya. Intuitive understanding of anomalies: A Paradox with regularization. *Int.J.Mod.Phys.*, A6:2913–2935, 1991.

[40] Sidney R. Coleman. The Quantum Sine-Gordon Equation as the Massive Thirring Model. *Phys.Rev.*, D11:2088, 1975.

[41] S. Mandelstam. Soliton Operators for the Quantized Sine-Gordon Equation. *Phys.Rev.*, D11:3026, 1975.

[42] Sidney R. Coleman. More About the Massive Schwinger Model. *Annals Phys.*, 101:239, 1976.

[43] C.J. Hamer, John B. Kogut, D.P. Crewther, and M.M. Mazzolini. The Massive Schwinger Model on a Lattice: Background Field, Chiral Symmetry and the String Tension. *Nucl.Phys.*, B208:413, 1982.

[44] Yitzhak Frishman and Jacob Sonnenschein. Non-Perturbative Field Theory – From Two Dimensional Conformal field Theory to QCD in Four Dimensions. 2010, 1004.4859.

[45] Yuri L. Dokshitzer, Valery A. Khoze, Alfred H. Mueller, and S.I. Troian. Basics of perturbative QCD. 1991.

[46] Florian Hebenstreit and Jürgen Berges. Connecting real-time properties of the massless Schwinger model to the massive case. 2014, 1406.4273.

[47] Frasher Loshaj and Dmitri E. Kharzeev. LPM effect as the origin of the jet fragmentation scaling in heavy ion collisions. *Int.J.Mod.Phys.*, E21:1250088, 2012, 1111.0493.

[48] G. Abbiendi et al. Charged particle momentum spectra in e+ e- annihilation at s**(1/2) = 192-GeV to 209-GeV. *Eur.Phys.J.*, C27:467–481, 2003, hep-ex/0209048.

[49] Werner Hofmann. Particle Composition in Hadronic Jets in e^+e^- Annihilation. *Ann.Rev.Nucl.Part.Sci.*, 38:279–322, 1988.

[50] R. Baier, Yuri L. Dokshitzer, Alfred H. Mueller, S. Peigne, and D. Schiff. Radiative energy loss of high-energy quarks and gluons in a finite volume quark - gluon plasma. *Nucl.Phys.*, B483:291–320, 1997, hep-ph/9607355.

[51] M. Gyulassy, P. Levai, and I. Vitev. Reaction operator approach to non-Abelian energy loss. *Nucl.Phys.*, B594:371–419, 2001, nucl-th/0006010.

[52] R. Baier, D. Schiff, and B.G. Zakharov. Energy loss in perturbative QCD. *Ann.Rev.Nucl.Part.Sci.*, 50:37–69, 2000, hep-ph/0002198.

[53] Xin-Nian Wang. Discovery of jet quenching and beyond. *Nucl.Phys.*, A750:98–120, 2005, nucl-th/0405017.

[54] L.D. Landau and I. Pomeranchuk. Limits of applicability of the theory of bremsstrahlung electrons and pair production at high-energies. *Dokl.Akad.Nauk Ser.Fiz.*, 92:535–536, 1953.

[55] Arkady B. Migdal. Bremsstrahlung and pair production in condensed media at high-energies. *Phys.Rev.*, 103:1811–1820, 1956.

[56] M.L. Ter-Mikaelian. . *JETP*, 25:289, 1953.

[57] CMS Collaboration. Detailed Characterization of Jets in Heavy Ion Collisions Using Jet Shapes and Jet Fragmentation Functions. 2012.

[58] Miklos Gyulassy and Xin-nian Wang. Multiple collisions and induced gluon Bremsstrahlung in QCD. *Nucl.Phys.*, B420:583–614, 1994, nucl-th/9306003.

[59] Jorge Casalderrey-Solana, Jose Guilherme Milhano, and Urs Achim Wiedemann. Jet Quenching via Jet Collimation. *J.Phys.*, G38:035006, 2011, 1012.0745.

[60] B.G. Zakharov. Fully quantum treatment of the Landau-Pomeranchuk-Migdal effect in QED and QCD. *JETP Lett.*, 63:952–957, 1996, hep-ph/9607440.

[61] Nestor Armesto, Brian Cole, Charles Gale, William A. Horowitz, Peter Jacobs, et al. Comparison of Jet Quenching Formalisms for a Quark-Gluon Plasma 'Brick'. *Phys.Rev.*, C86:064904, 2012, 1106.1106.

[62] J.F. Gunion and G. Bertsch. HADRONIZATION BY COLOR BREMSSTRAHLUNG. *Phys.Rev.*, D25:746, 1982.

[63] Dmitri E. Kharzeev and Frasher Loshaj. Jet energy loss and fragmentation in heavy ion collisions. *Phys.Rev.*, D87:077501, 2013, 1212.5857.

[64] Christof Roland. Jet measurements by the CMS experiment in pp and PbPb collisions. *J.Phys.*, G38:124020, 2011, 1107.3106.

[65] Georges Aad et al. Observation of a Centrality-Dependent Dijet Asymmetry in Lead-Lead Collisions at $\sqrt{s_{NN}} = 2.77$ TeV with the ATLAS Detector at the LHC. *Phys.Rev.Lett.*, 105:252303, 2010, 1011.6182.

[66] Serguei Chatrchyan et al. Observation and studies of jet quenching in PbPb collisions at nucleon-nucleon center-of-mass energy = 2.76 TeV. *Phys.Rev.*, C84:024906, 2011, 1102.1957.

[67] K. Aamodt et al. Suppression of Charged Particle Production at Large Transverse Momentum in Central Pb–Pb Collisions at $\sqrt{s_{NN}}$ = 2.76 TeV. *Phys.Lett.*, B696:30–39, 2011, 1012.1004.

[68] Jorge Casalderrey-Solana, Yacine Mehtar-Tani, Carlos A. Salgado, and Konrad Tywoniuk. New picture of jet quenching dictated by color coherence. *Phys.Lett.*, B725:357–360, 2013, 1210.7765.

[69] L. Adamczyk et al. Jet-Hadron Correlations in $\sqrt{s_{NN}}$ = 200 GeV Au+Au and $p + p$ Collisions. 2013, 1302.6184.

[70] F.E. Low. Bremsstrahlung of very low-energy quanta in elementary particle collisions. *Phys.Rev.*, 110:974–977, 1958.

[71] V.N. Gribov. Bremsstrahlung of hadrons at high energies. *Sov.J.Nucl.Phys.*, 5:280, 1967.

[72] P.V. Chliapnikov et al. Observation of Direct Soft Photon Production in K^+p Interactions at 70-GeV/c. *Phys.Lett.*, B141:276, 1984.

[73] F. Botterweck et al. Direct soft photon production in K+ p and pi+ p interactions at 250-GeV/c. *Z.Phys.*, C51:541–548, 1991.

[74] S. Banerjee et al. Observation of direct soft photon production in pi- p interactions at 280-GeV/c. *Phys.Lett.*, B305:182–186, 1993.

[75] A. Belogianni et al. Confirmation of a soft photon signal in excess of QED expectations in pi- p interactions at 280-Gev/c. *Phys.Lett.*, B408:487–492, 1997, hep-ex/9710006.

[76] A. Belogianni, W. Beusch, T.J. Brodbeck, D. Evans, B.R. French, et al. Further analysis of a direct soft photon excess in pi- p interactions at 280-GeV/c. *Phys.Lett.*, B548:122–128, 2002.

[77] A. Belogianni, W. Beusch, T.J. Brodbeck, F.S. Dzheparov, B.R. French, et al. Observation of a soft photon signal in excess of QED expectations in p p interactions. *Phys.Lett.*, B548:129–139, 2002.

[78] V. Balek, N. Pisutova, and Jan Pisut. The Puzzle of Very Soft Photon Production in Hadronic Interactions. *Acta Phys.Polon.*, B21:149, 1990.

[79] Edward V. Shuryak. The 'Soft Photon Puzzle' and Pion Modification in Hadronic Matter. *Phys.Lett.*, B231:175–177, 1989.

[80] P. Lichard and L. Van Hove. Cold quark - gluon plasma as source of very soft photons in high-energy collisions. *Phys.Lett.*, B245:605–608, 1990.

[81] Peter Lichard. Consistency of data on soft photon production in hadronic interactions. *Phys.Rev.*, D50:6824–6835, 1994, hep-ph/9812206.

[82] Gokce Basar, Dmitri Kharzeev, Dmitri Kharzeev, and Vladimir Skokov. Conformal anomaly as a source of soft photons in heavy ion collisions. *Phys.Rev.Lett.*, 109:202303, 2012, 1206.1334.

[83] A.A. Andrianov, V.A. Andrianov, D. Espriu, and X. Planells. Dilepton excess from local parity breaking in baryon matter. *Phys.Lett.*, B710:230–235, 2012, 1201.3485.

[84] Kenji Fukushima and Kazuya Mameda. Wess-Zumino-Witten action and photons from the Chiral Magnetic Effect. *Phys.Rev.*, D86:071501, 2012, 1206.3128.

[85] Kirill Tuchin. Electromagnetic radiation by quark-gluon plasma in magnetic field. *Phys.Rev.*, C87:024912, 2013, 1206.0485.

[86] Ho-Ung Yee. Flows and polarization of early photons with magnetic field at strong coupling. *Phys.Rev.*, D88(2):026001, 2013, 1303.3571.

[87] G.W. Botz, P. Haberl, and O. Nachtmann. Soft photons in hadron hadron collisions: Synchrotron radiation from the QCD vacuum? *Z.Phys.*, C67:143–158, 1995, hep-ph/9410392.

[88] Cheuk-Yin Wong. Anomalous Soft Photons in Hadron Production. *Phys.Rev.*, C81:064903, 2010, 1001.1691.

[89] Yoshitaka Hatta and Takahiro Ueda. Soft photon anomaly and gauge/string duality. *Nucl.Phys.*, B837:22–39, 2010, 1002.3452.

[90] J. Abdallah et al. Study of the Dependence of Direct Soft Photon Production on the Jet Characteristics in Hadronic Z0 Decays. *Eur.Phys.J.*, C67:343–366, 2010, 1004.1587.

[91] J. Abdallah et al. Evidence for an excess of soft photons in hadronic decays of Z0. *Eur.Phys.J.*, C47:273–294, 2006, hep-ex/0604038.

[92] J. Abdallah et al. Observation of the Muon Inner Bremsstrahlung at LEP1. *Eur.Phys.J.*, C57:499–514, 2008, 0901.4488.

[93] Dmitri E. Kharzeev and Frasher Loshaj. Anomalous soft photon production from the induced currents in Dirac sea. *Phys.Rev.*, D89:074053, 2014, 1308.2716.

[94] Dmitri Kharzeev. Parity violation in hot QCD: Why it can happen, and how to look for it. *Phys.Lett.*, B633:260–264, 2006, hep-ph/0406125.

[95] D. Kharzeev and A. Zhitnitsky. Charge separation induced by P-odd bubbles in QCD matter. *Nucl.Phys.*, A797:67–79, 2007, 0706.1026.

[96] Dmitri E. Kharzeev, Larry D. McLerran, and Harmen J. Warringa. The Effects of topological charge change in heavy ion collisions: 'Event by event P and CP violation'. *Nucl.Phys.*, A803:227–253, 2008, 0711.0950.

[97] Kenji Fukushima, Dmitri E. Kharzeev, and Harmen J. Warringa. The Chiral Magnetic Effect. *Phys.Rev.*, D78:074033, 2008, 0808.3382.

[98] Dmitri E. Kharzeev and Ho-Ung Yee. Chiral Magnetic Wave. *Phys.Rev.*, D83:085007, 2011, 1012.6026.

[99] J. Beringer et al. Review of Particle Physics (RPP). *Phys.Rev.*, D86:010001, 2012.

[100] A. Bialas. Fluctuations of string tension and transverse mass distribution. *Phys.Lett.*, B466:301–304, 1999, hep-ph/9909417.

[101] Zhong-Bo Kang and Dmitri E. Kharzeev. Quark fragmentation in the θ-vacuum. *Phys.Rev.Lett.*, 106:042001, 2011, 1006.2132.

[102] K. Schilling, G.S. Bali, and C. Schlichter. A Ginzburg-Landau analysis of the color electric flux tube. *Nucl.Phys.Proc.Suppl.*, 73:638–640, 1999, hep-lat/9809039.

[103] Paolo Cea, Leonardo Cosmai, and Alessandro Papa. Chromoelectric flux tubes and coherence length in QCD. *Phys.Rev.*, D86:054501, 2012, 1208.1362.

[104] Takumi Iritani, Guido Cossu, and Shoji Hashimoto. Analysis of topological structure of the QCD vacuum with overlap-Dirac operator eigenmode. 2013, 1311.0218.

[105] Dmitri E. Kharzeev and Frasher Loshaj. Partial restoration of chiral symmetry in a confining string. 2014, 1404.7746.

[106] Tigran Kalaydzhyan and Edward Shuryak. Self-interacting QCD strings and String Balls. 2014, 1402.7363.

[107] Paolo Cea, Leonardo Cosmai, Francesca Cuteri, and Alessandro Papa. Flux tubes in the SU(3) vacuum: London penetration depth and coherence length. *Phys.Rev.*, D89:094505, 2014, 1404.1172.

[108] Jr. Callan, Curtis G. and Jeffrey A. Harvey. Anomalies and Fermion Zero Modes on Strings and Domain Walls. *Nucl.Phys.*, B250:427, 1985.

[109] Erick J. Weinberg. Index Calculations for the Fermion-Vortex System. *Phys.Rev.*, D24:2669, 1981.

[110] Jeffrey Goldstone and Frank Wilczek. Fractional Quantum Numbers on Solitons. *Phys.Rev.Lett.*, 47:986–989, 1981.

[111] Stephen G. Naculich. Axionic Strings: Covariant Anomalies and Bosonization of Chiral Zero Modes. *Nucl.Phys.*, B296:837, 1988.

[112] Chi Xiong. QCD Flux Tubes and Anomaly Inflow. *Phys.Rev.*, D88(2):025042, 2013, 1302.7312.

[113] Chi Xiong. Phase of Quark Condensate and Topological Current in QCD. 2013, 1310.8657.

[114] John David Jackson. *Classical electrodynamics*. Wiley, New York, NY, 3rd ed. edition, 1999.

[115] I. S. Gradshteyn and I. M. Ryzhik. Table of Integrals, Series, and Products. *Academic Press, New York, 7th edition, 2007*, 2007.

[116] J.B. Kogut and M.A. Stephanov. The phases of quantum chromodynamics: From confinement to extreme environments. *Camb.Monogr.Part.Phys.Nucl.Phys.Cosmol.*, 21:1–364, 2004.

[117] R.A. Bertlmann. Anomalies in quantum field theory. 1996.